SHORT TERM CONTRACT FOR THE BIOLOGICAL STUDIES (ICCAT GBYP 08/2020) OF THE ATLANTIC-WIDE RESEARCH PROGRAMME FOR BLUEFIN TUNA (GBYP Phase 10)

Final Report

for:

ICCAT

Scientific coordinator:

Dr. Nicolas Goñi (AZTI)

Pasaia, July 12th, 2021

This project is co-funded by

the European Union

PARTNERS:

Fundación AZTI-AZTI Fundazioa

IFREMER

Instituto Español de Oceanografía

Universitá di Genova

University of Cagliari

Texas A&M University

GMIT

Universidad de Cádiz

National Oceanic and Atmospheric Administration

University of Maine

Fisheries and Oceans of Canada

SUBCONTRACTORS and COLLABORATORS:

Institute of Marine Research

IPMA

INRH

Univ. Arizona

CNRS

Sgiker (EHU)

Thermofisher

NordSIM

Univ. of Istambul

CBBA

TAXON

INDEX:

EXECUTIVE SUMMARY:

The main objective of this project is to enhance knowledge about Atlantic bluefin tuna (ABFT) population structure and mixing, but also to focus on age dynamics.

During Phase 10, following sampling protocols agreed in earlier Phases, the Consortium sampled a total of 713 bluefin tuna (32 YOY, 96 medium sized fish and 585 large fish) from different regions (113 from the Strait of Gibraltar, 7 from Morocco, 25 from the Canary Islands, 400 from Norway, 121 from the Central North Atlantic (sampled in 2019), 31 from the Western Mediterranean and 16 from the Bay of Biscay). In total, 1452 biological samples (348 otolith samples, 391 fin spines and 713 genetic samples) were collected by the Consortium and incorporated into the tissue bank. The Consortium also received samples from other ICCAT contracts with tagging teams and farm operators. In total, the Consortium handled 3947 biological samples (1243 otolith samples, 700 fin spines, 310 gonads and 1694 genetic samples from 1699 individuals).

On genetic analyses, we have developed a new cost-effective tool that includes more than 7000 genetic markers suitable for Atlantic bluefin tuna population genetics, sex determination, kinship finding and origin assignment. Using this tool, we have confirmed previous hypothesis on Atlantic bluefin tuna connectivity, including the presence of signals of adaptation that require further studies. Concerning origin assignment, we have concluded that improving the baseline with more samples from the Gulf of Mexico does not result in a better origin assignment and that the presumed incorrectly assigned samples and those unassigned are more likely due to a non complete genetic isolation between spawning components.

Regarding otolith microchemistry, new carbon and oxygen stable isotope ($\delta^{13}C$ and $\delta^{18}O$) analyses were carried out in 202 otoliths of Atlantic bluefin tuna captured in the Canary Islands, Central North Atlantic (east and west of the 45ºW boundary) and the Norwegian Sea, to determine their nursery area. $\delta^{13}C$ and $\delta^{18}O$ values measured in otolith cores indicated that samples from the Northeast Atlantic, Norwegian Sea and Canary Island were dominated by eastern origin individuals, whereas a considerable mixing of the two populations was detected in the western North Atlantic. These results are consistent with previous findings and suggest that Mediterranean bluefin tuna may be the principal contributor to the fisheries operating in the

eastern North Atlantic. Fisheries operating west of the 45ºW meridian are supported by both Mediterranean and Gulf of Mexico populations, and the proportions of each stock contributing to the catches may vary from year to year. Additionally, discrimination capacity of a new baseline created with reference otoliths from the Gulf of Mexico and Mediterranean spawners was evaluated using the otolith portion corresponding to the early life period (approx. 3 months). Discriminatory power of this new baseline was similar to that based on 1-year otolith portion, but preliminary results suggested that the combination of stable isotopes and trace elements may considerably improve our ability to identify the origin of tuna from the mixing zones.

In relation to life history analyses, secondary ion mass spectrometry (SIMS) was used to measure $\delta^{18}O$ along otolith growth profiles at a high temporal-resolution. The method proved effective at detecting variation in environmental histories, with results showing evidence of individual variability in early life history and possible trans-Atlantic migration of adult fish. It was also shown that trace elements and $\delta^{18}O$ provide a complementary ecological information, and thus combining both techniques may be useful to characterize otolith chemical patterns, and ultimately detect movements between the Mediterranean Sea and Atlantic Ocean.

On the otolith age calibration exercise, the findings show that there are differences in band counts between ICCAT expert readers and FAS readings. These differences start from specimens with more than 10 bands and are more pronounced for older specimens. The results of the present calibration (GBYP Phase 10) are very similar to those of the previous one (GBYP Phase 9). These differences in readings appear to be because FAS uses the entire section of the otolith to count annual bands, whereas ICCAT readers focus on the inner part of the ventral arm. Analyses conducted to establish which reading is more appropriate, growth function estimation and cohort follow-up analysis, seem to indicate that ICCAT readers are more accurate than FAS readers.

Regarding otolith edge type deposition along the year cycle, our preliminary results of edge type and MIA in otolith of ABFT clearly indicate that opaque bands are fully formed between August and November. However, poor data in the early part of the year prevent from reaching any conclusive results. Further sampling effort during winter months are recommended to fully cover the year and examine the relationship between month and index of completion.

In 2019, an ABFT larvae from August 2009 were found in the Bay of Biscay near the position 43º37’61N 4º10’92 W (Rodriguez et al.2019), confirming that ABFT can spawn in this area. For that reason, the search for ABFT larvae in samples collected in the 2020 acoustic survey in the Bay of Biscay was proposed for this study. The species identification was performed on plankton

samples preserved in ethanol, collected along the track of the acoustic survey, outside the continental shelf, where the probability to find ABFT was considered to be higher. All larvae were extracted and identified through microscopic identification and genetic sequencing would have been used in the case of necessity for confirmation. Among the 6 plankton hauls, preserved in ethanol, done during the 2020 survey, 99 larvae were found, of which none was an ABFT larva, the only scombrid larvae encountered being *Auxis sp.* larvae.

Finally, ABFT larvae from surveys conducted in the Balearic spawning ground were sorted and identified for potential genetic analyses. A total of 2258 bluefin tuna larvae were identified in 49 samples, and were suitable for genetic analyses.

Most of the objectives of the project were met. The analyses continue to provide important information that is relevant for the understanding of Atlantic bluefin tuna biology and improve stock assessment and management of this valuable resource.

1. CONTEXT

On June 19th 2020, the Consortium coordinated by Fundación AZTI-AZTI Fundazioa, formed by partners Fundación AZTI-AZTI Fundazioa, IFREMER, Universitá di Genova, National Research Institute of Far Seas Fisheries, GMIT, Texas A&M University, Universidad de Cádiz, University of Cagliari, Instituto Español de Oceanografía, National Oceanic and Atmospheric Administration, University of Maine, Fisheries and Oceans of Canada, with subcontracted parties IPMA, Institute of Marine Research, INRH, University of Arizona, CNRS, Sgiker (EHU), Thermofisher, NordSIM, Istambul University, CBBA and TAXON, presented a proposal to the call for tenders on biological and genetic sampling and analysis (ICCAT-GBYP 08/2020).

This proposal was awarded and the final contract between ICCAT and the Consortium represented by Fundación AZTI-AZTI Fundazioa was signed on July 20th 2020.

According to the terms of the amended contract, a draft final report (Deliverable # 4) needs to be submitted to ICCAT by 12th of July 2021, and the definitive final report, incorporating the suggestions from GBYP Coordination team (Deliverable 5), by 26th July. The present report was prepared in response to such requirements.

2. SAMPLING

Task Leader: Igaratza Fraile

Participants:

AZTI: Inma Martin, Naiara Serrano, Ainhoa Arevalo, Goreti Garcia, Nicolas Goñi, Naiara Rodriguez-Ezpeleta, Natalia Diaz, Iñaki Mendibil

UCA: Jose Luis Varela, Antonio Medina

NRIFSF: Yohei Tsukahara, Tomoyuki Itoh, Shuya Nakatsuka

IEO: Enrique Rodriguez Marín, Rosa Delgado de Molina

INRH: Noureddine Abbid

IMR: Ørjan Sørensen, Adam Custer, Christine Djønne, Erling Boge, Leif Nøttestad

IPMA: Pedro Lino, Rui Coelho

The sampling conducted under this project follows a specific design, aimed primarily at contributing to knowledge on population structure and mixing. As such, the sampling conducted under this project is independent from other routine sampling activities for fisheries and fishery resources monitoring (e.g. the Data Collection Framework).

2.1. Sampling accomplished

The sampling protocols, together with instructions, have been distributed within the Consortium as well as to ICCAT, so that they are distributed to other institutions conducting biological sampling (e.g. as part of tagging activities, Regional Observer Programs, farms, etc.).

The sampling tasks have finalized successfully in most of the areas. IEO has provided otolith and genetic samples from 25 individuals from Canary Islands caught in late 2020. NRIFSF provided otolith and genetic samples from 121 individuals caught by Japanese longliners in the central Atlantic Ocean in October 2019, all of them have arrived to AZTI. Among these 121 individuals, 35 were caught west of the 45ºW boundary, and 86 were captured east of the 45ºW boundary. Only one YOY bluefin tuna was captured in the Strait of Gibraltar by UCA. Although efforts have been made to target this size class, YOY bluefin tuna were not available in the area in 2020, same as in 2019. However, complete (genetic+otoliths+spines) samples of 31 YOY bluefin tuna were collected in

Alboran Sea off Murcia area, and provided by UCA, as a substitute for the ones missing from the strait of Gibraltar. Additionally, UCA also provided tissue samples from 96 medium-sized and 16 large individuals caught by baitboat in the Strait of Gibraltar. INRH has conducted sampling on fattened tuna in Morocco, with both otolith and muscle tissue sampled from 7 individuals. Although efforts have been made to sample these tunas, the access to the harvest locations was restricted due to sanitary restrictions.

Sampling in Norwegian waters was successfully conducted in September 2020. Samples were again taken from three Norwegian purse seine vessels, M/V "Brennholm", M/V "Orfjord" and M/V "Vibeke Helene". A total number of 165 genetic samples, 153 spines and 26 pair of otoliths have been taken from large Atlantic bluefin tuna. Because most of the BFT are sold with heads on, it was not possible to extract the otoliths from many of the individuals.

In the Bay of Biscay, 16 large bluefin tunas caucht in January and November 2020 were sampled by AZTI, which may be representative of a population fraction overwintering around this area.

In total, 713 bluefin tuna have been sampled by Consortium partners., i.e. 128% of the global target (table 1). Additional samples captured in 2019 and harvested in spring 2020 arrived from two different sources, respectively Maltese Ministry for Agriculture, Fisheries and Animal Rights – Department of Fisheries and Aquaculture and the company Taxon operating in the Spanish Mediterranean, as part of ICCAT/GBYP specific contracts for sampling adult BFT in the Mediterranean. They collected samples from 676 and 310 individuals, respectively (table 2).

In terms of number of samples, a total of 1452 samples were collected by the Consortium partners, i.e. 109% of the target, with a bigger proportion of genetic samples and lower proportion of otoliths than expected (table 3).

Table 1: Individuals sampled within the Consortium

		Age 0	**Juveniles**	**Medium**	**Large**	Total		
		<3 kg	**3-25 kg**	**25-100 kg**	**>100 kg**		**Target**	**%**
Gibraltar	Gulf of Cadiz	1		96	16	**113**	50	226%
East Atlantic-W.African coast	Morocco				7	**7**	50	14%
	Canary Islands				25	**25**	25	100%
Northeast Atlantic	Bay of Biscay				16	**16**	no	> 100%
	Portugal (Algarve)					**0**	30	0%
North Sea	Norway				400	**400**	100	400%
Central North Atlantic	Central North Atlantic				121	**121**	300	40%
Western Med	South Spain	31				**31**	no	> 100%
	TOTAL	**32**	**0**	**96**	**585**	**713**	555	128%

Table 2: TOTAL individuals sampled

Gran Area	**Area**	**Age 0** **<3 kg**	**Juveniles** **3-25 kg**	**Medium** **25-100 kg**	**Large** **>100 kg**	**Total**
Central Med	Malta				4	**4**
Western Med	South Spain	31				**31**
	Balearic				310	**310**
Gibraltar	Gibraltar	1		109	16	**126**
Northeast Atlantic	Bay of Biscay				15	**15**
	Portugal					**0**
East Atlantic	Canary Islands				25	**25**
North Sea	Norway				400	**400**
Central North Atlantic	Central and North Atlantic				180	**180**
	TOTAL	**32**	**0**	**109**	**950**	**1091**

Table 3: detail the number of otoliths, fin spines and genetic samples in each stratum sampled in the framework of the Consortium

		Size classes sampled				Material sampled				Responsible
		Age 0	Juveniles	Medium	Large					
		<3 kg	3-25 kg	25-100 kg	>100 kg	otoliths	spine	gonads	muscle/fin	
Strait of Gibraltar	Gibraltar	1		96	16	1	1		113	UCA
	Alboran Sea	31				31	31		31	
East Atlantic-West African Coast	Morocco				7	7			7	AZTI (INRH)
	Canary Islands				25	25			25	IEO
Northeast Atlantic	Bay of Biscay				16				16	
	Portugal (Algarve)				0					AZTI (IPMA)
North Sea	Norway				400	163	359		400	AZTI (IMR)
Central North Atlantic	Central and North Atlantic				121	121			121	NRIFSF
	TOTAL	32	0	96	585	348	391	0	713	
	TOTAL nº indivuals	713					TOTAL samples		1452	

A total of 1452 biological samples have been collected by the Consortium and incorporated to the tissue bank (348 otoliths, 391 fin spines and 713 genetic samples). These samples have been catalogued and stored together with the biological tissue bank.

Altogether (considering the samples collected by the Consortium and those that arrived from other contracts), the Consortium handled 2433 biological samples (1243 otoliths, 700 fin spines and 1694 genetic samples).

2.2. Sampling difficulties encountered and global balance

Sampling by IPMA in the Portuguese traps was not possible in 2020, due to restricted access of the samplers to harvest locations. Otoliths, spines and muscles were intended to be sampled from 30 individuals but this sampling was not possible during this phase. Likewise, the sampling of individuals with abnormally long second dorsal fin, initially planned to be done by Taxon, was not done. For the same reasons, only 14% of the target was reached in Moroccan sampling locations.

For the same reasons, access to Japanese longline vessels for sampling was not possible during 2020, although samples collected in 2019 were provided.

In the Gulf of Cadiz, the problem encountered was the absence of YOY individuals in the area, they were substituted by YOY individuals from northern Alboran Sea, and individuals from older age groups in the Strait of Gibraltar. Additional samples (n=300) were also provided from the North Sea, and 16 initially non planned samples from the Bay of Biscay.

The original plan, according to the Consortium contract, was to acquire samples from 555 individuals. Thus, the current sampling status by the Consortium represents 128% of the target in terms of total number of individuals. Analyzing the objectives by strata, most areas were covered according to the sampling plan. In the Atlantic side of the Strait of Gibraltar, the target was the acquisition of 50 YOY bluefin tuna. This objective was not achieved due to the lack of small fish in this area during 2020, but instead, medium and large category bluefin tuna were sampled. In the other areas, the number of individuals caught was larger than expected.

3. GENETICS

Task Leader: Naiara Rodriguez-Ezpeleta (AZTI)

Participants: Natalia Diaz-Arce, Iñaki Mendibil, Haritz Arrizabalaga

3.1. Introduction

Despite recent efforts on understanding the population structure and connectivity of Atlantic bluefin tuna, numerous questions remain. Perhaps the most important question is how much and since when the two presumed populations, Gulf of Mexico and Mediterranean, interbreed, and what is the role of the Slope Sea in this interbreeding. Interbreeding has been mostly identified to happen in the Slope Sea. We think this region facilitates interbreeding, but we do not know since when it does, and if it is an old interbreeding region we do not know why the East-West differentiation still exists. Another hypothesis would be that western spawners migrated to the Slope Sea in more recent years. In recent endeavours we have used RAD-seq data to tackle these questions. These data have provided unprecedented information about the population structure of Atlantic bluefin tuna, revealing connectivity mediated through the Slope Sea, signals of adaptation and nuclear introgression from albacore. The discovery of the genome markers leading to know these results allow the development of more cost-effective approaches for genotyping, which will allow to upscale Atlantic bluefin tuna population studies by enabling the analyses of much more samples. Additional analyses using alternative approaches are also needed to confirm previous findings on connectivity and potential adaptation, not only because they rely on different genotyping technologies, but also because they allow inclusion of more samples. In parallel to study population connectivity of Atlantic bluefin tuna, it is important to continue monitoring feeding aggregates through small scale assays such as the 96 SNP traceability panel developed in previous phases. The baseline for this panel was based on a few Gulf of Mexico larvae, which was a limitation. Thus, there is scope to improve it by including more larvae from the Gulf of Mexico as they become available. In this Phase, genetic analyses have focused on further confirming previous results on the population structure of Atlantic bluefin tuna by using a new developed assay and on testing assignment of feeding aggregates with an improved origin traceability panel through the use of an enlarged baseline.

3.2. Materials and methods

3.2.1. DNA extraction

DNA of 170 new samples was extracted. From those, 154 were larvae from the Gulf of Mexico and 16 were Mediterranean adults with normal and abnormal fin lengths (8 of each). This number is less than that originally planned (350) because we received less abnormal fin length adults than expected and because the Slope Sea individuals selected for analyses had DNA already extracted from previous phases. DNA was extracted using the Wizard® Genomic DNA Purification kit (Promega, WI, USA) following manufacturer´s instructions for "Isolating Genomic DNA from Tissue Culture Cells and Animal Tissue". The starting material was approximately 20 mg of tissue or whole larvae and after extraction all samples were suspended in equal volumes of Milli-Q water. DNA quantity (ng/µl) was evaluated on the Qubit® 2.0 Fluorometer (Life Technologies) and DNA integrity was assessed by electrophoresis.

3.2.2. Assay for chromosomal inversion detection

In order to determine the break point of the potential chromosomal inversion, we calculated inter-chromosomic pairwise SNP squared correlation values based on genotypic allele counts (r^2) using PLINK (Purcell et al. 2007). The count, for each SNP, of the number of high linkage correlations (r^2>0.1) was screened along both reference scaffolds to identify approximate break points, considering that only reduced representation of the genome is available. Two primer sequence pairs for amplification of the region covering one of the break points corresponding to the potentially inverted and non-inverted versions were designed based on the nearest tag sequences available (Figure 1). The designed primers were used to amplify the target genomic region performing a long range Polymerase Chain Reaction (PCR) in a total volume of 20 µl with 10 µl of Taq Master Mix (New England Biolabs LongAmp Taq 2X Master Mix ref.174M0287S), 1 µl of each primer and 50 ng of total DNA using the following profile: an initial denaturation step at 94°C during 3 min, 30 cycles of 30 sec at 94°C, 30 sec at 56°C and 25 min at 65°C, and a final extension of 65°C for 10 minutes. Products were visualized on 1.7% agarose gels. Both primer pairs were tested on 3 sample pairs that cluster in the common-homozygous (homozygous for the non-inverted), rare-homozygous (homozygous for the inverted), and the heterozygous haplotypes for the inversion.

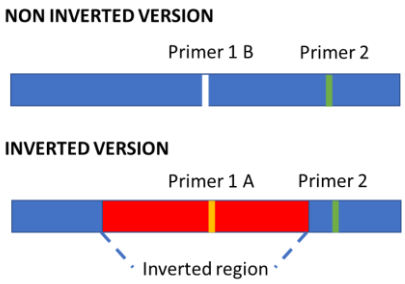

Figure 1. *Scheme depicting primer design for amplification of inverted and non-inverted versions, which are represented in red and blue, respectively. Shared and non-shared amplification ends are represented in green and in white or orange, respectively.*

3.2.3. SNP Array design and genotyping

We targeted the development of an Axiom array (Thermo Fisher) of 10,000 SNPs, which is what the budget allowed. For that aim, we submitted an initial set of 18,003 of candidate probes to be validated by the Axiom array design center. The candidate markers covered neutral SNPs and adaptive SNPs (including those within the potential chromosomal inversion) derived from the RAD-seq dataset as well as markers of mitochondrial variation (including signal for introgression), sex determination, and origin assignment (the 96 SNPs included in the panel developed in Phase 6) (Table 4).

Table 4*. Number of markers of each type for which corresponding probes were submitted for quality analysis and included in the SNP array. For some markers more than one probe pair was included. The total number of probes included for markers of each type is also indicated.*

Type	Submitted	Included	Probe pairs
Neutral SNPs	17,612	9,610	9,610
Neutral SNPs located within potential inversion	141	108	108
Outlier SNPs	134	109	150
Mitochondrial introgression	7	5	5
Mitochondrial variants	8	8	11
Sex markers	5	5	10
96-SNP panel	96	83	106
TOTAL	18,003	**9,928**	**10,000**

The RAD tags containing the selected SNPs were mapped to the Pacific bluefin tuna reference genome (Suda et al. 2019) to extract the flanking regions for each SNP using an in-house script. The probe design requires at least 36bp length monomorphic flanking sequences at both sides of the SNP. To avoid loss of valuable markers due to the presence of rare variants, we considered those polymorphisms in the flanking regions with minimum allele frequency lower than 0.003 monomorphic. Probes for mitochondrial variants (including those informative for albacore introgression) were identified by comparing available genus representative COI sequences (Diaz-Arce *et al.* unpublished) to the Atlantic bluefin tuna mitochondrial reference genome (accession number NC_014052). Five probes for sex determination were developed to genotype 4 sex-specific SNPs and a 6bp male-specific insertion located within the genomic regions covered by the three sex discriminative PCR assays developed in Suda et al. (2019).

The suitability of the total 18,003 probes for their inclusion in the SNP array was assessed by the Thermo Fisher Scientific Center. A final set of 9,928 markers were selected giving priority to adaptive SNPs, markers of mitochondrial introgression, sex markers and the 96 SNPs from the discrimination panel, which were excluded only if their corresponding probes were assessed as "not_possible". Double strand probes were included for 72 of these priority markers for which its design was possible. The rest of the markers were included in the final set following the suitability assessment. The final array, which included 10,000 probes targeting 9,928 markers, was sent for design and manufacture to the Thermo Fisher Scientific Center.

A total of 384 DNA samples were genotyped with the 10,000 SNP array, including larvae from the Gulf of Mexico, candidate spawners of the Slope Sea captured in the West Atlantic, a subset of long/short fin Atlantic bluefin tuna individuals, 25 Gulf of Mexico and Mediterranean samples already genotyped with RAD-seq for replicability analyses (Table 5). Although originally only 250 were planned, the array design required 384 samples, which compensated the reduction of DNA extractions and number of SNPs included.

Table 5. *Total number of samples of each type genotyped using the newly designed SNP array*

Sample Type	**n**
GoM larvae	154
Long/Short fin	16
Slope Sea "spanwners"	189
RAD-sequenced	25
TOTAL	384

3.2.4. SNP array genotype analysis

Obtained genotypes were analyzed using Axiom Analysis Suite specific software and genotypes were assessed using default parameters. Genotypes of the nuclear SNPs excluding markers for sex determination, for the 25 samples that were available from SNP array genotyping and from RAD-sequencing were compared and percentage of mismatch genotypes, excluding missing genotypes, was estimated to test for SNP genotyping reproducibility with both methods.

Genetic relatedness of the newly genotyped individuals was assessed based on neutral markers building a genetic relatedness matrix using the software GCTA (Yang et al. 2011) and one individual of each pair of relatives, or all individuals in case of groups of related individuals, were removed from the dataset for further analysis. Genotypes for neutral and outlier SNPs obtained using the SNP array were split into separated genotype tables using PLINK (Purcell et al. 2007) and exported to structure format using PGDSpider (Lischer, Excoffier 2011). Principal Component Analysis (PCA) was performed using the *adegenet* R package (Jombart 2008) and individual proportions of ancestral populations (assuming two ancestral populations, K=2) were estimated using ADMIXTURE (Alexander, Novembre, Lange 2009). Proportion of individuals of each type showing the albacore like mitochondrial haplotype was estimated based on successfully genotyped mitochondrial introgression markers.

3.2.5. 96 SNP panel assignments based on newly generated baselines

Genotyping of 94 larvae samples captured in the Gulf of Mexico for the 96-SNPs traceability panel from Rodríguez-Ezpeleta et al. (2019) was performed on the BiomarkTM HD platform using Flex Six™ and 96.96 Dynamic Array IFCs, and the resulting data set was analyzed with the Fluidigm Genotyping Analysis Software. Two new baselines were generated based on the i) old baseline ("original baseline"), by ii) incorporating the newly genotyped larvae from the Gulf of Mexico ("enlarged baseline"), and by iii) additionally excluding genotypes from adult individuals from the Gulf of Mexico ("filtered baseline"). Assignment rate using the newly generated baselines was calculated following the same procedure described in Phases 6 and 9. Assignments were performed with GENECLASS2 (Piry et al. 2004) using the Rannala and Mountain (1997) criterion (0.05 threshold) considering two (Gulf of Mexico and Mediterranean) populations as baselines. For each individual not involved in the 96 SNP selection process (see Phase 6), assignment scores (*i.e.*, probability of belonging to each of the baseline populations) were calculated using a leave-one-out approach using the different baselines excluding the sample being assigned for each calculation. Assignment rates were calculated considering only assignment scores >80%. A total of 2,487 adult

samples of unknown origin captured at different feeding grounds in the North Atlantic (see Phase 9) were assigned with GENECLASS2 (Piry et al. 2004) using the Rannala and Mountain (1997) criterion (0.05 threshold) using the location informed or the newly generated genetic-informed baseline and considering results applying 80% threshold for assignment scores.

3.3. Results

3.3.1. The developed chromosomal inversion detection assay was not successful

The number of inter-chromosomic SNP relations under linkage disequilibrium starts increasing from position 237,098 of scaffold BKCK01000111 and decreasing from position 750,383 of scaffold BKCK01000075 (Figure 2). This is a high-linkage disequilibrium region, which covers nearly the entire scaffold BKCK01000111; for that reason, primers were designed to amplify the region around the break-point located within the scaffold BKCK01000075. Therefore, the second primer of the two designed pairs was based on the tag starting at position 750,447 of scaffold BKCK01000075, while first primer of the pair targeting the non-inverted and inverted versions were designed based on tags starting at position 721,935 of the scaffold BKCK01000075 and position 237,098 of the scaffold BKCK01000111 (Table 6).

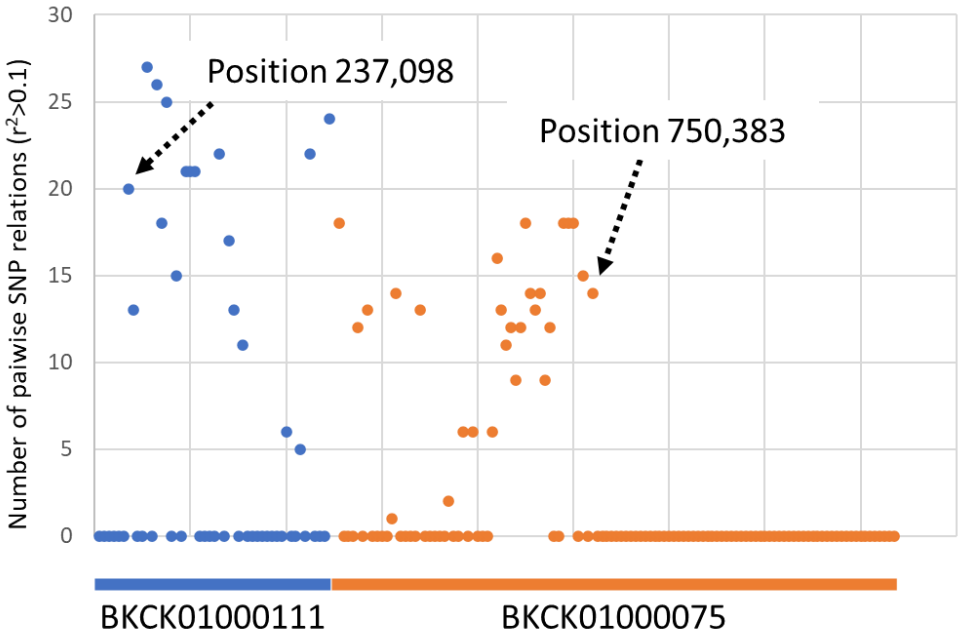

Figure 2. *Number of inter-chromosomic SNPs correlation under high-linkage disequilibrium (r2>0.1) (y-axis) at the 167 SNPs concatenated in order along the scaffolds BKCK01000111 and*

BKCK01000075 of the reference genome of Pacific bluefin tuna (x-axis). Candidate break-point positions for the chromosomal inversion along the respective scaffolds are indicated.

Table 6. *Sequences of the primer pairs designed targeting the non-inverted and inverted chromosomic versions of the genomic region surrounding one of the inversion break-points. Starting position and the reference scaffold of the Pacific bluefin tuna genome (Suda et al. 2019) is indicated.*

TARGET	Name	Sequence 5´to 3´	Start position
Non-inverted	BFT-1A	AACCTCCCCAGGGACACC	722018; BKCK01000075
	BFT-2	GAACCCTGCAGAAACCCTGCA	750,447; BKCK01000075
Inverted	BFT-1B	GGAGGCTCATCCGTGATCACATTC	327,025; BKCK01000111
	BFT-2	GAACCCTGCAGAAACCCTGCA	750,447; BKCK01000075

Both primer pairs failed to clearly amplify regions of the expected length (Figure 3). Despite several different bands of different sizes being obtained, none resulted to be the expected size. This could be due to technical issues or to differences between the expected and real genomic sequences. Better understanding of the size and nature of the potential inversion would be needed to develop assays that could effectively detect its presence. The failure of this assay has prevented us testing the presence of adaptive markers in as many samples as expected as we had to rely on the array (see below) for this and only a limited sample number was possible.

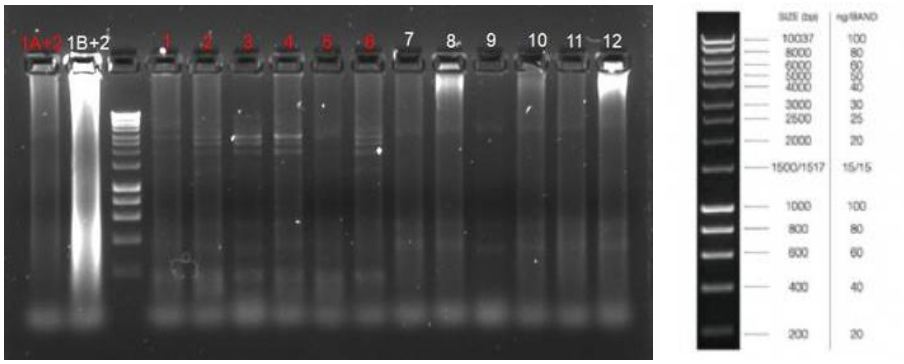

Figure 3. *PCR amplification results using the primers for detecting the inverted (red) and non-inverted (white) versions. Samples 1-2, 7-8 and 5-6, 11-12 are homozygous for the rare and the common version respectively, and samples 3-4, 9-10 are heterozygous.*

3.3.2. The SNP array performed very well compared to RAD-seq

After filtering samples and genotypes obtained using the newly designed SNP array, in total 7,930 markers were successfully genotyped including markers of all types (Table 7).

Table 7. *Number of markers of each type that passed genotyping quality filtering and were included in the dataset.*

Marker type	**Passed markers**	**% probes**	**Succesful**
Neutral SNPs	7,673	79.8	
Neutral SNPs located within potential inversion	75	69.4	
Outlier SNPs	94	62.6	
Mitochondrial introgression	2	40	
Mitochondrial variants	6	54.5	
Sex markers	5	50	
96-SNP panel	75	70.7	
TOTAL	**7,930**		

The average genotyping rate per sample, estimated based on the 7,842 RAD-seq derived nuclear SNPs that successfully genotyped is 0.96457, which is slightly lower than that obtained when converting RAD-seq derived SNPs to the SNP panel, 98% (Rodríguez-Ezpeleta et al. 2019).

3.3.3. The population structure of Atlantic bluefin tuna inferred form the array is equivalent to that inferred from RAD-seq markers

In total, 27 pairs of newly genotyped individuals show genetic relatedness values over 0.1, ranging from 0.16 to 0.52, suggesting the presence of kin pairs within the dataset. All kin pairs involved only larvae captured within the same period in the Gulf of Mexico. After checking that average heterozygosity values were not abnormal for any sample, we excluded one randomly selected sample of each pair, and a group of 4 samples that were involved in 6 different kin pairs with average genetic relatedness values of 0.23. After filtering, 339 individuals were included in the SNP array derived genotype table. Both PCA and ADMIXTURE analysis performed using this dataset showed differentiation between Mediterranean and Gulf of Mexico individuals, while adult individuals from

the West Atlantic cover the whole range from pure Gulf of Mexico like to pure Mediterranean like (Figure 4). These results confirm the patterns observed with the RAD-seq dataset including the identification of Gulf of Mexico individuals with Mediterranean genetic background.

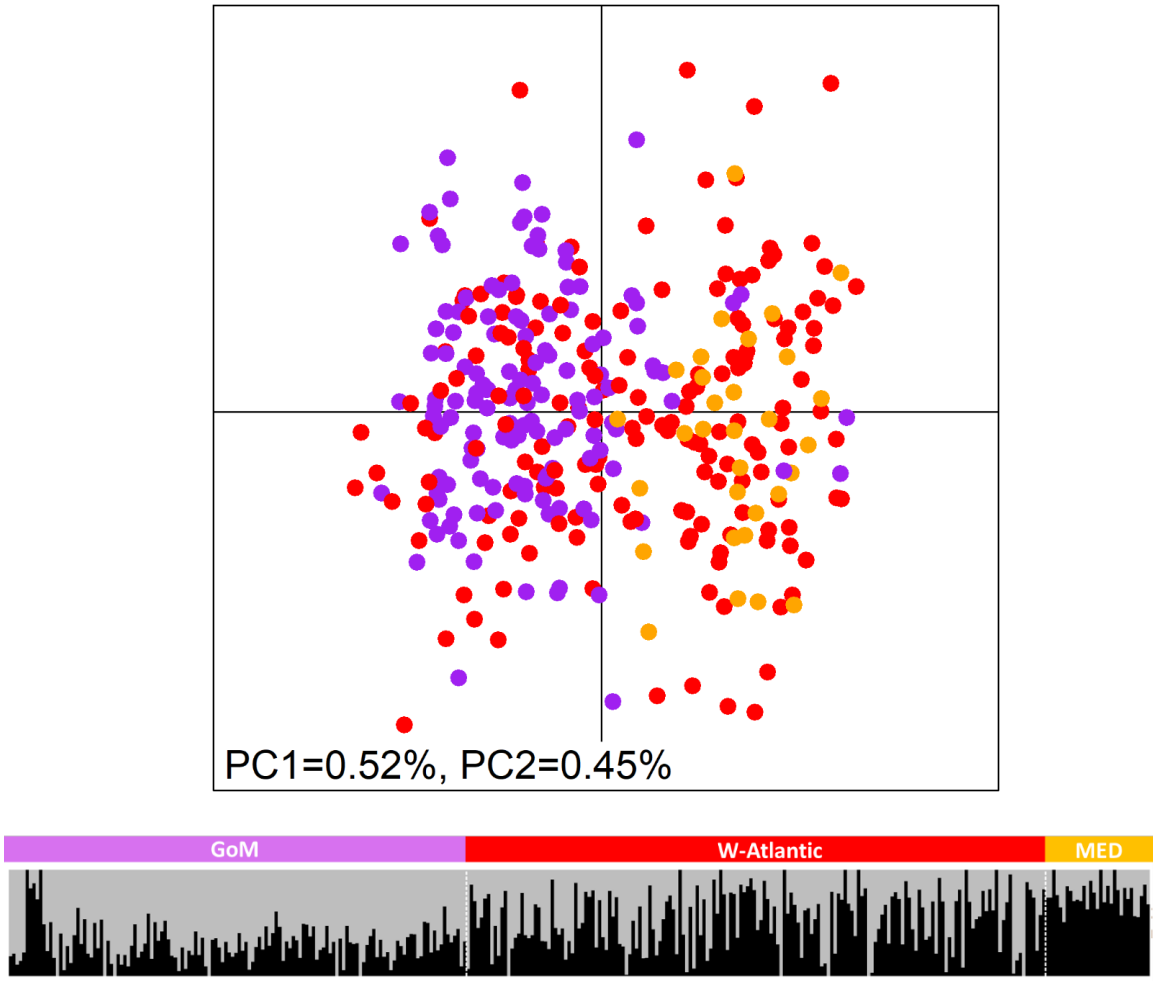

Figure 4. *PCA (top) and ADMIXTURE analysis (below) performed based on the SNP array derived genotypes for the neutral markers, where each dot and bar represent one individual respectively. Colors indicate sample origin and type, which include larvae individuals captured in the Gulf of Mexico (purple), adult individuals captured in the West Atlantic (red) and individuals of different age classes captured in the Mediterranean Sea (orange). Black and grey bars represent individuals' proportions of ancestral genetic components when assuming two ancestral populations.*

3.3.4. Potentially adaptive and mitochondrial markers

PCA based on outlier markers displayed samples into three different clusters, as observed using RAD-sequencing data (Figure 5).

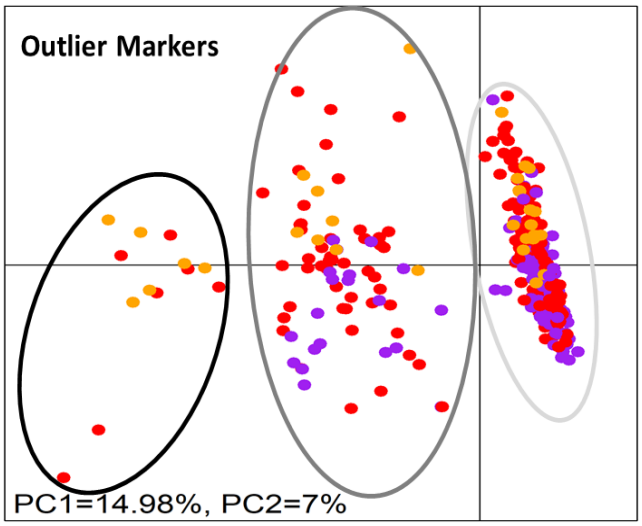

Figure 5. *PCA based on the SNP array derived genotypes for the outlier markers, where each dot represents one individual. Colors indicate Gulf of Mexico (purple), West Atlantic (red) and Mediterranean Sea (orange) origin.*

The two successfully genotyped markers for mitochondrial introgression were, as expected, homozygous for all individuals providing with only two possible haplotypes that were consistent with previous genotypes obtained for the 25 RAD-sequenced individuals. Excluding these individuals, 326 and 13 individuals showed the Atlantic bluefin tuna and the alalunga like mitochondrial haplotypes respectively. The individuals presenting the later were adults from the West Atlantic (10) and long fin individuals (3), but none larvae from the Gulf of Mexico neither short fin individuals showed the introgressed mitochondrial haplotype, confirming previous observations based on RAD-sequencing data.

Concerning short vs long second dorsal fin individuals, one of them had the potential inversion, however, it is difficult to conclude anything being only 8 the individuals analyzed. Concerning potentially Slope Sea spawners, about 30% had the inversion, and only about 4% had it homozygous. Although the inversion could still play a role in the understanding of the Atlantic Bluefin tuna connectivity, more analyses are needed.

3.3.5. Baseline improvement

Incorporation of additional larvae from the Gulf of Mexico to the baseline does not clearly improve correct assignment rates to origin. The percentage of both correctly and incorrectly assigned individuals from the Gulf of Mexico decreased when using the enlarged and filtered baselines, while the percentage of unassigned individuals increased. Besides, the enlarged baseline performed worst in assigning Mediterranean individuals, providing with lowest correct assignments and highest wrong and unassigned sample percentages. On the other hand, the filtered baseline provided with highest and

lowest correct and unassigned percentages respectively for Mediterranean samples and provided with the least correctly and incorrectly assigned individuals from the Gulf of Mexico, in return for higher percentages of unassigned individuals. Excluding the Gulf of Mexico adults from the baseline excludes the Mediterranean-like individuals from the Gulf of Mexico baseline, narrowing and purifying the representation of corresponding genetic profiles. However, the slightly heterogeneous genetic profile of the Gulf of Mexico individuals could contribute to steep increase of unassigned individuals from the Gulf of Mexico. Indeed, the percentages of incorrectly assigned individuals is always higher among samples captured in the Gulf of Mexico than in the Mediterranean (Table 8).

n

ORIGINAL

	CORRECT	WRONG	UNASS
GOM	121	16	12
MED	126	5	25

ENLARGED

	CORRECT	WRONG	UNASS
GOM	193	20	29
MED	121	7	28

FILTERED

	CORRECT	WRONG	UNASS
GOM	67	5	21
MED	130	6	20

%

ORIGINAL

	CORRECT	WRONG	UNASS
GOM	81.2	10.7	8.1
MED	80.8	3.2	16.0

ENLARGED

	CORRECT	WRONG	UNASS
GOM	79.8	8.3	12.0
MED	77.6	4.5	17.9

FILTERED

	CORRECT	WRONG	UNASS
GOM	72.04	5.38	22.58
MED	83.33	3.85	12.82

Table 8. *Numbers (left) and percentages (right) of correct (assignment match catch location), wrong (assignment does not match catch location) and unass (assignment scores below 80%) assigned individuals using the three different baselines analyzed: the original baseline, the enlarged baseline which includes newly genotyped larvae from the Gulf of Mexico, and the filtered baseline, which was generated by removing adult individuals from the Gulf of Mexico to the enlarged baseline.*

3.3.6. Feeding aggregate origin assignments

Assignment of feeding aggregates based on the original, enlarged, and filtered baselines result in virtually identical results (Figure 6), as expected considering the few differences in assignment rates using samples of known origin (see above).

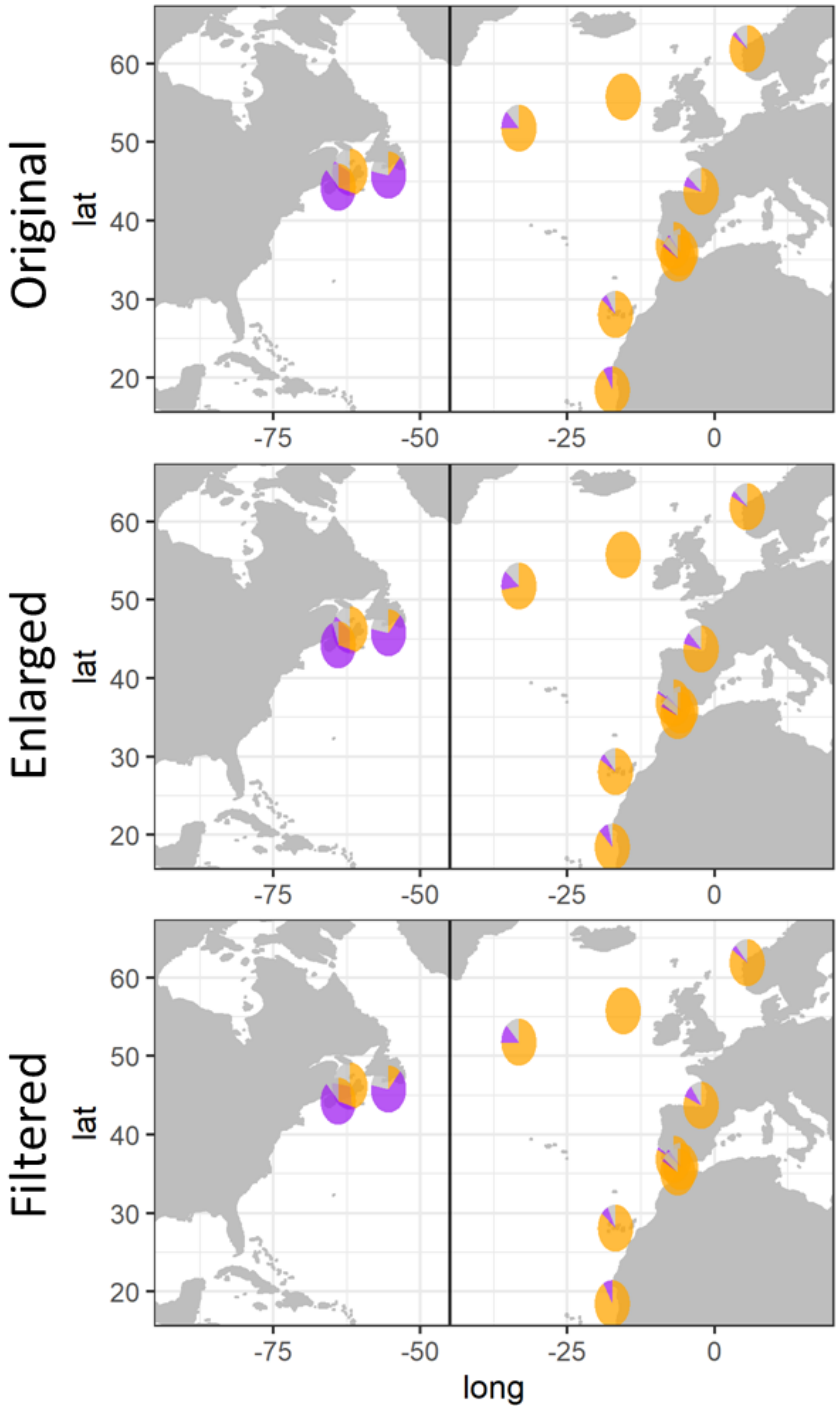

Figure 6. *Proportion of samples assigned to Mediterranean (orange) or Gulf of Mexico (purple origin and unassigned (grey) from different locations using the three different baselines analyzed.*

3.4. Conclusions

Array development:

- A genotyping array consisting of 7,930 markers has been successfully developed. This array includes neutral and outlier SNP markers for population structure analyses as well as markers for traceability (derived from the 96 SNP panel), markers for mitochondrial introgression and markers for sex determination.
- The results obtained with the array are consistent with those obtained with the RAD-seq data, confirming the suitability of this tool as a cost-effective approach for bluefin tuna population studies. Compared to RAD-sequencing, the array does not require reprocessing the whole dataset when adding new samples, involves easier bioinformatic data analyses and costs about three times less per sample.
- Additionally, this array has been proven useful to detect kins, making it suitable for applications such as Close-kin Mark Recapture

Population structure:

- The array-based analyses confirm that the Mediterranean individuals have all Mediterranean genetic background, that the Gulf of Mexico individuals include mostly Gulf of Mexico genetic background individuals but also Mediterranean and mixed background individuals, and that the Western Atlantic individuals corresponding to potential Slope Sea spawners have mixed background.
- The array-based analyses also detect a potential chromosomal inversion that separates samples in three groups, two being homozygous for the inversion and one heterozygous.
- Altogether these results confirm previous findings on the population structure of Atlantic bluefin tuna, suggesting that the observed "unexpected" findings were not due to artifacts of the used methodology.

Origin assignment:

- Our results show that improving the baseline by adding more Gulf of Mexico larvae and/or removing Mediterranean origin Gulf of Mexico adult do not result in significant changes in origin assignment rate. This suggests that the number of "incorrectly" assigned or unassigned individuals is most likely due to these individuals having a different genetic and catch origin or to having a mixed genetic background.
- Assignment of feeding aggregates using the alternative baselines result in similar pictures about the origin distribution in the different areas, with most eastern samples being of Mediterranean origin and most Western samples of Gulf of Mexico origin.

3.5. References

Alexander, DH, J Novembre, K Lange. 2009. Fast model-based estimation of ancestry in unrelated individuals. Genome research 19:1655-1664.

Jombart, T. 2008. adegenet: a R package for the multivariate analysis of genetic markers. Bioinformatics 24:1403-1405.

Lischer, HEL, L Excoffier. 2011. PGDSpider: an automated data conversion tool for connecting population genetics and genomics programs. Bioinformatics 28:298-299.

Purcell, S, B Neale, K Todd-Brown, et al. 2007. PLINK: A Tool Set for Whole-Genome Association and Population-Based Linkage Analyses. The American Journal of Human Genetics 81:559-575.

Suda, A, I Nishiki, Y Iwasaki, A Matsuura, T Akita, N Suzuki, A Fujiwara. 2019. Improvement of the Pacific bluefin tuna (Thunnus orientalis) reference genome and development of male-specific DNA markers. Scientific Reports 9:14450.

Yang, J, SH Lee, ME Goddard, PM Visscher. 2011. GCTA: A Tool for Genome-wide Complex Trait Analysis. The American Journal of Human Genetics 88:76-82.

4. OTOLITH MICROCHEMISTRY

Task Leader: Igaratza Fraile (AZTI), Deirdre Brophy (GMIT) & Jay Rooker (TAMU)

Participants:

AZTI: Nicolas Goñi, Iraide Artetxe, Patricia Lastra

IPREM: Christophe Pecheyran, Fanny Claverie

GMIT: Elizabeth Tray, Louise Vaughan

NordSIM: Martin Whitehouse, Heejin Jeon, Kerstin Linden

NOAA: Beverly Barnett, Robert Allman, John Walter, Ashley Pacicco

4.1. Determining nursery origin of bluefin tuna captured in the potential mixing zones

4.1.1. Introduction

The results from previous phases suggested that western origin contributions were negligible in the Mediterranean Sea, Bay of Biscay and Strait of Gibraltar, but mixing rates could be considerable, in some years, in the central North Atlantic, Canary Islands and western coast of Morocco. To further assess the spatial and temporal variability of mixing proportions, 103 otoliths captured in the eastern North Atlantic by fisheries in the Canary Islands (49 and 54 captured in 2018 and 2019 respectively) and 79 otoliths from the central North Atlantic (both east and west of 45ºW boundary) were analyzed for stable carbon and oxygen isotopes ($\delta^{13}C$ and $\delta^{18}O$). Additionally, 20 otoliths of bluefin tuna captured by Norwegian fisheries were also analyzed for first time using the same methodology.

4.1.2. Material and Methods

In this section, we investigate the origin of bluefin tuna collected in the eastern North Atlantic (Canary Islands) and Norwegian Sea, using stable $\delta^{13}C$ and $\delta^{18}O$ isotopes in otoliths. Samples utilized for this study were collected in the preceding years under the GBYP program. In the case of the Eastern North Atlantic, samples utilized for this study (N=100) were collected between March 2015 and April 2019 by Spanish baitboat fisheries operating around the Canary Islands. Samples from the central North Atlantic were captured by the Japanese longliners operating in the central North Atlantic Ocean in 2017. Otoliths from Norwegian Sea (N=20) were collected in 2019 by Norwegian purse

seiners targeting bluefin tuna. Some of these bluefin tuna were also captured as bycatch in blue whiting fisheries. (Fig. 7).

Otolith handling followed the protocols previously described in Rooker et al. (2008). Briefly, following extraction by GBYP participants, sagittal otoliths of bluefin tuna were cleaned of excess tissue with nitric acid (1%) and deionized water. One sagittal otolith from each bluefin tuna specimen was embedded in Struers epoxy resin (EpoFix) and sectioned using a low speed ISOMET saw to obtain 1.5 mm transverse sections that included the core. Following attachment to a sample plate, the portion of the otolith core corresponding to approximately the yearling periods of bluefin tuna was milled from the otolith section using a New Wave Research MicroMill system. A two-vector drill path based upon otolith measurements of several yearling bluefin tuna was created and used as the standard template to isolate core material following Rooker et al. (2008a). The pre-programmed drill path was made using a 500 µm diameter drill bit and 15 passes each at a depth of 50 µm was used to obtain core material from the otolith. Powdered core material was transferred to plastic vials and later analyzed for $\delta^{13}C$ and $\delta^{18}O$ on an automated carbonate preparation device (KIEL-III) coupled to a gas-ratio mass spectrometer (Finnigan MAT 252). Stable $\delta^{13}C$ and $\delta^{18}O$ isotopes are reported relative to the PeeDee belemnite (PDB) scale after comparison to an in-house laboratory standard calibrated to PDB.

Region-specific estimates of nursery origin of bluefin tuna were based on comparing stable isotope signals of otolith 'cores' (otolith material deposited during the first year of life or yearling period) of adult bluefin tuna with reference samples from Mediterranean and Gulf of Mexico nurseries revised in GBYP-Phase 3 and presented in Rooker et al. (2014). HISEA software (Millar 1990) was used to generate direct maximum likelihood estimates of mixed-stock proportions in each of the mixing zones. HISEA computes the likelihood of fish coming from each nursery area with a characterized isotopic signature. Maximum likelihood estimator is defined as the composition that maximizes the likelihood of the entire mixed fishery sample (Millar 1990). Uncertainty in estimation is addressed by re-sampling the baseline data 500 times with replacement and bootstrapping the mix data (n=1000). Mixed-stock proportions in Canary Islands were estimated for each of the sampled years and for all years combined.

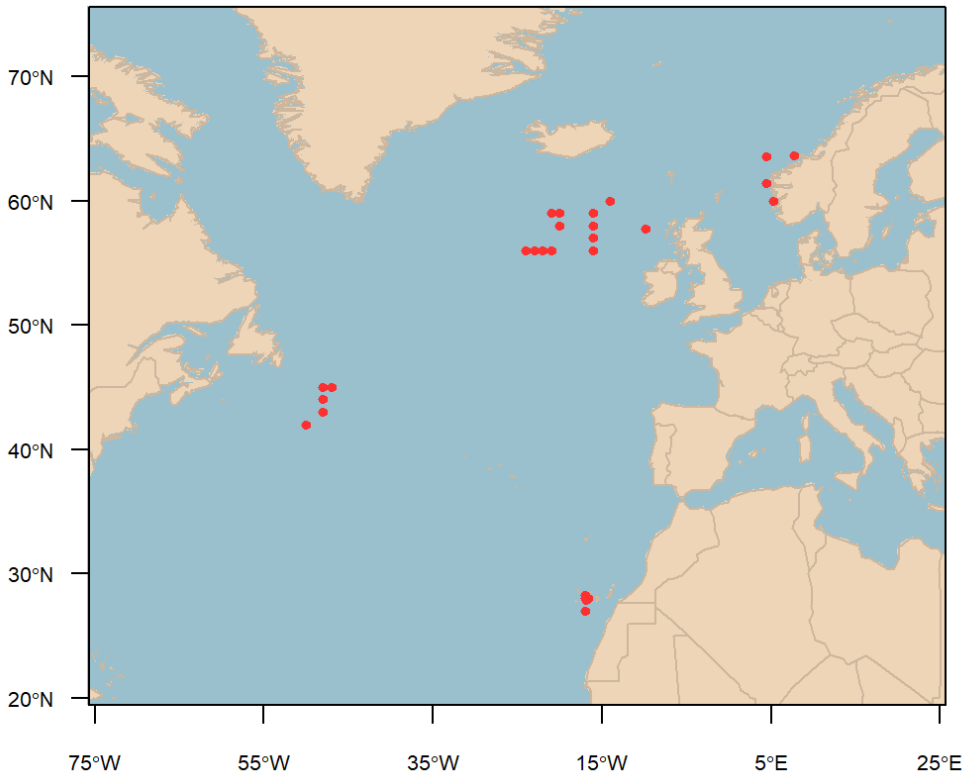

***Figure 7**: Sample distribution. Otoliths were collected by Norwegian purse-seiners in 2019 and baitboat fisheries from Canary Islands in 2015, 2018 and 2019.*

4.1.3. Results and Discussion

Management of Atlantic bluefin tuna has traditionally been based on separate stock assessments east and west of the 45°W stock boundary, assuming that the effects of mixing are negligible. It is crucial for stock evaluation to characterize stock composition and the degree to which each area is influenced by the mixing of the two stocks, since it has large implications for the sustainable management of the species.

$\delta^{13}C$ and $\delta^{18}O$ were measured in the otolith cores of bluefin tuna from the central North Atlantic (east and west of the 45ºW boundary), Canary Islands and Norwegian Sea, and compared to baseline populations from the Mediterranean and Gulf of Mexico (Fig. 8).

Otolith $\delta^{18}O$ and $\delta^{13}C$ values of adult bluefin tuna generally corresponded well with those measured in yearling otoliths from the eastern and western nurseries. However, some $\delta^{13}C$ values measured in otoliths from tuna captured in 2018 and 2019 near the Canary Islands were slightly enriched compared to baseline samples. The enrichment of $\delta^{13}C$ has been previously reported in previous phases of the project, and we think the reason for such enrichment may be attributed to several factors. On the one hand, it must be noted that the carbon forming the otolith aragonite is derived

from a mixture of carbon from dissolved inorganic carbon in the surrounding seawater and carbon from the diet, released through respiration. Thus, fluctuations in fish metabolic rate may influence otolith $\delta^{13}C$ values (Chung et al. 2019). On the other hand, a temporal enrichment of $\delta^{13}C$ has been previously reported in bluefin tuna otoliths (Schloesser et al. 2009, Fraile et al. 2016) and was attributed to the increase in atmospheric CO_2 derived from the combustion of fossil fuels and deforestation. Finally, it must be considered that $\delta^{13}C$ values could be altered in storage, especially after being milled, either through sorption of atmospheric CO_2 on crystal surfaces or through diffusive exchange. Due to the availability of the mass spectrometer the time spent between the milling and the isotopic analyses varies from year to year, and this may cause slight variations in $\delta^{13}C$ values. More likely, the shift in otolith $\delta^{13}C$ observed in our dataset between the mixed sample and the reference values occurred due to a combination of these factors. In any case, the primary marker for eastern and western stock discrimination is $\delta^{18}O$, and the bias introduced by variations in $\delta^{13}C$ are insignificant.

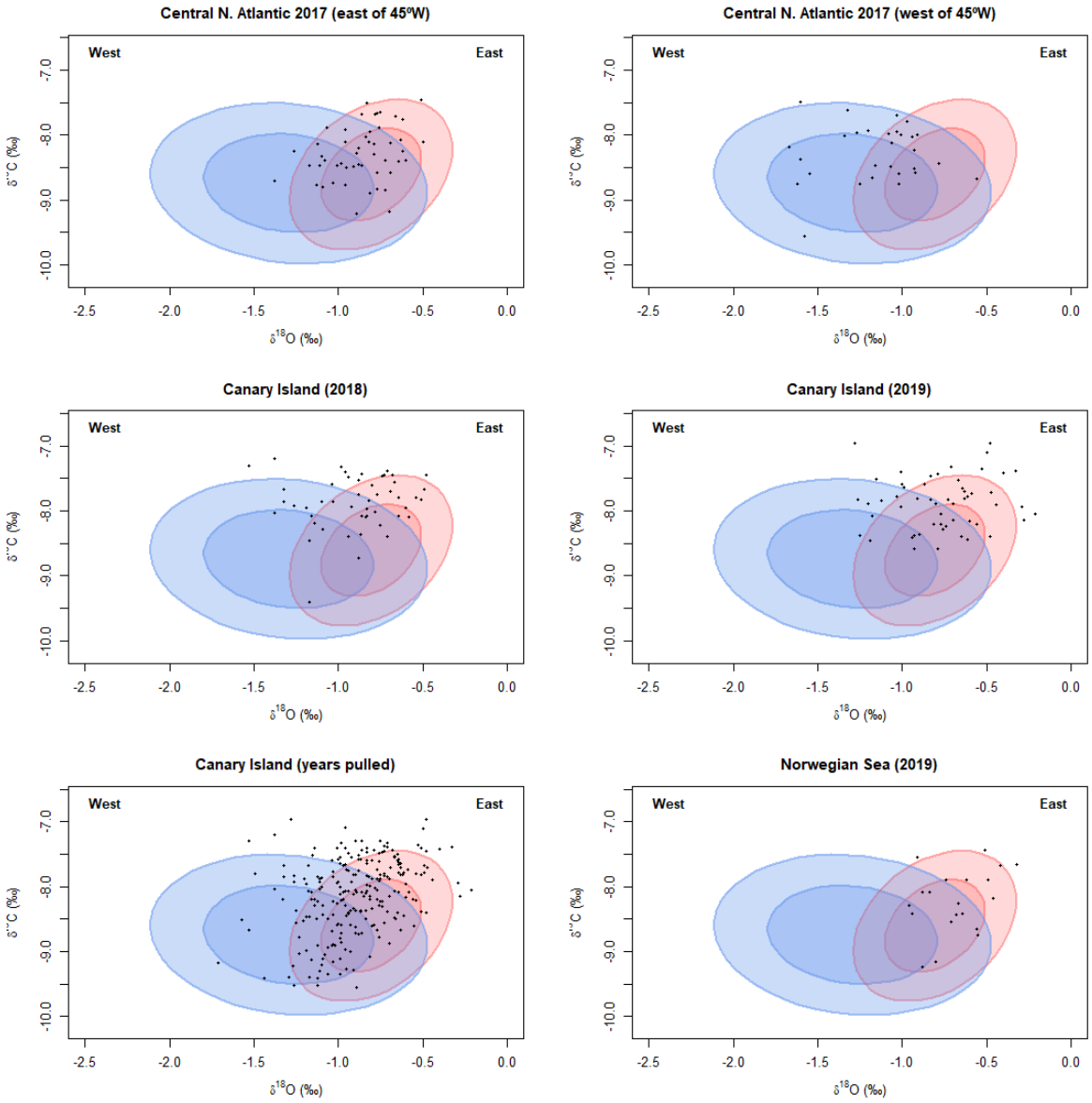

Figure 8: *Confidence ellipses (1 and 2 SD or ca. 68% and 95% of sample) for otolith $\delta^{13}C$ and $\delta^{18}O$ values of yearling bluefin tuna from the east (red) and west (blue) nurseries along with the isotopic values (black) for otolith cores of bluefin tuna captured by Japanese longliners operating in the central North Atlantic in 2017 (east and west of the 45ºW boundary; N=79), Spanish baitboat fishery around the Canary Islands in 2018 (N=49) and 2019 (N=54), and by Norwegian purse-seiners in 2019 east (N=20).*

Otolith samples from the central North Atlantic collected by Japanese longliners are from two distinct regions: a northern geographic region situated east of the 45ºW boundary and between 55ºN and 60ºN, and a second geographic area at lower latitudes (40-45ºN) in the western North Atlantic (Fig.7). Mixing proportions in these two areas differ considerably and are analyzed separately. In the northern area, mixed-stock analyses using the MLE procedure indicated that catches are comprised exclusively of the Mediterranean population. West of 45ºW, mixing of the eastern and western population occurs,

and our results indicate that about 74% of the catches in 2017 derived from the western population (Table 9 and Fig. 8).

The results from the current phase confirmed previously observed patterns: East of 45ºW boundary, catches have been largely dominated by the Mediterranean population, except for 2013, when a high fraction of western migrants was found. Overall, our results suggest that Mediterranean bluefin tuna may be the principal contributors to the Japanese fishery operating east of the 45ºW boundary and north of 50ºN. In the western North Atlantic, strong mixing of eastern and western individuals occurs, but mixing rates vary considerably among years. For example, in 2012, catches were almost exclusively from the western population, whereas in 2014 Mediterranean population was clearly dominant. Overall, our results indicate that a considerable fraction of bluefin tuna is originated from Mediterranean Sea, and that interannual variability of trans-Atlantic migrations may be important in the western North Atlantic.

Around the Canary Islands, mixed-stock analyses indicated that in 2018 and 2019, catches were almost exclusively comprised of the Mediterranean population (97% and 100% respectively). Mixing rate estimates around the Canary Islands using this methodology varied in preceding years. Catches in 2013 and 2019 were found to be exclusively composed of the Mediterranean population, but in 2013, 2015 and 2016 a substantial contribution of western migrants was found in this area (Fig. 9). The fishery around Canary Islands may be sustained partly by the western migrants. After all, catches have been largely dominated by the Mediterranean population and we conclude that Mediterranean bluefin tuna may be the principal contributors to the Spanish fishery operating in the Canary Islands.

In the Norwegian Sea (N=20) we found no evidence of population mixing, as 100% of the catches were estimated to be from the Mediterranean population.

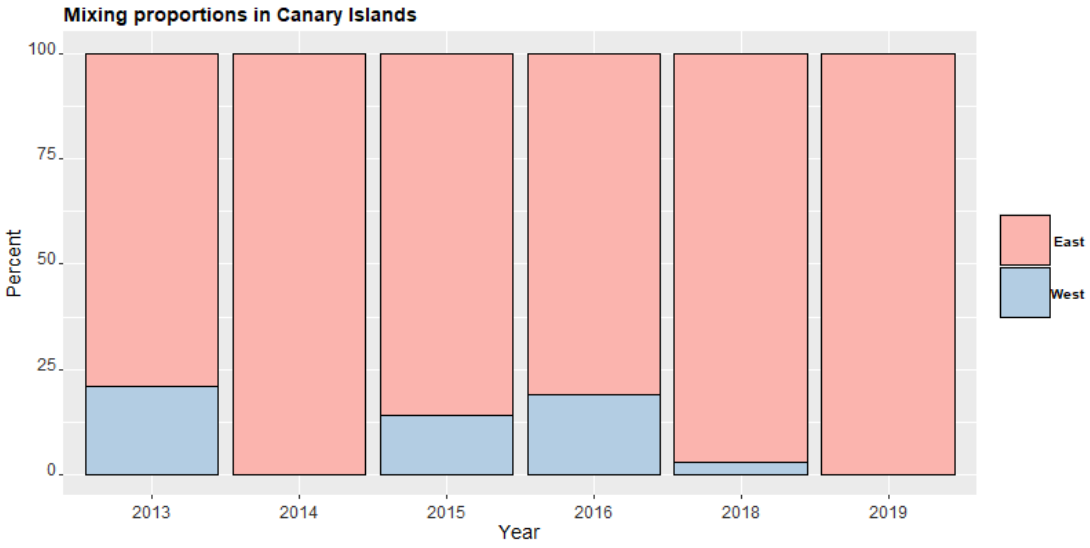

***Figure 9**: Interannual variation of the mixing proportions in the Canary Islands estimated by Maximum Likelihood Estimator (HISEA program). Data from 2018 and 2019 were analyzed during the current phase.*

***Table 9**: Maximum-likelihood estimates of the origin of bluefin tuna from the eastern North Atlantic (Canary Islands and Norwegian Sea) analyzed under the current contract. Estimates are given as percentages. The mixed-stock analysis (HISEA program) was run under bootstrap mode with 1000 runs to obtain standard deviations around estimated percentages (± %).*

Area	Year	West	East	SD	N
Canary Islands	**2018**	3.2%	96.8%	3.1	49
	2019	0%	100%	0.0	54
	Pulled (2013-2019)	3.8%	96.2%	2.8	229
Central North Atlantic (east of 45°W)	**2017**	0.2%	99.8%	0.8	50
Central North Atlantic (west of 45°W)	**2017**	73.6%	26.4%	17.5	29
Norwegian Sea	**2019**	0%	100%	0.0	20

4.2. Individual origin assignment

4.2.1. Introduction

Samples analyzed in Task 1 were also assigned to origin individually, with associated levels of probability. The identification of individual origin is needed for at least two main reasons: the construction of stock-age-length-keys, and the comparison/improvement of individual assignments based on different types of markers (i.e. genetic, otolith shape and stable isotopes). Moreover, it allows for tabulation of the results according to any stratification that might be used during the stock assessment or MSE process.

4.2.2. Material and Methods

During the current project, 79 individual bluefin from the central North Atlantic (east of 45ºW, N=50; west of 45ºW, N=29), 103 from the Canary Islands and 20 from the Norwegian Sea were assigned to their natal origin (Gulf of Mexico or Mediterranean Sea).

$\delta^{13}C$ and $\delta^{18}O$ values of bluefin tuna otoliths were statistically analyzed and individuals were assigned to source populations with associated levels of probability. Among the classification methods tested with the baseline dataset, it has been shown that Quadratic Discriminant Function Analysis (QDFA) performs the best attaining the highest classification accuracy (Fraile et al. 2015). Thus, QDFA was used to provide posterior probabilities for each pair of $\delta^{13}C$ and $\delta^{18}O$ values. During GBYP Phase-8 it was shown that higher classificatory power was attained by using the adult baseline, composed of spawning adults from the Mediterranean and Gulf of Mexico rather than the classical yearling baseline. Individual probabilities using the adult and yearling baselines (presented in GBYP Phase-8 and Phase-3 respectively) were estimated.

4.2.3. Results and Discussion

Individual origin assignments based on QDFA suggest that population mixing occurs in all studied regions at variable rates (Table 10). Individual origin assignment was performed using the yearling baseline revised in GBYP-Phase 3 and the adult baseline samples of spawner groups presented in GBYP-Phase 8. Overall, individual assignments by QDFA (using either yearling or adult baseline) yield higher mixing proportions than MLE method in the central North Atlantic and Canary Islands. The source of bluefin tuna captured in the Norwegian Sea predicted by QDFA was 100% Mediterranean, the same as predicted by MLE. Considering the confidence intervals around the estimated averages (i.e. mean±2*s.d), the results are generally concordant.,

Full posterior probabilities of the bluefin tuna otoliths analyzed in the current phase have been included in the appendix of the current report.

Table 10: Proportions of eastern and western contributions in the central North Atlantic (east and west of the 45ºW boundary), Canary Island and Norwegian Sea based on individual origin assignment approach. Results based on yearling and spawning adult reference samples were compared. Quadratic Discriminant Function Analysis was used to estimate individual origin.

	YEARLING BASELINE				ADULT BASELINE			
Central North Atlantic (west of 45ºW)								
Year	**West**	**East**			**West**	**East**		**N**
2017	55%	45%			52%	48%		29
Central North Atlantic (east of 45ºW)								
2017	18%	82%			18%	82%		50
Canary Islands								
2018	27%	73%			29%	71%		49
2019	20%	80%			16%	84%		55
Norwegian Sea								
2019	0%	100%			0%	100%		20

4.3. Life-history analyses: comparison of trace element vs $\delta^{18}O$ profiles (LA-ICPMS vs SIMS)

4.3.1. Introduction

During phase 9 otoliths of young-of-the-year and adult bluefin tuna captured in different regions were measured for $\delta^{18}O$ along the otolith growth axis at with very high spatial resolution using secondary ion mass spectrometry (SIMS). By combining otolith $\delta^{18}O$ with available maps of $\delta^{18}O$ in seawater and temperature, and using a fractionation equation, an attempt to reconstruct movements of bluefin tuna between different water masses was presented. However, variability in otolith $\delta^{18}O$ among individuals was found to be very high, even for fish that were exposed to the same conditions.

During Phase-10, we measured Sr and Ba concentration using the Laser Ablation Inductively Coupled-Mass Spectrometry (LA-ICPMS) in the same otolith spots as previously analyzed for $\delta^{18}O$. By combining and integrating trace elements and stable isotopic profiles the inferential power can be substantially increased. The results presented in this section will help to better understand biomineralization processes of tuna otoliths, and to better resolve environmental reconstructions and seasonal migrations patterns based on chemical proxies.

4.3.2. Material and Methods

A total of 20 otoliths that had been analyzed for $\delta^{18}O$ using SIMS during the previous GBYP phase were selected for LA-ICPMS and prepared for trace element analysis. This selection included YOY from the Atlantic Ocean (N=5), YOY from the Mediterranean Sea (N=5), free moving adults in the Mediterranean Sea (N=5) and adults captured in the Mediterranean and held in the Croatian farms for several years (N=5) (Fig.10) (Table 11). Otolith samples were analyzed with an IR 1030 nm femtosecond laser (Alfamet-Novalase, France) in conjunction with an Elan DRC II (Perkin Elmer) located at the Institut des Sciences Analytiques et de Physico-Chimie pour l'Environnement et les Matériaux (IPREM), Pau, France. Trace element analyses were performed adjacent to $\delta^{18}O$ measurements. Prior to analysis, samples were pre-ablated to remove any potential surface contamination. The laser was fired at a rate of 20 Hz and energy of 4.4 μJ per pulse. The ablation strategy consisted in 5 scanning discs of 20μm (with a 1μm step) at a scanner speed of 0.25mm/s. It resulted in a spot ablation of 20 μm. The mass spectrometer was used in the low-resolution mode (R = 300). Relative abundance of three isotopes, 86Sr and 138Ba and 44Ca, were measured by fs-LA-ICPMS. Ca was used as an internal standard for each ablation to correct for variation in ablation yield. The concentration of Ca in the otoliths was assumed to be constant at 383.000 $\mu g.g^{-1}$. Data reduction

including background subtraction, standardization to calcium and concentration calculation was conducted using an in-lab developed VBA excel program (FOCAL 2.39). External calibration was performed by ablating two glass reference materials (NIST 612 and NIST 610; National Institute of Standards and Technology, USA) and an aragonite reference material, FEBS-1 (National Research Council, Canada), was analyzed to check for the analytical accuracy and precision. All the reference materials were measured at the beginning, middle and the end of each session for calibration and drift correction. The background signal (i.e., the period during which only the carrier gas composition is measured) was used to calculate the limit of detection (LOD) which was calculated as the mean background level plus 3 times standard deviation. Concentrations below LOD were not included in the statistical analysis.

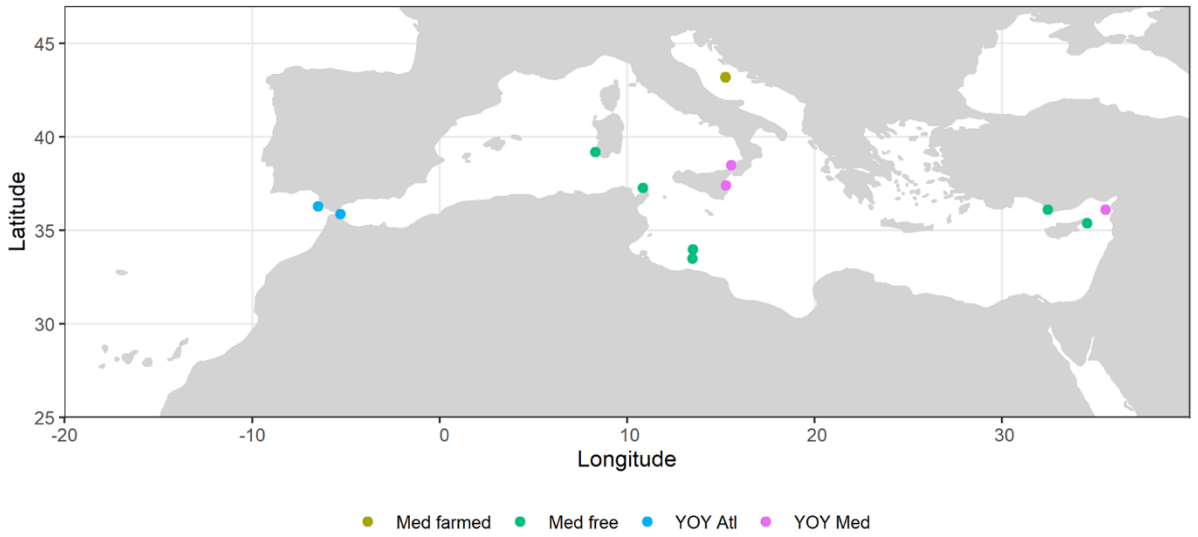

***Figure 10**: Sampling locations of bluefin tuna of disputed origin, farmed in the Croatian farms, free living in the Mediterranean Sea and young-of-the-year (YOY) from the Atlantic Ocean and Mediterranean Sea.*

***Table 11**: Summary of fish used for trace element analyses.*

Group	n	Length mean (±sd)	Length range	Capture year
Mediterranean farmed	5	152 (±3.9)	145.0-156.0	2013
Mediterranean free	5	168 (±20.3)	140.0-191.0	2015,2016
YOY Atlantic	5	30 (±2.7)	25.6-33.5	2015, 2017
YOY Mediterranean	5	36 (±11.2)	24.1-49.0	2017

Statistical analyses were performed in R software version 3.6.1. Sr:Ca, Ba:Ca and $\delta^{18}O$ measures were plotted along the same otolith trajectories of each individual. Normality of variables Sr:Ca, Ba:Ca and $\delta^{18}O$ was examined using Shapiro test. As variables ere not bivariate normal, Kendall´s rank tau (τ) coefficient was used for correlation measures. This non-parametric approach is less sensitive to outliers and more accurate with smaller sample sizes.

4.3.3. Results and Discussion

There was little similarity between trace element and $\delta^{18}O$ profiles within each fish (Figs. 11 to 14). No significant correlation between otolith Sr:Ca and $\delta^{18}O$ was detected in any of the individuals analyzed separately (Table 11), nor when data from all individuals was pooled ($\tau(343)=0.06$, $p=0.083$, Fig. 15). A few fish (n=5) showed significant correlation between otolith Ba:Ca and $\delta^{18}O$, but no consistent pattern was found in the direction of these associations (Table 12). Both positive and negative correlations were found, which may reflect the weak relationship observed ($\tau(343)=0.09$, $p=0.013$) when all individuals were pooled (Fig. 15). Significant positive correlation was detected between Sr:Ca and Ba:Ca ($\tau(343)=0.50$, $p<0.01$) (Fig. 11). Sr and Ba have similar atomic radii and identical charge (+2) to that of Ca, and therefore these elements are most often incorporated into the otolith directly by substituting Ca in the crystal lattice (Thomas et al. 2017, Hüssy et al. 2020). However when correlations of Sr:Ca and Ba:Ca were analyzed individually for each fish, most of the significant correlations were in young fish (Table 2). The relationship between the environment and the biogeochemical composition of the otolith becomes less predictable in older organisms if physiological processes become more complex (Grammer et al. 2017), for instance a decrease in environmental sensitivity in Sr has been suggested as fish grow (Macdonald et al. 2020).

Overall, the observed results prevent the construction of a predictive relationship between otolith trace element (Sr:Ca and Ba:Ca) and $\delta^{18}O$ profiles measured by LA-ICPMS and SIMS, respectively. This suggests that the uptake of Sr and Ba into the otoliths of bluefin tuna is controlled by different processes than $\delta^{18}O$ fractionation, which is known to be determined primarily by temperature and the isotopic composition of the water. Therefore, trace elements and oxygen stable isotopes can provide complementary information that may help to infer the lifetime movements of Atlantic bluefin tuna. When variations in $\delta^{18}O$ occur along individual otolith growth profiles, it is often difficult to disentangle whether observed differences are due to movements between different water masses, or if they represent changes in the environmental conditions at a given area. The combination of two independent profiles such as trace element and $\delta^{18}O$ data can help with this issue. It may be therefore worthy to combine SIMS alongside with LA-ICPMs transects in otoliths so that they can provide new insights into habitat use and migration of bluefin tuna, especially when combined with growth information, such as microstructural analyses of the otoliths.

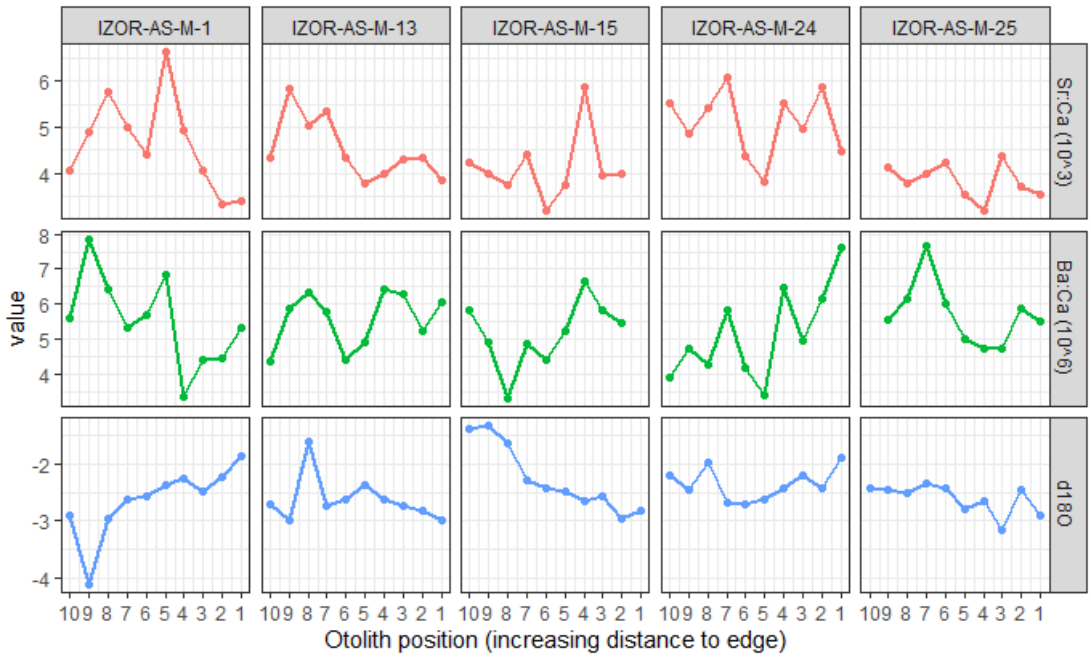

***Figure 11**: Observed Sr:Ca, Ba:Ca and $\delta^{18}O$ measurements from taken from the core towards the edge of otoliths from the Mediterranean farmed group.*

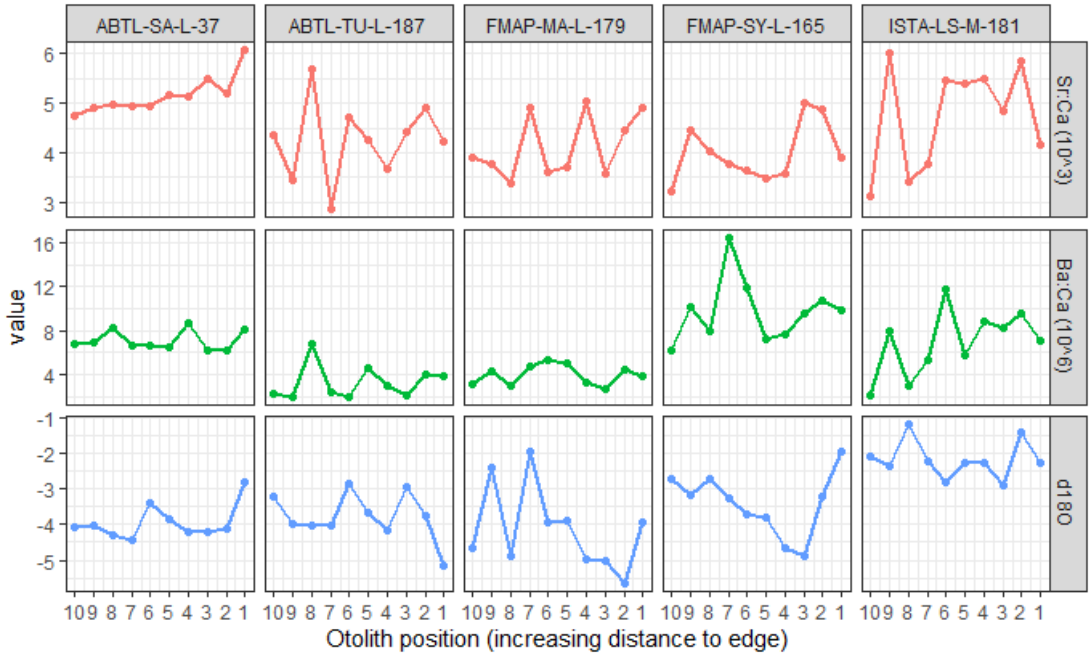

***Figure 12**: Observed Sr:Ca, Ba:Ca and $\delta^{18}O$ measurements from taken from the core towards the edge of otoliths from the Mediterranean free group.*

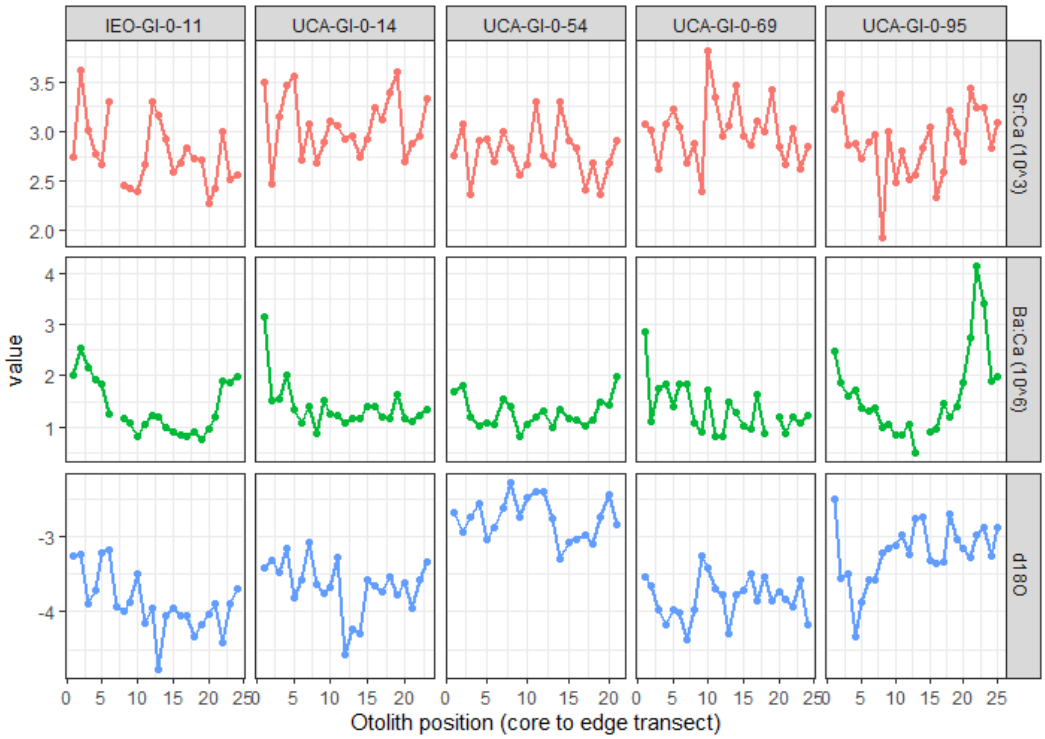

***Figure 13**: Observed Core to edge Sr:Ca, Ba:Ca and $\delta^{18}O$ profiles in otoliths of young of the year collected in the Atlantic Ocean.*

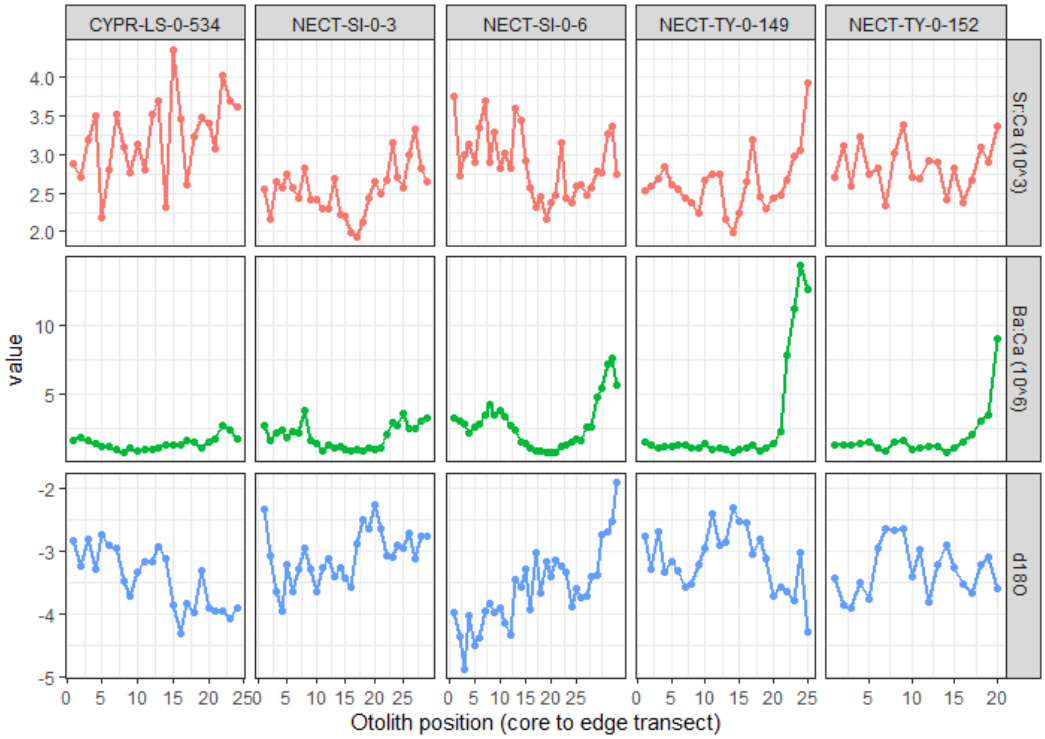

***Figure 14**: Observed Core to edge Sr:Ca, Ba:Ca and $\delta^{18}O$ profiles in otoliths of young of the year collected in the Mediterranean.*

***Table 12**: Kendall´s tau (τ) correlation coefficient between elements analyzed in each fish otolith. Significant correlations are highlighted with *and ** at p<0.05 and 0<0.01, respectively. Colour indicate the direction of the significant correlation, positive (blue) or negative (red).*

Group	Fish ID	N spot	Kendall`s τ correlation		
			Sr:Ca vs $\delta^{18}O$	Ba:Ca vs $\delta^{18}O$	Sr:Ca vs Ba:Ca
Mediterranean farmed	IZOR-AS-M-1	10	-0.16	-0.29	0.33
	IZOR-AS-M-13	10	-0.20	-0.02	0.22
	IZOR-AS-M-13	10	-0.11	-0.38	0.38
	IZOR-AS-M-24	10	0.04	0.22	0.24
	IZOR-AS-M-25	10	0.20	0.65*	0.28
Mediterranean Free	ABTL-SA-L-37	10	0.15	0.02	-0.2
	ABTL-TU-L-187	10	0.33	-0.33	0.24
	FMAP-SY-L-165	10	-0.02	-0.11	0.38
	ISTA-LS-M-181	10	-0.27	-0.40	0.64**
YOY Atlantic	IEO-GI-0-11	24	-0.09	0.32*	0.32*
	UCA-GI-0-14	23	0.13	0.33*	0.40**
	UCA-GI-0-54	21	-0.06	0.07	0.26
	UCA-GI-0-69	24	0.02	-0.35*	0.23
	UCA-GI-0-95	25	0.11	0.06	0.38**
YOY Mediterranean	CYPR-LS-0-534	24	-0.21	-0.22	0.05
	NECT-SI-0-3	29	0.09	0.07	0.51**
	NECT-SI-0-6	33	-0.17	-0.08	0.38**
	NECT-TY-0-149	25	-0.14	-0.52**	0.40**
	NECT-TY-0-152	20	-0.01	-0.15	0.36**

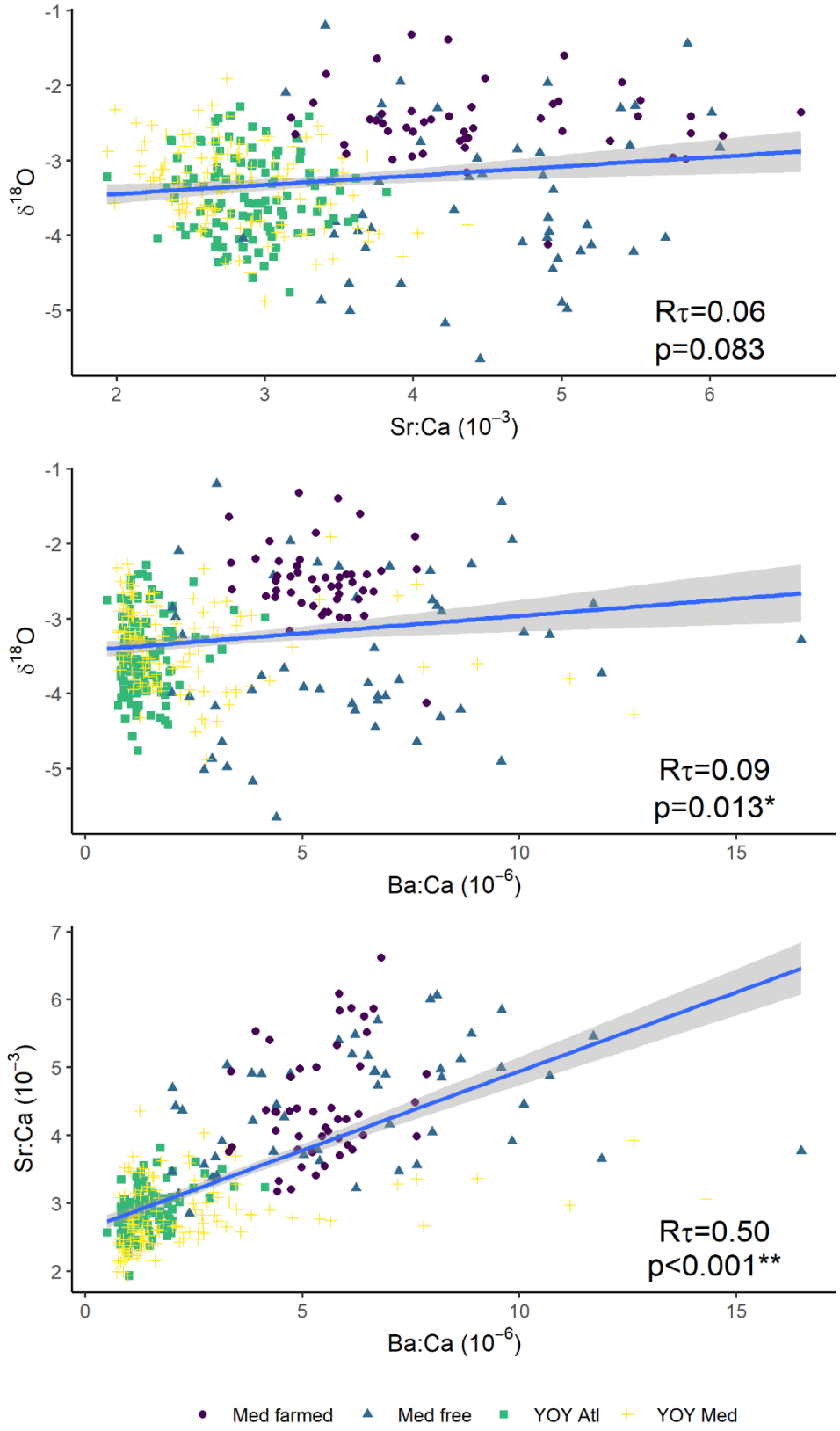

***Figure 15**: Scatter plots with Kendall´s tau correlation coefficient (τ) and p values for the associations between otolith Sr:Ca, Ba:Ca and $\delta^{18}O$ measurements. Linear interpolation (blue line) is also shown.*

4.4. Creation of a new baseline for Mediterranean vs. Gulf of Mexico origin tuna based on the young-of-the-year otolith signature

4.4.1. Introduction

Atlantic bluefin tuna is managed as two different stocks: the eastern and western Atlantic stocks spawning in the Mediterranean Sea and Gulf of Mexico respectively. In the Atlantic Ocean, mixing of the two populations occurs at variable rates. Within the GBYP program, year and region-specific mixing proportions have been quantified using otolith carbon and oxygen stable isotopes ($\delta^{13}C$ and $\delta^{18}O$). The reference samples for stock assignment are yearling (ca. 12 to18 mo. old) bluefin tuna captured in the eastern and western production zones (Mediterranean Sea and Gulf of Mexico), with the assumption being that no transatlantic movement occurs before this age (Rooker et al. 2014). Cross-validated classification accuracy of yearlings to eastern and western nurseries using the yearling reference otoliths was of 80%, indicating that approximately 20% of the fish will be incorrectly assigned using this baseline. Part of the inaccuracy is associated with the overlap of $\delta^{18}O$ signatures between the two populations. The overlap of $\delta^{18}O$ signatures may arise, at least partly, because measurements are made in otolith portions accreted from birth to approximately 18 months. These measurements integrate part of the time living within the nursery areas (Mediterranean or Gulf of Mexico), but may also combine with the time living in the open North Atlantic Ocean.

In this section, we aim to refine the existing baselines and increase the classificatory power of the methodology. For that, we selected otoliths of bluefin tuna from the spawning aggregations in the Mediterranean and Gulf of Mexico, and measured $\delta^{13}C$ and $\delta^{18}O$ composition on the portion of the otoliths corresponding to the YOY period (from birth to 6 mo.). Reducing the portion of the otolith targeted for analyses, we ensure that the isotopic signature represents the signature of the nursery area by minimizing the incorporation of material accreted while living in the open Atlantic Ocean.

4.4.2. Material and Methods

A total of 127 otoliths of bluefin tuna spawning in the Mediterranean Sea (N=107) and Gulf of Mexico (N=20) bluefin tuna were selected for the current task. Samples from the Mediterranean Sea included tuna captured in the Balearic Sea, Malta, Tunisia, Gulf of Syrta and Levantine Sea, and were collected under the GBYP program between 2015 and 2018 (Fig. 16). Otoliths from the Gulf of Mexico spawners were collected between 2010 and 2014 as part of NOAA sampling program (Table 13). Previous genetic analyses have found that a fraction of the spawning adults in the Gulf of Mexico are genetically of Mediterranean origin. Therefore, for the selection of Gulf of Mexico reference otoliths genetic results were revised and individuals genetically identified as “pure Gulf of Mexico”

were selected. In contrast, in the Mediterranean Sea, we found no sign of mixing of the two populations, and therefore no further genetic analyses were performed for the otolith selection.

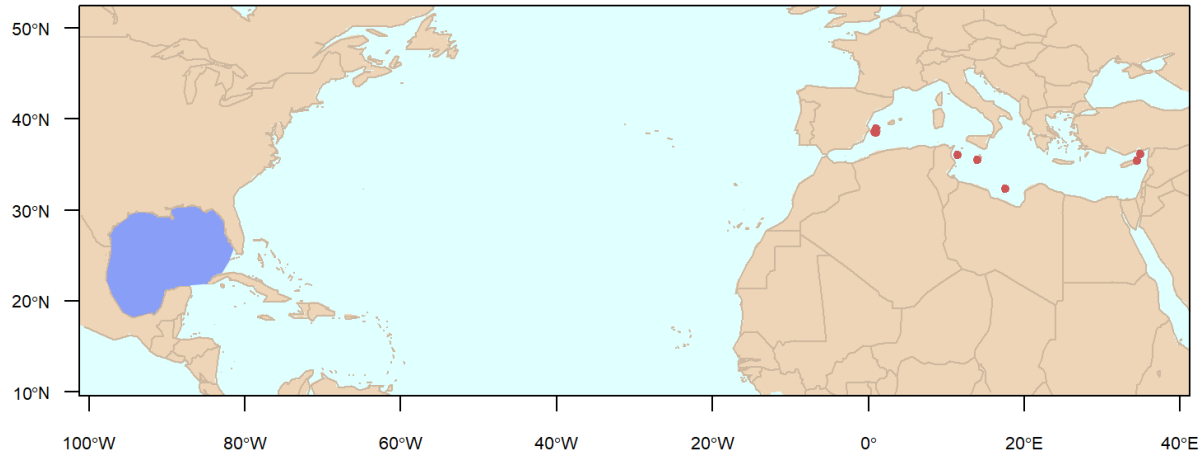

***Figure 16**: Bluefin tuna spawning aggregations sampled in the Mediterranean Sea (red dots) and Gulf of Mexico (blue area) nurseries*

Prior to analyses, samples were prepared following the established protocol. Sagittal otoliths of bluefin tuna were cleaned with deionized water and dried under laminar air flow. One sagittal otolith from each bluefin tuna specimen was embedded in two-part epoxy resin (Araldite 2020) and polished with silicon carbide sandpapers of a range of grit sizes under running water until the core was exposed (Fig. 17). Following attachment to a sample plate, the portion of the otolith core corresponding to approximately 3 months of life was milled using a New Wave Research MicroMill system (hereafter called "core"). A milling template was created using distance measurements on a reference otolith previously aged by daily increment counting. The pre-programmed drill path was made using a 300 µm diameter drill bit and 12 passes each at a depth of 55 µm was used to obtain core material from the otolith. Powdered core material was transferred to plastic vials and later analyzed for $\delta^{13}C$ and $\delta^{18}O$ on an automated carbonate preparation device (KIEL-III) coupled to a gas-ratio mass spectrometer (Finnigan MAT 252). Stable $\delta^{13}C$ and $\delta^{18}O$ isotopes are reported relative to the PeeDee belemnite (PDB) scale after comparison to an in-house laboratory standard calibrated to PDB.

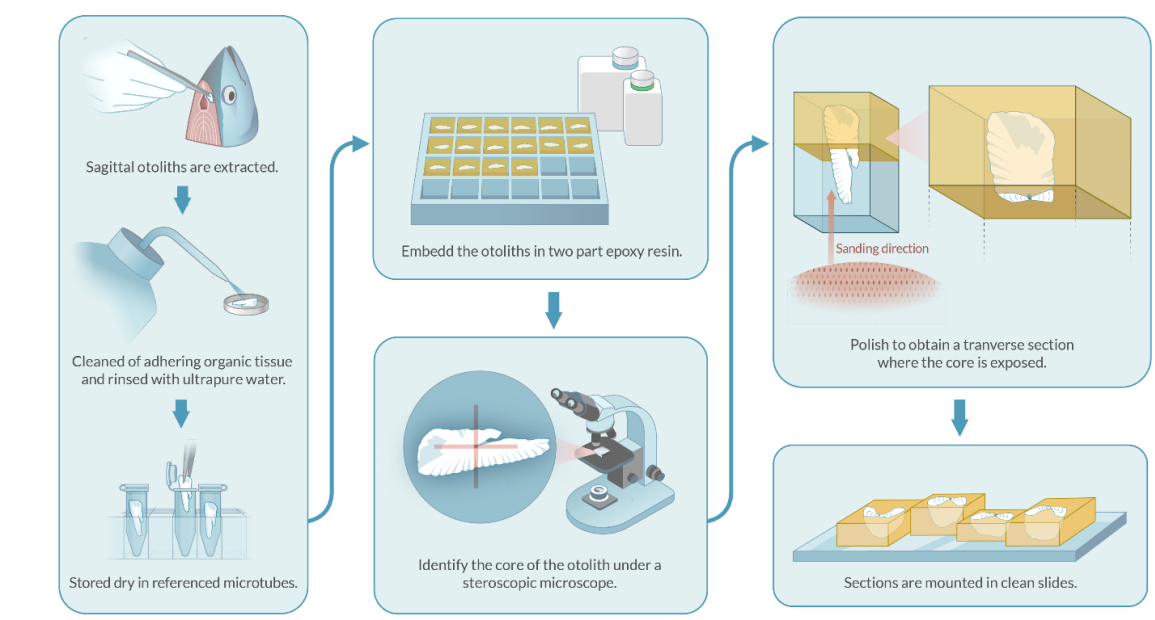

***Figure 17**: Sample preparation process from otolith extraction until the attachment to the glass slide (illustration from Artetxe-Arrate, 2021).*

Within-group normality was assessed with quantile-quantile plots and Shapiro-Wilk normality test, and homogeneity of variance between the two groups was evaluated by F-test. Multivariate analysis of variance (MANOVA) was used to test for differences in otolith $\delta^{13}C$ and $\delta^{18}O$ values of bluefin tuna from eastern and western nurseries, and significance was based on Pillai-Bartlett's statistic. Univariate tests were also performed individually for otolith $\delta^{13}C$ and $\delta^{18}O$ values using an analysis of variance (ANOVA). Quadratic Discriminant Function Analysis (QDFA) and Random Forest (RF) machine learning algorithms conducted on otolith $\delta^{18}O$ values were used to classify the reference samples to their known groups. A leave-one-out cross-validation method was performed to evaluate the classification ability of the baseline samples using different models. Statistical analyses were carried out using "MASS", "dplyr" and "RandomForest" packages available for R statistical software (R version 4.0.3).

Table 13: Otoliths of spawning adults from the Mediterranean Sea (Med) and Gulf of Mexico (Gom) used as reference samples to assess the classification accuracy of the YOY otolith portion.

Area	Capture Yearss	Nursery	N
Balear Sea	11-28 September 2011	Med	26
Malta	15 September – 7 November 2013	Med	25
Tunisia	23-24 October 2011	Med	19
Gulf of Syrta	10 September – 23 October 2013	Med	6
Levantine Sea	10-20 August 2011	Med	31

Gulf of Mexico	12 July 2012-28 August 2013	Gom	20

Prior to stable isotope analyses, a selection of otoliths from the Gulf of Mexico and Mediterranean Sea were analyzed with laser ablation inductively coupled mass spectrometry (LA-ICPMS) (available at the Institut des Sciences Analytiques et de Physico-Chimie pour l'Environnement et les Matériaux, Université de Pau et des Pays de l'Adour/CNRS, Pau, France) to create two dimensional maps of trace element concentration across the otolith sections. To correct for short-term instrumental drift, two standards (NIST-610 and NIST-612) were measured at the beginning and the end of each session. Measurement accuracy was determined based on an otolith certified reference material for trace elements (FEBS-1). Sr, Ba and Mg concentrations were converted to color images to visualize trace element patterns. Two-dimensional plots (2-D maps) of chemical variation throughout an otolith, adds important insights that can help to find differences between the eastern and western stocks.

4.4.1. Results and Discussion

From the total of 127 otoliths analyzed, five samples could not be analyzed precisely due to the small amount of otolith powder recovered, and were therefore, excluded. The remaining samples were successfully analyzed with a precision of 0.03‰ (SD) and ± 0.04‰ (SD) for $\delta^{13}C$ and $\delta^{18}O$ respectively. Both $\delta^{13}C$ and $\delta^{18}O$ values were normally distributed within groups. Otolith $\delta^{13}C$ and $\delta^{18}O$ values of spawning bluefin tuna captured in the Gulf of Mexico and Mediterranean Sea nurseries were distinct (MANOVA, $p < 0.001$, Fig. 18), but differences were only due to oxygen composition. Otolith $\delta^{13}C$ values in our baseline samples did not significantly differ between the two populations (ANOVA, $p > 0.05$). In contrast, the difference in otolith $\delta^{18}O$ values of spawning bluefin tuna from Gulf of Mexico and Mediterranean nurseries was more pronounced, with bluefin tuna captured in the Mediterranean Sea having higher values (mean ± SD = −0.74 ± 0.19‰) relative to those spawning in the Gulf of Mexico (−1.25 ± 0.18‰) (ANOVA, $p < 0.001$).

Cross-validated classification accuracy of adult spawners to Gulf of Mexico and Mediterranean nurseries based on QDFA parameterized with otolith $\delta^{13}C$ and $\delta^{18}O$ values was 76 and 97% respectively (overall 94%). Classification success from QDFA based on $\delta^{18}O$ alone was the same as the full model, indicating that carbon isotopes do not contribute to the differentiation of both stocks. Random Forest classifier was also tested using $\delta^{18}O$ as the only explanatory variable, and the results confirmed a high discriminatory power of this new baseline, although slightly lower than the classical QDFA (65% and 95% for eastern and western nurseries respectively, overall 91%). The capacity of this new baseline to discriminate eastern and western stock is similar to the adult baseline presented in Brophy et al. (2020) and GBYP Phase-8 (using yearling otolith portion), and higher than the yearling baseline presented in Rooker et al. (2014) (Fig. 18 and Table 14).

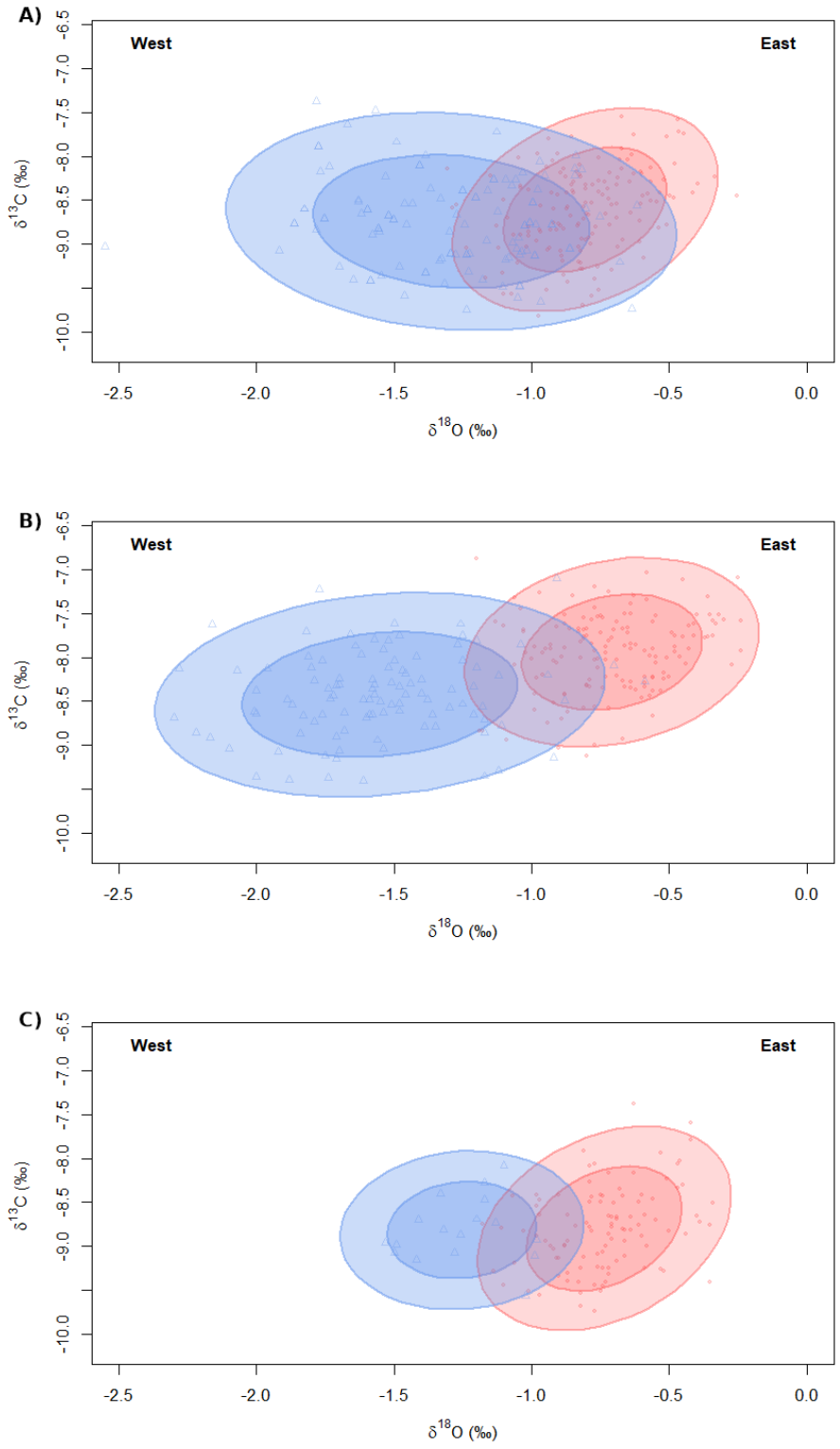

***Figure 18**: Stable $\delta^{13}C$ and $\delta^{18}O$ isotopes of bluefin tuna otoliths used as a reference for East and West stock discrimination (confidence intervals of 1σ and 2σ). A) Yearling (age-1) tuna from the Gulf of Mexico Mediterranean Sea (GBYP-Phase3 and Rooker et al. 2014); B) Yearling (Age-1) otolith portion of spawning adults from the Gulf of Mexico Mediterranean Sea (GBYP Phase8); C) Young-of-the-year (Age-0) otolith portion of spawning adults from the Gulf of Mexico Mediterranean Sea (GBYP current Phase10).*

***Table 14**: Classification accuracy of Quadratic Discriminant Function Analysis (QDFA) and Random Forest (RF) classificators using only $\delta^{18}O$ isotope measurements a) from the spawning adult baseline using YOY otolith portion (current GBYP-Phase10), b) from the yearling baseline samples (GBYP-Phase3 and Rooker et al. 2014), and c) from the spawning adult baseline using yearling otolith portion (GBYP-Phase8 and Brophy et al. 2020).*

	a) Adult baseline (YOY signature)		**b) Yearling baseline**		**c) Adult baseline (Yearling signature)**	
	Estimated origin		Estimated origin		Estimated origin	
Origin	Accuracy QDFA (%)	Accuracy RF (%)	Accuracy QDFA (%)	Accuracy RF (%)	Accuracy QDFA (%)	Accuracy RF (%)
Med	97.1	95.2	91.7	81.9	97.5	95
Gom	76.2	64.7	67	78.3	93.4	92.5
Total	**94.2**	**90.9**	**80.7**	**80.3**	**95.6**	**93.9**

Significant differences in $\delta^{18}O$ were found among the three main basin of the Mediterranean Sea (western, central, and eastern). However, the capacity of QDFA and RF classifiers to discriminate among the three areas was almost null Fig. 19). These results indicate that oxygen stable isotopes are an important tracer to differentiate bluefin tuna from the Gulf of Mexico and Mediterranean population, but by itself is insufficient for sub-stock structure investigations within the Mediterranean Sea.

In addition to the stable isotope analyses, 2-dimensional maps of Sr, Ba and Mg concentration were built with a selection of 6 otoliths from the Gulf of Mexico and Mediterranean Sea (Fig. 20 to 22). Full 2-D mapping of trace elements enables visualizing trace metal concentration along and across de otolith growth axis, providing an insight on otolith composition and spatial heterogeneity.

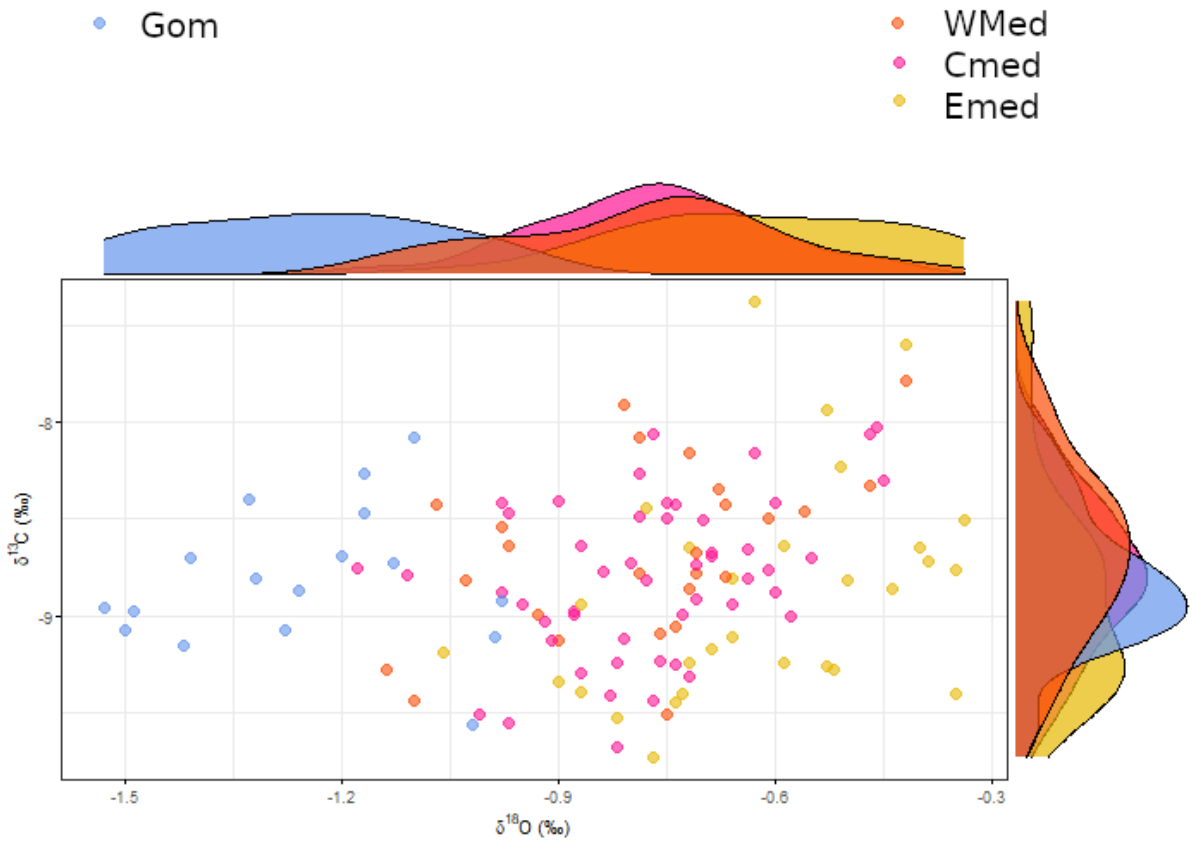

***Figure 19**: Scatter and density plots of $\delta^{13}C$ and $\delta^{18}O$ values in otoliths of adult bluefin tuna spawning in the Gulf of Mexico (Gom) and western, central and eastern Mediterranean Sea (WMed, CMed and EMed respectively).*

In all the six otoliths analyzed, Sr concentrations were lower during the early life stage (Fig. 20). However, the pattern of Sr variability differed between the Gom and Med samples. In otoliths collected in the Gulf of Mexico a gradual and diffuse increase in Sr concentration was visible during approximately the first year of life. After that, a cyclicity in Sr concentration could be appreciated related likely to migrations or seasonal variations of water mass properties. In contrast, Sr concentration in otoliths of bluefin tuna captured in the Mediterranean Sea was lowest during the first month of life, and an abrupt increase was observed in the three otoliths before the Age-1. Cyclicity of Sr concentration during the adolescent and adult stages was more pronounced than that observed in Gulf of Mexico samples.

Differences in intra-otolith Ba distribution between Gulf of Mexico and Mediterranean samples were similar to those found in Sr concentration: Otoliths from the Mediterranean tuna presented a clearly well-defined zone of low Ba concentration during the YOY period compared to a more diffuse zonation visible in otoliths from the Gulf of Mexico (Fig. 21).

In contrast to Sr and Ba, Mg concentrations were found to be higher at the early life stages (Fig. 22). In this case, the YOY period was not as clearly defined as Sr and Ba, and a gradual but pronounced decrease is observed during the first months. In case of Mg, the main difference found between the two stocks was the evidence of bands with high Mg concentration on the external margin of the otoliths from the Mediterranean Sea. This pattern was less clear in the Gulf of Mexico tuna otoliths.

If differences found in the subset of otoliths selected for 2-D mapping can be extended to the rest of the population, trace element maps may become a useful tool to reliably predict the origin of individual bluefin tuna to their corresponding nursery origin.

A similarity found in all samples was the presence of a marginal band with high Sr and Ba concentration, particularly well-defined on the distal side of the otolith, adjacent to the core. We suspect that this material was accreted during the adult stages, and thus, do not represent the signature of the nursery origin. The accretion of material around the core until the first inflexion point during the adult stages is a feature previously reported in the literature (Fraile et al. 2015, Shiao et al. 2009). Yet, when integrating the signature of a larger otolith portion, the effect of the material accreted during the adult stages, and thereby, its influence in the origin estimation is attenuated. However, this characteristic may have large implications in otolith chemistry applications, especially when using single and small spot sizes. Special care is needed in studies focusing on natal origin determination using LA-ICPMS, and a prior 2-dimensional mapping is highly recommended to differentiate parts of the otolith accreted on different life stages. Additionally, a gradient in Mg concentration perpendicular to the growth axis was visible in all otoliths analyzed, and although this is probably a feature not related to fish's life history, it must be considered when choosing the locations of spots or transects.

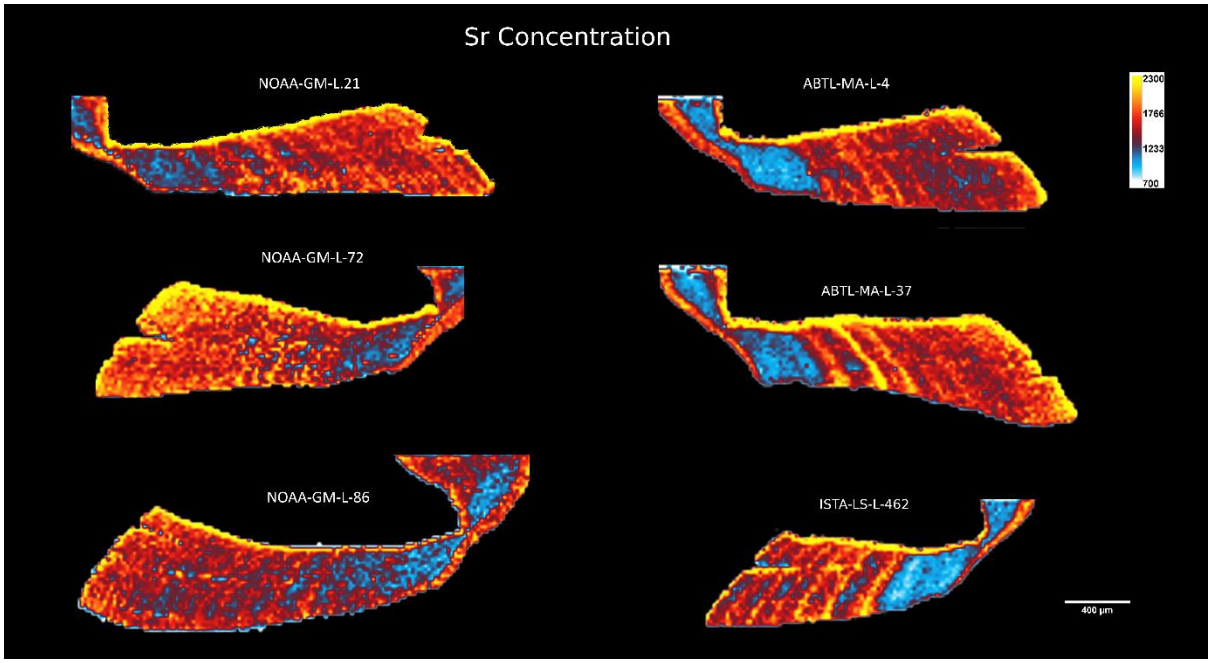

***Figure 20**: Two-dimensional map of Sr concentration (in ppm) across otoliths of spawning bluefin tuna captured in the Gulf of Mexico (left panels) and Mediterranean Sea (right panels).*

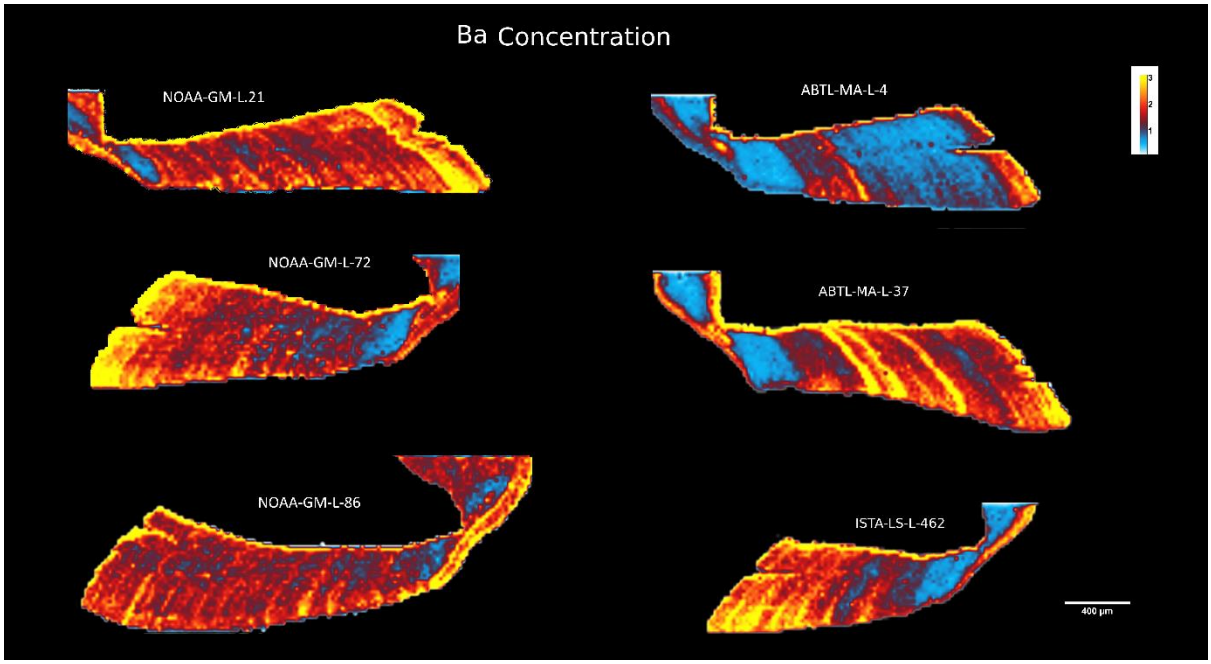

***Figure 21**: Two-dimensional map of Ba concentration (in ppm) across otoliths of spawning bluefin tuna captured in the Gulf of Mexico (left panels) and Mediterranean Sea (right panels).*

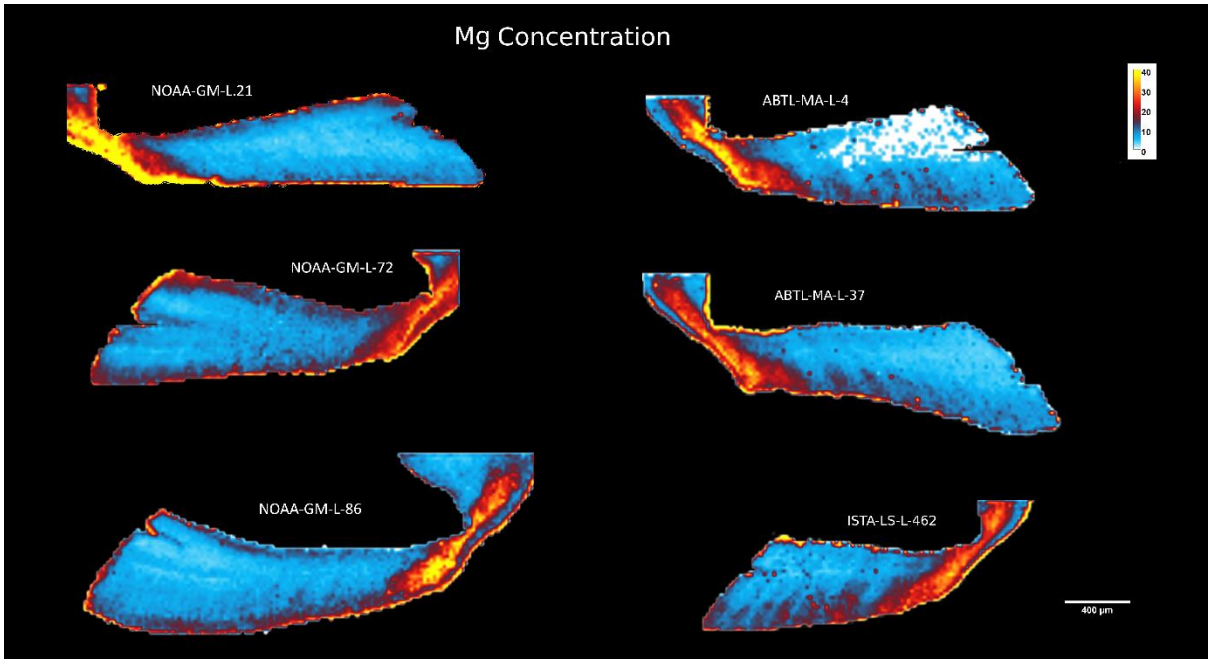

***Figure 22**: Two-dimensional map of Mg concentration (in ppm) across otoliths of spawning bluefin tuna captured in the Gulf of Mexico (left panels) and Mediterranean Sea (right panels).*

4.5. Do Otolith oxygen isotopes measured by high-precision secondary ion mass spectrometry (SIMS) reflect movements between the Mediterranean Sea and the Atlantic Ocean?

4.5.1. Introduction

The oxygen isotope ratio ($\delta^{18}O$ value) of fish otoliths is dependent on the temperature and the $\delta^{18}O$ value of the ambient water and can thus reflect the environmental history of a fish. Secondary ion mass spectrometry (SIMS) can be used to measure $\delta^{18}O$ along otolith growth profiles at a much higher temporal-resolution compared to isotope ratio mass spectrometry (IRMS). When $\delta^{18}O$ values are overlaid on visible otolith growth zones they may provide a chronological record of fish's thermal experience over its life history. Given the differences in temperature and ^{18}O composition of the seawater between the Mediterranean Sea and the Atlantic Ocean, otolith $\delta^{18}O$ values along otolith growth profiles are likely to vary, depending on whether the tuna inhabited the Mediterranean Sea or the open Atlantic Ocean. The SIMS approach is particularly powerful because it allows for the detection of habitat shifts with high temporal resolution (< 1 month).

During Phase 9, SIMS was used to provide, for the first time, high resolution estimates of $\delta^{18}O$ along otolith growth transects from Atlantic bluefin tuna from the Mediterranean and North Atlantic. The method proved effective at detecting variation in environmental histories, with results showing evidence of individual variability in early life history and possible trans-Atlantic migration of adult fish. However, $\delta^{18}O$ signatures in individuals from the same environment (Mediterranean farms) showed considerable variability, probably due to individual physiological effects or differences in behaviour (e.g. depth preferences), which will reduce the accuracy of life history reconstructions. The results also showed that due to methodological differences, $\delta^{18}O$ values obtained using SIMS are markedly lower than values recorded by IRMS, making comparison with previous studies difficult.

The application of the SIMS technique to the analysis of Atlantic bluefin tuna otoliths is in its infancy. Progress made in phase 9 was built on in phase 10 by using the relationship between temperature and $\delta^{18}O$ in the otoliths of farmed fish to develop a fractionation equation to allow for the more accurate reconstruction of temperature histories. Patterns of $\delta^{18}O$ during early life was examined in Mediterranean spawners. By aligning $\delta^{18}O$ profiles with the position of annual growth marks in the otolith it was possible to infer the timing of movement away from the main spawning areas. The fractionation equation was used to estimate the range of otolith $\delta^{18}O$ values that could be expected to occur in the otoliths of bluefin residing in different areas of the Atlantic Ocean and Mediterranean Sea and to infer possible migrations patterns in adult bluefin from observed otolith $\delta^{18}O$ profiles.

4.5.2. Methods

Otolith selection and preparation for SIMS analysis

Otoliths were selected from the GBYP tissue bank held by AZTI (Figure 23). A total of 53 otoliths were analyzed using SIMS in this phase. Of these, 47 otoliths were from large adult bluefin collected in the Western Mediterranean in May and June (2017 and 2018), held for between 3 and 8 months in a farm located in Spanish Mediterranean coasts and sampled between September 2016 and January 2017 or September 2017 and January 2018. An additional 4 otoliths were from adults in the medium size category, captured in the Adriatic Sea and held in a Croatian farm for 32 months (June 2013-January 2016); these otoliths had also been analyzed in phase 9. In phase 10, additional transects were analyzed to collect data at a higher temporal resolution. Finally, 2 otoliths from fish of disputed origin (assigned to the Western population based on IRMS stable isotope analysis and to the Eastern population based on genetics) that had been analyzed during phase 9, were reanalyzed to ensure that the transect properly intersected the larval growth period. These data were combined with data from phase 9 to generate core to edge profiles for 5 fish of disputed origin.

Otoliths were prepared according to protocols described in (Rooker et al., 2008). Briefly, following extraction, sagittal otoliths of bluefin tuna were cleaned of excess tissue with nitric acid (1%) and deionized water. One sagittal otolith from each individual was embedded in Struers epoxy resin (EpoFix) and sectioned on the transverse plane using a low speed ISOMET saw to obtain 1.5 mm transverse sections that included the core. In preparation for SIMS analysis, sections were polished to expose a smooth surface and attached to a 60mm diameter epoxy block custom made for the SIMS chamber.

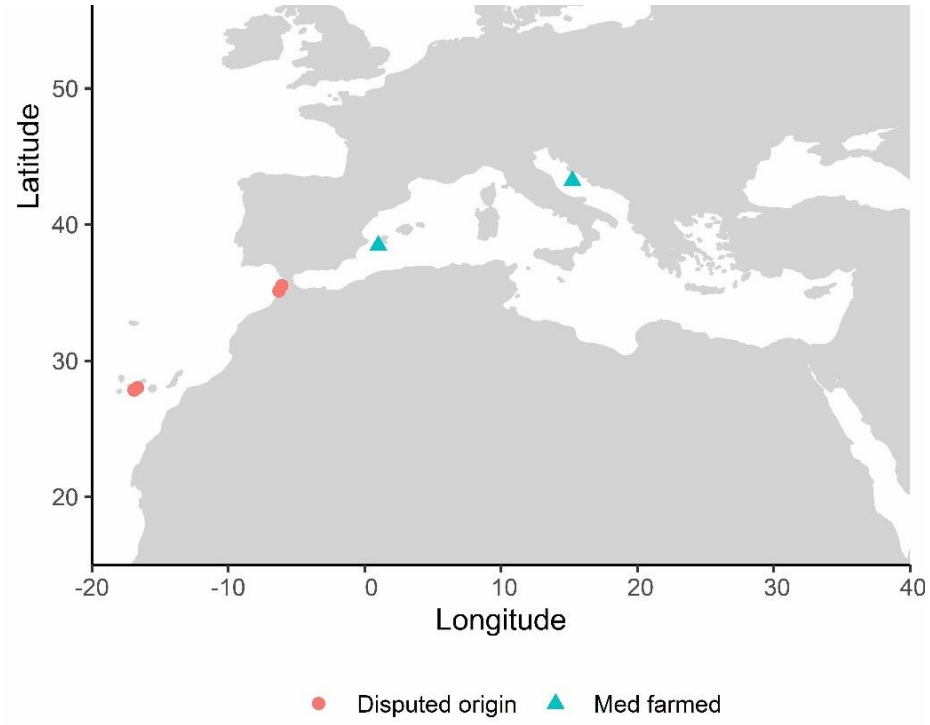

***Figure 23**: Map of the capture locations for bluefin tuna including in the SIMS analysis in phase 10.*

SIMS analysis

Otoliths were analyzed at the Nordsim-laboratory in the Swedish Museum of Natural History in Stockholm, Sweden. The instrument used for the analysis was a CAMECA IMS 1280 ion microprobe. Samples were recast with grains of a calcite standard and repolished using 3µm and 1µm diamond solutions. To facilitate navigation during analysis, a tiled image of each mount was generated using image analysis software. The mounts were coated with a layer of gold before analysis in the ion microprobe machine.

Oxygen isotope measurements were taken from 10µm spots with a distance of 40 µm between spots (centre to centre). Sample analyses were performed in blocks of 6, bracketed by two analyses of the standards. The results were reported in per mil (‰) relative to the Pee Dee belemnite (PDB) standard with a mean reproducibility of ± 0.13‰. On 20 of the large fish that were held in farms, and on all 5 of the disputed origin fish, a transect from the core to the edge was analyzed. For the remaining fish from the farm in the Western Mediterranean, 6 spots at the otolith edge were analyzed to represent the period immediately prior to sampling (3-8 months) when the fish were held in the farm. For the 4 fish from the farm in the Adriatic, a transect of ~800 µm length starting from the edge was analyzed in

order to capture the growth period during the period of captivity (32 months). On one of these fish (IZOR-AS-M-11), a complete core to edge transect was analyzed.

Relating SIMS measurements to IRMS measurements if otolith $\delta^{18}O$

The SIMS analysis in phase 9 showed that $\delta^{18}O$ otolith measurements obtained using SIMS were markedly higher than $\delta^{18}O$ otolith measurements obtained using IRMS. Similar differences were observed in an analysis of cod otoliths (Helser et al., 2018). They may arise because protein and hydrous components are removed from the otolith material by acid digestion prior to IRMS or due to differences in the bicarbonate standards that are used in each type of analysis. The AZTI database was used to identify otoliths from this analysis that had previously been analyzed using IRMS. Otoliths from 5 fish had been analyzed using both methods; all of these fish belonged to the disputed origin group. Reanalysis of otoliths from other fish in this group using IRMS indicated that the original IRMS measurements may have been too low. Given the uncertainty associated with the IRMS measurements, cross calibration with the SIMS measurements from this analysis was not conducted. Instead, the equation of Helser et al. (2018) was used to convert the $\delta^{18}O$ values from SIMS to the equivalent $\delta^{18}O$ values from IRMS to allow for comparison with previous studies based on IRMS.

Relating oxygen stable isotope signatures to water chemistry

The isotopic composition of oxygen in otoliths ($\delta^{18}O_{oto}$) is linearly related to the isotopic composition ($\delta^{18}O_w$) and temperature (T) of the seawater in which the fish resides through the fractionation equation:

$$\delta^{18}O_{oto} - \delta^{18}O_w = \gamma T + \beta$$

By coupling an empirically derived fractionation equation with estimates of $\delta^{18}O_w$ and sea surface temperature (SST) it is possible to use otolith oxygen isotope ratios as geolocators, although the successful application of this approach is somewhat limited by uncertainties surrounding small scale variation in $\delta^{18}O_w$ and species-specific variation in the fractionation equation (Trueman et al., 2012).

A 1°X1° grid of $\delta^{18}O_w$ was obtained from the dataset published by LeGrande and Schmidt (2006). Estimates of mean monthly seawater temperature at 25m depth at the location of the fish farms during the period of captivity were obtained from the MET Office Hadley Centre Observations dataset (Good et al., 2013).

Two approaches were used to examine the relationship between $\delta^{18}O$ in the otolith and temperature:

Cross individual analysis

For the large fish that were held in the farm in the western Mediterranean for 3-8 months, fish had been collected over 5 months of the year (September, October, November, December and January). The $\delta^{18}O$ values at the otolith edge should reflect the water temperature prior to capture. To test this, a general linear model was used to compare otolith $\delta^{18}O$ values at the otolith edge between fish collected in different months. The relationship between $\delta^{18}O$ at the otolith edge and estimated temperature at the farm location in the month of capture was examined. Water samples were collected at the farm location from September to December 2020 and analyzed for $\delta^{18}O$; this provided direct measurements of $\delta^{18}O$ in the water to compare with the estimates from the LeGrand and Schmidt (2006) dataset.

Within individual analysis

For the medium size category fish that were held in the farms in the Adriatic the period of captivity was 32 months. $\delta^{18}O$ profiles for the period of captivity (edge to 800µm) should reflect seasonal cycles in water temperature at the farm location. Examination of the temperature data confirmed that the water temperature at 25m was at a minimum in March a maximum in September. As $\delta^{18}O$ in the otolith is inversely correlated with temperature, maxima and minima in the $\delta^{18}O$ profiles were assumed to correspond to growth during March and September respectively while the data point at the otolith edge represented growth immediately prior to capture. A polynomial regression was used to relate distance along the otolith transect to days prior to capture; for the data points in between the temperature extremes, time of formation was estimated by interpolation. The seasonal temperature cycle at the farm location during the period of captivity was modelled using a general additive model with a cubic regression spline; this model was used to estimate temperature at each point along the SIMS analysis transect, based on the estimated time of formation for that point in the otolith. According to the Le Grande and Schmidt dataset, the estimated $\delta^{18}O$ composition of the water at the farm location at 20m depth was 1.42 ‰ relative to the Vienna Standard Mean Ocean Water (VSMOW). A general linear model was fit to the $\delta^{18}O$ otolith values and the estimated temperature at each point of the transect as follows:

$$glm((\delta^{18}O_{oto_{nx}} - \delta^{18}O_{water}) \sim \gamma T_{nx} + \beta)$$

Where $\delta^{18}O_{oto_{nx}}$ is the otolith $\delta^{18}O$ value at the nth point on the transect from fish y and T_nx is the estimated temperature during the period of formation at the nth point on the transect from fish y.

Relating oxygen stable isotope profiles to age

Seventeen of the individuals that were analyzed using SIMS had previously been aged using visual inspection of growth bands in the otoliths. For these fish, images of the sectioned otoliths, annotated with the position of the annual growth bands, were available from AZTI. The images were measured

to determine the position of each growth band along a core to edge transect. To align with the position of the SIMS data points, distance measurements were divided by the total transect length to provide a proportional distance measure that could be compared across the stable isotope and ageing transect. This provided a temporal context for interpreting the $\delta^{18}O$ profiles.

4.5.3. Results and Discussion

Estimated relationship between otolith $\delta^{18}O$ and water temperature

The most robust approach to deriving a field-based fractionation equation for Atlantic bluefin tuna would be to relate otolith $\delta^{18}O$ values to direct measurements of $\delta^{18}O$ and temperature from the rearing water of fish held in pens. If both measurements were obtained at regular intervals during the year, seasonal changes in water temperature and otolith $\delta^{18}O$ could be used to estimate the fractionation coefficients. In this case, no field measurements of water chemistry were available, so modelled estimates from the available ocean $\delta^{18}O$ and seawater temperature datasets were used.

Cross individual analysis

For the large bluefin that were held at the farm in the western Mediterranean for 3-8 months, the $\delta^{18}O$ values at the otolith edge showed no significant variation between fish collected in different months (glm, $p>0.05$). This most likely reflects the fact that the fish were held for a relatively short period of time and due to their large size, the rate of otolith growth was slow. Otolith measurements from the aged fish indicated that 1 month of growth corresponded to ~4µm along the SIMS analysis transect. The spatial resolution of the analysis (10 µm spots spaced 40 µm apart), combined with the possible loss of otolith edge material during polishing meant it was difficult to accurately measure $\delta^{18}O$ in the month prior to capture and to compare the same time-period across individuals.

Monthly measurements of water chemistry at the farm location between September and December 2020 showed that $\delta^{18}O$ of the water was 0.9 + 0.1 ‰ VSMOW at 25m. This was lower than value obtained from the gridded dataset of (LeGrande and Schmidt, 2006) of 1.18 ‰ VSMOW.

Within individual analysis

For the medium size category fish, the time in captivity was longer (32 months) and the rate of otolith growth much faster (1 month corresponded to ~30µm on the SIMS analysis transect). In three of the four fish that were analyzed, a clear decrease in $\delta^{18}O$ was evident, moving from the edge (January) towards the core (towards the most recent temperature maximum). In these three fish, the $\delta^{18}O$ values subsequently increased, showing a clear cyclical pattern that could be linked to the seasonal temperature cycle (Figure 18). In the 4th fish, $\delta^{18}O$ values increased from the edge to the core and no

seasonal cycle was apparent (IZOR-AS-M-11, last panel in Figure 19). This may have been caused by a failure to section the otolith along the correct plane or by over polishing, although neither was apparent in the otolith images. For one of the fish, an aged otolith image was available; the position of the outer annual growth bands aligned well with the cycle in the $\delta^{18}O$ measurements (Figure 18). The annual growth bands appeared to roughly align with the $\delta^{18}O$ minima (temperature maxima in September). In one fish (IZOR-AS-M-2) two annual cycles of similar magnitude were visible. In the other two fish (IZOR-AS-M-12 and IZOR-AS-M-14), 1.5 annual cycles were visible and the magnitude of the maxima and minima varied along the same otolith transect.

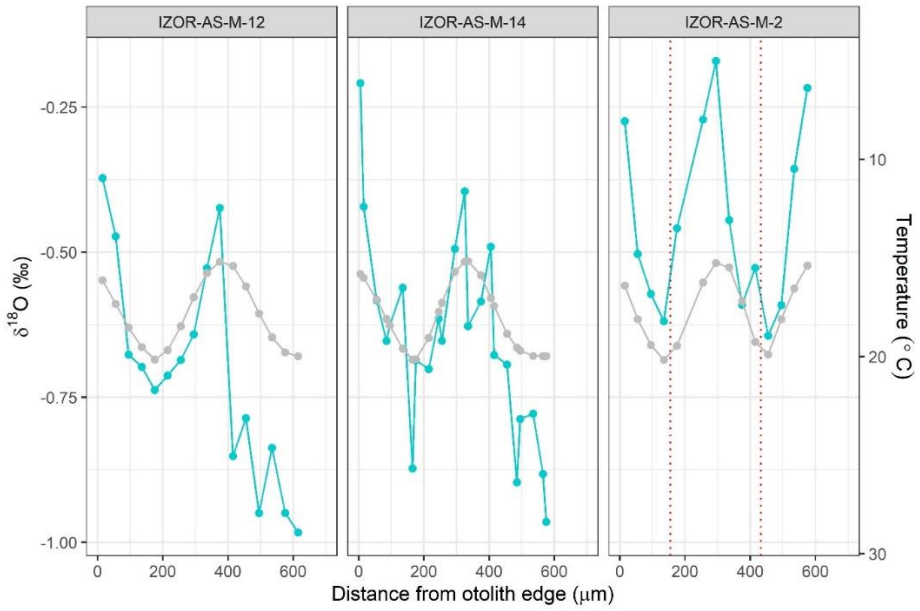

***Figure 24**: $\delta^{18}O$ measurements (blue points) at the edge of otoliths at a fish farm in the central Mediterranean (43.19° latitude, 15.24° longitude) between June 2013 and January 2016. The mean SIMS measurements were converted to the equivalent IRMS values using the equation of Helser et al. (2018). The estimated mean temperature at 25m depth during the otolith growth period (up to 23 months prior to capture) is shown in grey (from the dataset published by Good et al., 2013). Note that the temperature axis is shown in reverse. For one fish that was aged by counting annual bands on the otolith, the positions of the annual bands are indicated by vertical dashed red lines.*

After aligning the $\delta^{18}O$ measurements along the otolith transects from the three individuals, with the corresponding estimated temperatures, a fractionation equation was estimated for each fish separately and for all fish combined (Figure 20). The parameters of the four fractionation equations varied, indicating individual variability in the relationship between temperature and $\delta^{18}O$ in the otolith. The fit of the individual glms also varied across individuals (R2 = 0.66, 0.62 and 0.3 for IZOR-AS-M-2, IZOR-AS-M-14 and IZOR-AS-M-12 respectively, R2 = 0.42 for the combined glm).

Analysis using general linear mixed models, with a random effect on fish ID showed individual variability in the intercept but not the slope of the fractionation equation. For the glm, 32% of the

variance in otolith $\delta^{18}O$ was due to individual variance and 34% was due to the effect of temperature (marginal R2 = 0.34; conditional R2 = 0.66). The parameters of all the fractionation equations were markedly different to the relationship between otolith $\delta^{18}O$ and temperature reported by Kitagawa et al. (2013) for larval Pacific bluefin tuna.

$\delta^{18}O_{oto} - \delta^{18}O_w = -0.27(T°C) + 5.193$ from Kitagawa *et al.* 2013
$\delta^{18}O_{oto} - \delta^{18}O_w = -0.69(T°C) - 0.075$ combined fractionation equation from this study

Estimates of $\delta^{18}O$ in the otolith under different temperature and water $\delta^{18}O$ values (see isoscape map in Figure 27) were more consistent with the values reported in the literature for bluefin tuna than estimates previously obtained using the equation of Kitagawa et al. (2013) (see Brophy et al., 2020).

Variation in $\delta^{18}O$ across life histories of adult bluefin tuna

Patterns in $\delta^{18}O$ were examined across entire core to edge transects in otoliths from 26 adult bluefin; 21 had been collected in the Mediterranean during the spawning season (the Mediterranean farmed group), 5 had been collected in the Atlantic Ocean in April and were of uncertain population origin (the disputed origin group: Figure 19). Age information was available for 16 of the Mediterranean farmed group.

In most of the otoliths, $\delta^{18}O$ values in the area corresponding to the first year of life were relatively stable, indicating that fish had remained within the same area for this period. In the second year of life, $\delta^{18}O$ values increased steadily. This may reflect migration to waters with higher $\delta^{18}O$ or lower temperatures or movement to deeper waters. After the second year of life, regular fluctuations in $\delta^{18}O$ between high and low values occurred at a frequency that appeared to be roughly annual. This could reflect seasonal changes in water temperature, seasonal movements between water bodies or depths, or a combination of all three. The annual fluctuations were more marked in some individuals (e.g. BALF-BA-L-115; BALF-BA-L-176; BALF-BA-L-304) than in others (e.g. BALF-BA-L-493; IZOR-AS-M-11; BALF-BA-L-317). In some fish, $\delta^{18}O$ values fluctuated markedly in parts of the transect, but were more stable in others (e.g. BALF-BA-L-284, BALF-BA-L-272).

During strong annual fluctuations, $\delta^{18}O$ changed by ~ 1 ‰ within a year of growth. This exceeded the annual fluctuations observed during the period of captivity in the farmed fish from the Central Mediterranean (max change ~ 0.4 ‰; Figure 24) and the maximum predicted change at any single location across the three areas of the Mediterranean (Table 7). For the fish from the Mediterranean farmed group that showed strong annual fluctuations, $\delta^{18}O$ minima were within the range of predicted

values for fish residing in the Mediterranean (Figure 25) and various region in the Atlantic Ocean where bluefin tuna are known to occur (Table 7). These changes could therefore also reflect movement within the Mediterranean or from the Mediterranean into the Atlantic. Given the magnitude of the changes, it seems unlikely that they reflect temperature variation within a restricted area.

For the disputed origin group, $\delta^{18}O$ values in the otolith core region were similar to values in the Mediterranean fish, suggesting a common spawning origin in the Mediterranean Sea. However, in the later part of the transects (particularly IEO-CI-L-11, IEO-CI-L-154 and INRH-MO-L-277) $\delta^{18}O$ values dropped below the range of predicted values for fish residing in the Mediterranean Sea. This might reflect movement out of the Mediterranean into the Atlantic (Table 15, Figure 27). Given the level of uncertainty associated with the fractionation equation and the observed degree of individual variability, migration patterns cannot be definitely inferred from the $\delta^{18}O$ profiles. However, the patterns suggest that the disputed origin group that were captured near the Canary Islands and Morocco had undergone more extensive migrations than the fish that were collected in the Mediterranean during the spawning season.

Overall, examination of the otolith profiles indicated three general patterns of movement: 1) residency within a relatively restricted area during adulthood; 2) annual movement of adults between areas of different water chemistry with $\delta^{18}O$ values rarely decreasing below -1.3 ‰; 3) annual movement of adults between areas of different water chemistry with $\delta^{18}O$ values frequently dropping below -1.5 ‰.

***Table 15**: Predicted annual minimum (min. $\delta^{18}O_{oto}$) and maximum (max. $\delta^{18}O_{oto}$) $\delta^{18}O$ values in the otolith for bluefin tuna residing in various known spawning and feeding areas (see locations in Figure 26). The absolute difference between these gives the area wide max. change (allowing for free movement across the whole area) while the location specific max. change is the maximum change at any one specific location. Predicted values were estimated by inputting the seawater temperature at 25m (Good et al., 2013) and $\delta^{18}O$ of seawater at 20m (LeGrande and Schmidt, 2006) into the fractionation equation from this study (Figure 25). For the temperature data, 2014 was used as the reference year.*

Area	**Area number**	**min. $\delta^{18}O_{oto}$ (‰)**	**max. $\delta^{18}O_{oto}$ (‰)**	**Area wide max. change (‰)**	**Location specific max. change (‰)**
Gulf of Mexico	1	-2.20	-1.30	0.90	0.77
Bahamas	2	-1.99	-1.20	0.79	0.49
Slope Sea	3	-2.97	-1.09	1.88	1.39
Offshore Slope Sea	4	-3.24	-1.13	2.11	1.37
Central Atlantic	5	-2.14	-0.87	1.27	1.07
Western Mediterranean	6	-1.29	-0.36	0.93	0.77
Central Mediterranean	7	-1.31	-0.30	1.00	0.80
Eastern Mediterranean	8	-1.22	-0.12	1.09	0.80
Bay of Biscay	9	-1.57	-1.00	0.57	0.56
Gibraltar	10	-1.46	-0.86	0.60	0.60
Canaries	11	-1.63	-0.87	0.76	0.56
Norwegian Sea	12	-2.03	-0.56	1.47	0.73

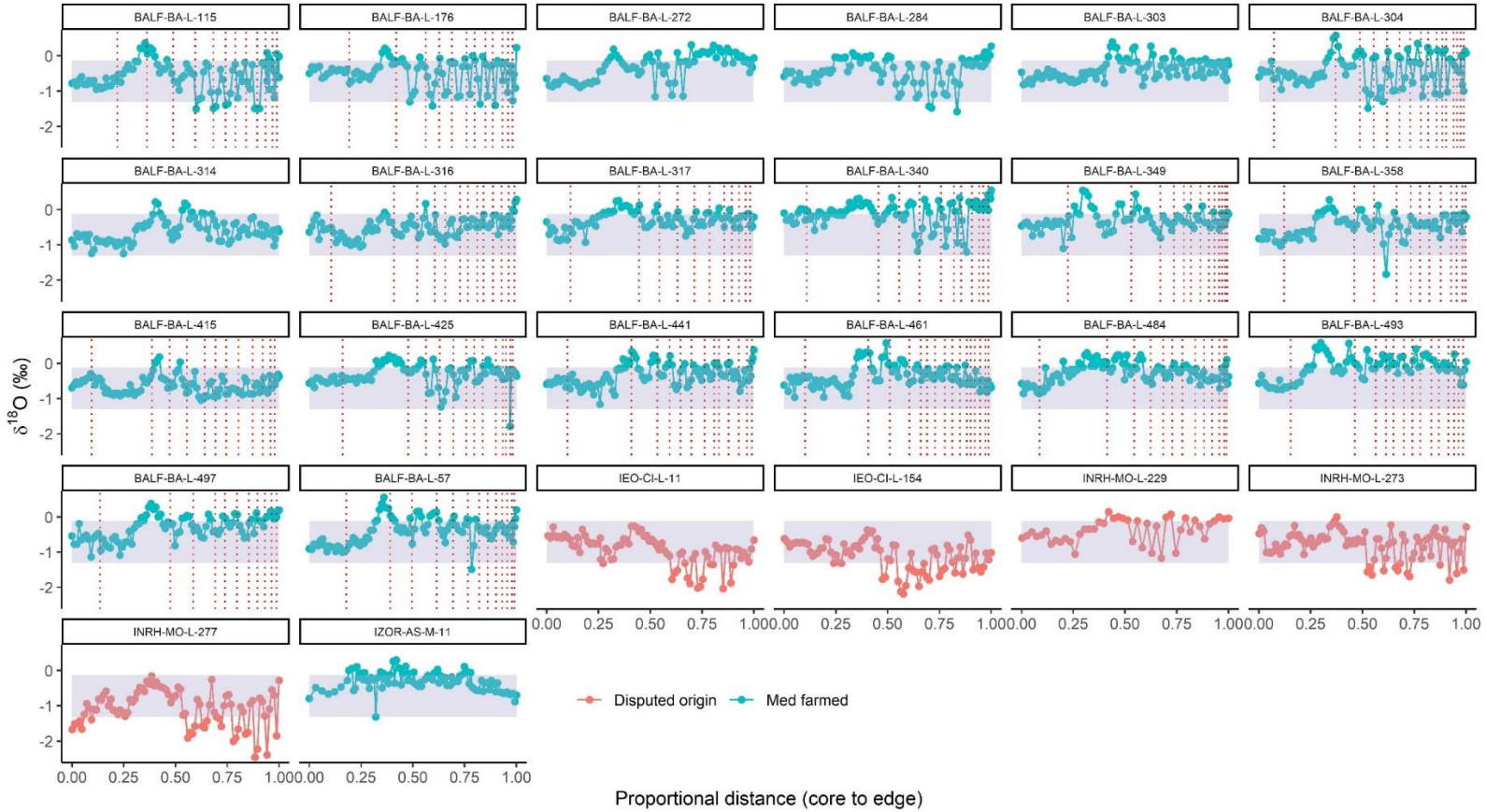

***Figure 25**: $\delta^{18}O$ measurements along core to edge transects in otoliths of bluefin tuna. SIMS measurements were converted to the equivalent IRMS values using the equation of Helser et al. (2018). For fish that were aged by counting annual bands on the otolith, the positions of the annual bands are indicated by vertical dashed red lines. The grey shaded areas represent the range of $\delta^{18}O$ values in the otolith of bluefin tuna residing in the Mediterranean Sea, predicted using the fractionation equation estimated from the farmed fish (equation 1). The disputed origin fish (shown in red) were previously assigned to the west Atlantic population based on IRMS analysis of the otolith core and assigned to the east Atlantic population using genetics. Of the Mediterranean farmed fish (shown in blue), one was held in a farm in the central Mediterranean for 963 days (IZOR-AS-M-11) while the remainder were held in a farm in the western Mediterranean for 3-8 months.*

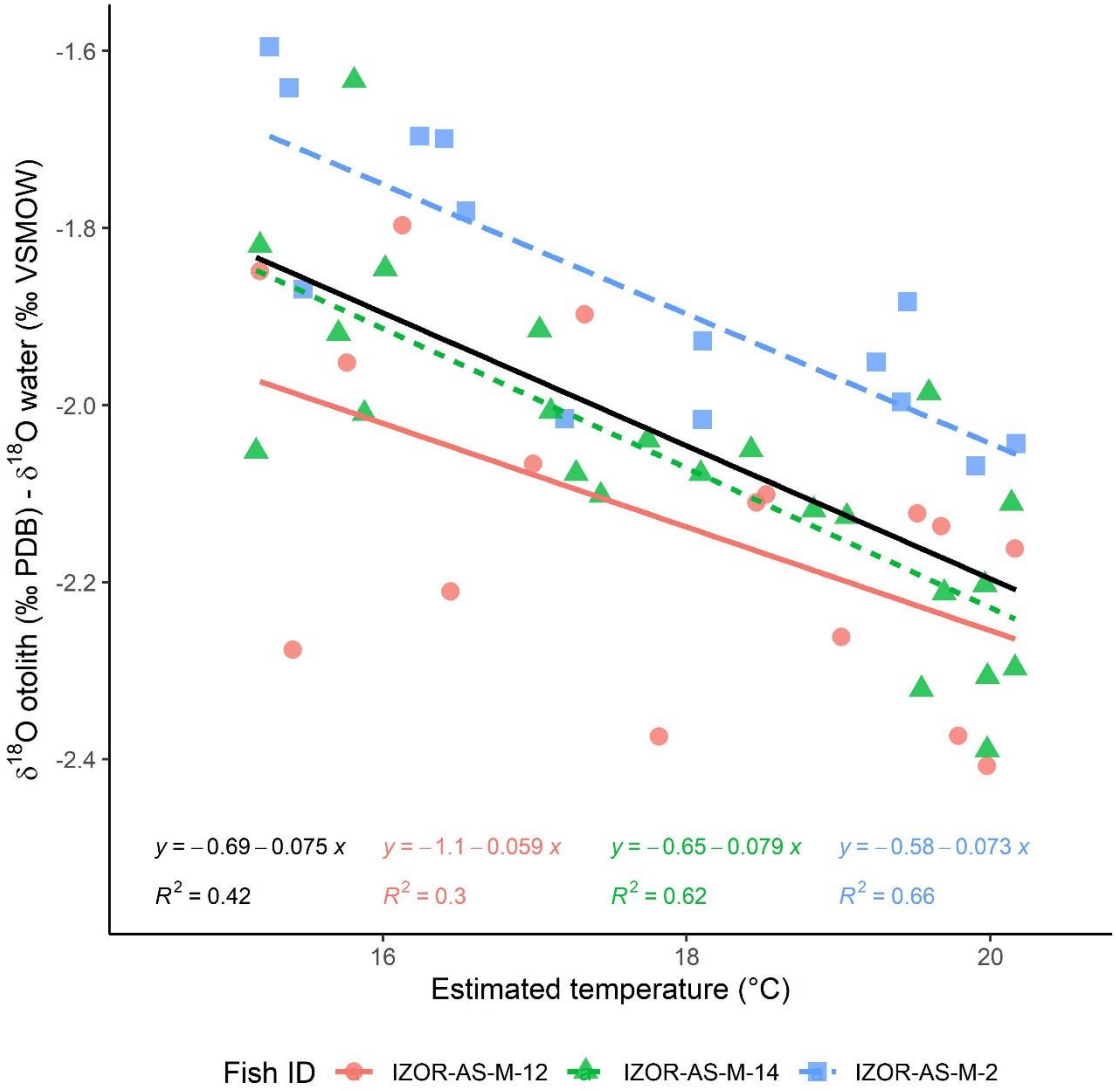

***Figure 26**: Difference between observed $\delta^{18}O$ along otolith growth trajectories and estimated $\delta^{18}O$ in the water (from the dataset published by LeGrande and Schmidt, 2006) plotted against the estimated mean temperature at 25m depth during the corresponding month of otolith growth (from the dataset published by Good et al., 2013) for bluefin held at a fish farm in the central Mediterranean (43.19° latitude, 15.24° longitude) between June 2013 and January 2016. Regression parameters are shown in colour for individual fish and in black for the three fish combined.*

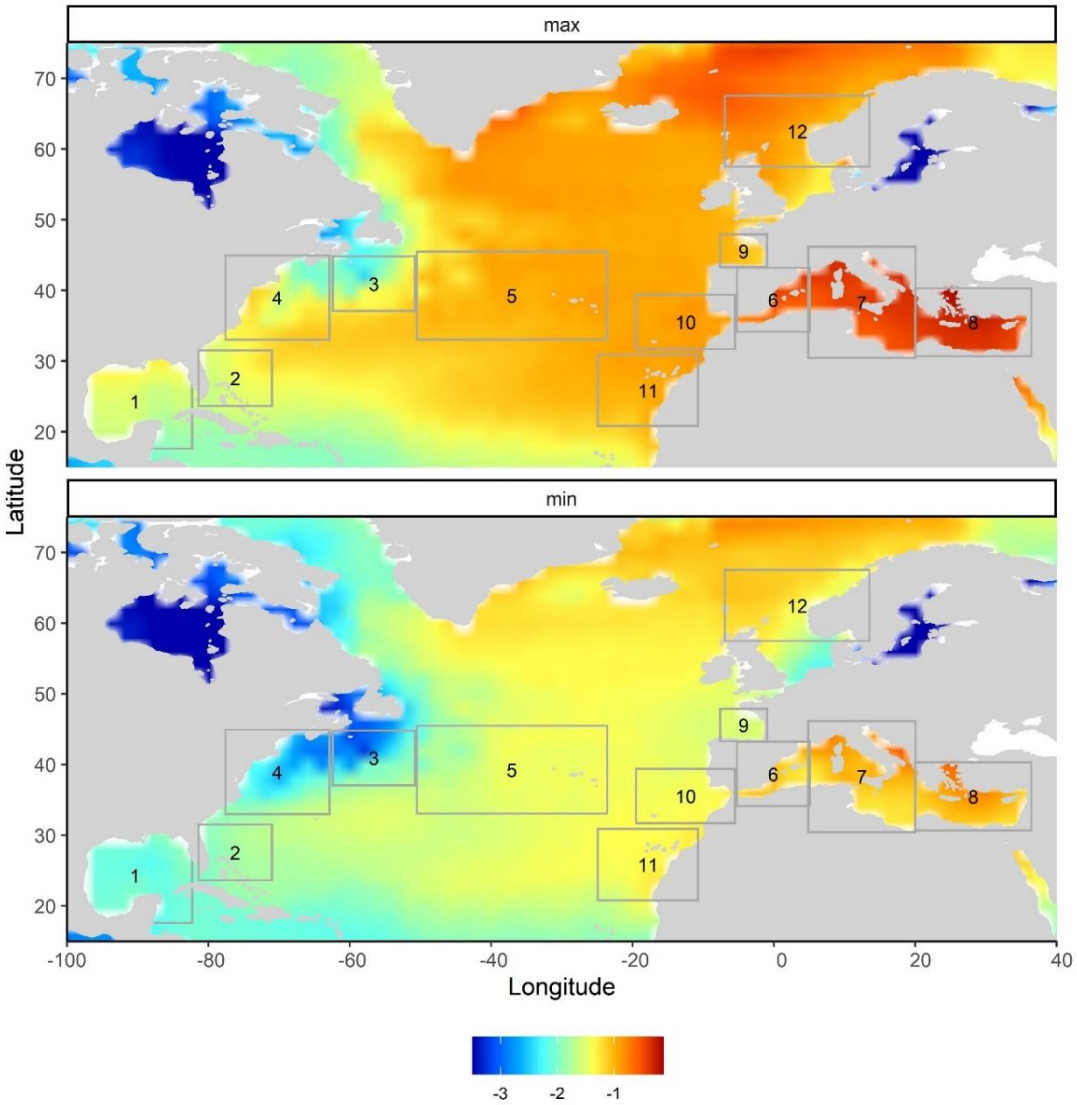

***Figure 27**: Map of predicted annual maximum (top) and minimum (bottom) $\delta^{18}O$ values in the otolith for bluefin tuna, estimated by inputting the seawater temperature at 25m (Good et al., 2013) and $\delta^{18}O$ of seawater at 20m (LeGrande and Schmidt, 2006) into the fractionation equation from this study (Figure 18). For the temperature data, 2014 was used as the reference year. For display purposes, all estimates equal to or lower than -3.5 ‰ were assigned a value of -3.5 ‰. The numbered boxes are areas where bluefin commonly occur; the limits of the predicted $\delta^{18}O_{oto}$ values for these areas are shown in Table 15.*

Conclusions

The SIMS analysis has furthered the development of an "isoscape approach" for reconstructing movements of Atlantic bluefin tuna between spawning, nursery and feeding areas. More detailed analysis of $\delta^{18}O$ profiles in bluefin from the medium size category, held in farms in the Mediterranean for 32 months has enabled the estimation of a fractionation equation that describes the relationship between otolith $\delta^{18}O$, stable isotope composition of the water and temperature. The fractionation equation provided a moderate fit to the $\delta^{18}O_{oto}$ measurements and the $\delta^{18}O_{seawater}$ and temperature

estimates (R^2 = 0.42). Its accuracy for predicting $\delta^{18}O_{oto}$ at a given time and location is reduced by individual variability in the relationship and uncertainties associated with modelled temperature and $\delta^{18}O_{seawater}$ estimates. In the future, recording of individual depth profiles and temperature histories using archival tags in fish held within the farms and direct measurements of seawater $\delta^{18}O$ could help to determine the sources of individual variability and to refine the fractionation equation.

In bluefin from the large size category, it was not possible to detect seasonal changes in $\delta^{18}O$ at the otolith edge due to the slow rate of otolith growth. However, seasonal cycles were apparent in otolith growth profiles for the first 8-10 years of life. It is recommended that bluefin from the small or medium size categories are used in future investigations of otolith chemistry-environment relationships. The reconstruction of migration pathways from otolith chemistry profiles after 10 years of age is challenged by the temporal resolution of currently available methods.

Alignment of $\delta^{18}O$ profiles with the position of otolith growth bands provided some first insights into age specific movements and possible migration behaviours. Although movements between the Mediterranean and Atlantic cannot yet be accurately reconstructed using stable isotope profiles, comparison of relative changes across individuals allowed for the detection of groups of fish with characteristic migratory patterns. The results provide some support for the hypothesis that there is a migratory and a resident contingent within the Eastern stock of Atlantic bluefin tuna (Aranda et al., 2013). By refining the fractionation equation we could reduce uncertainties on the modelled temperature, and thus, improve the accuracy for predicting $\delta 18O_{oto}$ at a given time and location. If a given fish shifts between migratory and resident contingents within the first 8-10 years of life, otolith $\delta 18O$ profiles could be used to detect the timing of the behaviour change. However, changes in behaviour will be difficult to detect after that age due to the limitations on the resolution of the current available methods.

References

Aranda, G., F. J. Abascal, J. L. Varela, and A. Medina. 2013. Spawning behaviour and post-spawning migration patterns of atlantic bluefin tuna (Thunnus thynnus) ascertained from satellite archival tags. PLoS One 8:e76445.

Arrizabalaga, H., Arregui, I., Medina, A., Rodríguez-Ezpeleta, N., Fromentin, J.-M. and Fraile, I. (2019) Life History and Migrations of Mediterranean Bluefin Tuna In: The Future of Bluefin Tunas: Ecology, Fisheries Management, and Conservation.B. Block (ed.) Johns Hopkins University Press, pp. 67-93.

Brophy, D, Rodríguez-Ezpeleta, N, Fraile, I and Arrizabalaga, H. (2020). Combining genetic markers with stable isotopes in otoliths reveals complexity in the stock structure of Atlantic bluefin tuna (Thunnus thynnus). Scientific Reports, 10, 14675. https://doi.org/10.1038/s41598-020-71355-6.

Chung, M.T., Trueman C.N., Aanestad J. and Grønkjær P. (2019). Otolithd13C values as a metabolic proxy: approaches andmechanical underpinnings. Marine and Freshwater Research, 70, 1747–1756.

Darnaude, A. M., A. Sturrock, C. N. Trueman, D. Mouillot, Eimf, S. E. Campana, and E. Hunter. 2014. Listening In on the Past: What Can Otolith δ18O Values Really Tell Us about the Environmental History of Fishes? PLoS One 9:e108539.

Fraile, I., Arrizabalaga, H. and Rooker, J.R. (2015) Origin of Atlantic bluefin tuna (Thunnus thynnus) in the Bay of Biscay. ICES Journal of Marine Science: Journal du Conseil 72: 625-634.

Fraile, I., Arrizabalaga, H., Groeneveld, J., Kölling, M., Santos, M.N., Macías, D., Addis, P., Dettman, D.L., Karakulak, S. and Deguara, S. (2016) The imprint of anthropogenic CO 2 emissions on Atlantic bluefin tuna otoliths. Journal of Marine Systems 158: 26-33.

Good, S. A., Martin, M. J. & Rayner, N. A. (2013). EN4: Quality controlled ocean temperature and salinity profiles and monthly objective analyses with uncertainty estimates. Journal of Geophysical Research: Oceans 118, 6704-6716.

Grammer G.L., Morrongiello J.R., Izzo C., Hawthorne P.J., Middleton J.F., Gillanders B.M. (2017). Coupling biogeochemical tracers with fish growth reveals physiological and environmental controls on otolith chemistry. Ecological Monogr. 87(3):487–507. doi:10.1002/ecm.1264

Helser, T. E., C. R. Kastelle, J. L. McKay, I. J. Orland, R. Kozdon, and J. W. Valley. 2018. Evaluation of micromilling/conventional isotope ratio mass spectrometry and secondary ion mass spectrometry of δ18O values in fish otoliths for sclerochronology. Rapid Communications in Mass Spectrometry 32:1781-1790.

Hüssy, K., Limburg K.E., de Pontual H., Thomas O.R.B., Cook P.K., Heimbrand Y., Blass M. and Sturrock A.M. (2020). Trace Element Patterns in Otoliths: The Role of Biomineralization. Reviews in Fisheries Science & Aquaculture, DOI:10.1080/23308249.2020.1760204.

Kitagawa, T., Ishimura, T., Uozato, R., Shirai, K., Amano, Y., Shinoda, A., Otake, T., Tsunogai, U. & Kimura, S. (2013). Otolith d18O of Pacific bluefin tuna Thunnus orientalis as an indicator of ambient water temperature. Marine Ecology Progress Series 481, 199-209.

LeGrande, A. N., and G. A. Schmidt (2006). Global gridded data set of the oxygen isotopic composition in seawater. Geophysical Research Letters 33.

Macdonald J.I., Drysdale R.N., Witt R., Csagoly Z. and Marteinsdottir G. (2020). Isolating the influence of ontogeny helps predict island-widevariability in fish otolith chemistry. Review Fish Biology & Fisheries, 30:173–202.

Matta, M. E., I. J. Orland, T. Ushikubo, T. E. Helser, B. A. Black, and J. W. Valley. 2013. Otolith oxygen isotopes measured by high-precision secondary ion mass spectrometry reflect life history of a yellowfin sole (Limanda aspera). Rapid Communications in Mass Spectrometry 27:691-699.

Millar, R.B. (1990) Comparison of methods for estimating mixed stock fishery composition. Canadian Journal of Fisheries and Aquatic Sciences 47: 2235-2241.

Rooker, J. R., H. Arrizabalaga, I. Fraile, D. H. Secor, D. L. Dettman, N. Abid, P. Addis, S. Deguara, F. S. Karakulak, A. Kimoto, O. Sakai, D. Macias, and M. N. Santos. 2014. Crossing the line: migratory and homing behaviors of Atlantic bluefin tuna. Marine Ecology Progress Series 504:265-276.

Rooker, J. R., D. H. Secor, G. De Metrio, R. Schloesser, B. A. Block, and J. D. Neilson. 2008a. Natal Homing and Connectivity in Atlantic Bluefin Tuna Populations. Science 322:742-744.

Rooker, J. R., D. H. Secor, G. DeMetrio, A. J. Kaufman, A. B. Rios, and V. Ticina. 2008b. Evidence of trans-Atlantic movement and natal homing of bluefin tuna from stable isotopes in otoliths. Marine Ecology Progress Series 368:231-239.

Schloesser, R. W., Rooker, J. R., Louchuoarn, P., Neilson, J. D., and Secor, D. H. (2009) Interdecadal variation in seawater d13C and d18O recorded in fish otoliths. Limnology and Oceanography 54: 1665–1668.

Thomas, O. R. B., Ganio, K., Roberts, B. R., and Swearer, S. E. (2017). Trace element-protein interactions in endolymph from the inner ear of fish: implications for environmental reconstructions using fish otolith chemistry. Metallomics 9, 239–224. doi: 10.1039/c6mt00189k

Trueman, C. N., K. M. MacKenzie, and M. R. Palmer. 2012. Identifying migrations in marine fishes through stable-isotope analysis. Journal of Fish Biology 81:826-847.

APPENDIX

Table 1: Individual probabilities of being from the western population using Quadratic Discriminant Analysis Function, using as a reference samples yearlings from the east and west nurseries (YB) and spawning adults (AB).

ID	AREA	Date	Lat.	Lon.	Fork Length [cm]	Total Weight [Kg]	prob (0-1) West (YB)	prob (0-1) West (AB)
IEO-CI-L-219	MC	26/03/2018	28	-17	239	286	0.752	0.792
IEO-CI-L-220	MC	26/03/2018	28	-17	237	216	0.037	0.010
IEO-CI-L-222	MC	26/03/2018	28	-17	270	300	0.071	0.032
IEO-CI-L-223	MC	26/03/2018	28	-17	223	249	0.396	0.178
IEO-CI-L-224	MC	27/03/2018	28	-17	201	145	0.029	0.008
IEO-CI-L-226	MC	28/03/2018	28	-17	230	199	0.009	0.002
IEO-CI-L-227	MC	28/03/2018	28	-17	252	244	0.026	0.007
IEO-CI-L-228	MC	28/03/2018	28	-17	233	267	0.092	0.040
IEO-CI-L-229	MC	26/03/2018	28	-17	235	249	0.100	0.048
IEO-CI-L-230	MC	26/03/2018	28	-17	245	265	0.637	0.892
IEO-CI-L-231	MC	26/03/2018	28	-17	250	247	0.044	0.013
IEO-CI-L-232	MC	26/03/2018	28	-17	234	230	0.048	0.015
IEO-CI-L-233	MC	26/03/2018	28	-17	246	308	0.171	0.162
IEO-CI-L-234	MC	02/04/2018	28	-17	256	284	0.017	0.003
IEO-CI-L-235	MC	02/04/2018	28	-17	245	255	1.000	0.998
IEO-CI-L-236	MC	02/04/2018	28	-17	248	264	0.034	0.011
IEO-CI-L-237	MC	02/04/2018	28	-17	234	194	0.125	0.070
IEO-CI-L-238	MC	02/04/2018	28	-17	225	208	0.065	0.029
IEO-CI-L-239	MC	26/03/2018	28	-17	250	281	0.219	0.186
IEO-CI-L-240	MC	26/03/2018	28	-17	231	221	0.139	0.098
IEO-CI-L-241	MC	26/03/2018	28	-17	241	253	0.990	0.981
IEO-CI-L-242	MC	26/03/2018	28	-17	230	245	0.205	0.117
IEO-CI-L-243	MC	04/04/2018	28	-17	232	228	0.314	0.139
IEO-CI-L-244	MC	04/04/2018	28	-17	242	263	0.498	0.344
IEO-CI-L-245	MC	04/04/2018	28	-17	232	243	0.994	0.984
IEO-CI-L-246	MC	04/04/2018	28	-17	245	270	0.895	0.842
IEO-CI-L-247	MC	04/04/2018	28	-17	233	225	0.174	0.069
IEO-CI-L-248	MC	04/04/2018	28	-17	233	264	0.108	0.059
IEO-CI-L-249	MC	05/04/2018	28	-17	242	291	1.000	1.000
IEO-CI-L-250	MC	06/04/2018	28	-17	250	299	0.027	0.008
IEO-CI-L-251	MC	05/04/2018	28	-17	241	243	0.080	0.029
IEO-CI-L-252	MC	04/04/2018	28	-17	259	274	0.814	0.765
IEO-CI-L-253	MC	04/04/2018	28	-17	245	255	0.493	0.230
IEO-CI-L-254	MC	26/03/2018	28	-17	232	287	0.062	0.023
IEO-CI-L-255	MC	28/03/2018	28	-17	258	269	0.036	0.011
IEO-CI-L-256	MC	27/03/2018	28	-17	259	243	0.576	0.554
IEO-CI-L-257	MC	27/03/2018	28	-17	245	284	0.718	0.584
IEO-CI-L-258	MC	27/03/2018	28	-17	263	351	0.030	0.008
IEO-CI-L-259	MC	28/03/2018	28	-17	243	258	0.151	0.055
IEO-CI-L-260	MC	27/03/2018	28	-17	261	297	0.613	0.389
IEO-CI-L-261	MC	28/03/2018	28	-17	251	272	0.966	0.944
IEO-CI-L-262	MC	27/03/2018	28	-17	248	289	0.013	0.002
IEO-CI-L-263	MC	26/03/2018	28	-17	197	127	0.018	0.004
IEO-CI-L-264	MC	26/03/2018	28	-17	215	186	0.101	0.052
IEO-CI-L-265	MC	27/03/2018	28	-17	255	300	0.028	0.008
IEO-CI-L-266	MC	27/03/2018	28	-17	213	180	0.739	0.707
IEO-CI-L-267	MC	27/03/2018	28	-17	203	145	0.156	0.072
IEO-CI-L-268	MC	26/03/2018	28	-17	245	289	0.066	0.031
IEO-CI-L-269	MC	26/03/2018	28	-17	256	294	0.995	0.992
IEO-CI-L-276	MC	15/03/2019	28	-17	245	291	0.047	0.017
IEO-CI-L-277	MC	15/03/2019	28	-17	245	353	0.110	0.039
IEO-CI-L-278	MC	15/03/2019	28	-17	247	236	0.205	0.167
IEO-CI-L-279	MC	15/03/2019	28	-17	235	254	0.035	0.010
IEO-CI-L-280	MC	15/03/2019	28	-17	234	198	0.006	0.001
IEO-CI-L-281	MC	15/03/2019	28	-17	245	272	0.013	0.002

IEO-CI-L-282	MC	15/03/2019	28	-17	248	286	0.007	0.001
IEO-CI-L-284	MC	19/03/2019	28	-17	230	226	0.021	0.002
IEO-CI-L-285	MC	19/03/2019	28	-17	229	223	0.034	0.008
IEO-CI-L-286	MC	19/03/2019	28	-17	243	256	0.856	0.815
IEO-CI-L-287	MC	19/03/2019	28	-17	221	200	0.063	0.029
IEO-CI-L-288	MC	19/03/2019	28	-17	225	203	0.912	0.923
IEO-CI-L-289	MC	20/03/2019	28	-17	233	215	0.039	0.002
IEO-CI-L-290	MC	20/03/2019	28	-17	226	214	0.073	0.036
IEO-CI-L-291	MC	20/03/2019	28	-17	232	229	0.168	0.127
IEO-CI-L-292	MC	20/03/2019	28	-17	211	173	0.998	0.988
IEO-CI-L-293	MC	20/03/2019	28	-17	275	338	0.972	0.948
IEO-CI-L-294	MC	18/03/2019	28	-17	261	281	0.100	0.044
IEO-CI-L-295	MC	18/03/2019	28	-17	233	200	0.197	0.102
IEO-CI-L-296	MC	18/03/2019	28	-17	224	214	0.006	0.001
IEO-CI-L-298	MC	18/03/2019	28	-17	250	273	0.023	0.006
IEO-CI-L-299	MC	26/03/2019	27	-17	233	248	0.007	0.001
IEO-CI-L-300	MC	26/03/2019	27	-17	226	215	0.912	0.786
IEO-CI-L-301	MC	20/03/2019	28	-17	253	285	0.037	0.010
IEO-CI-L-302	MC	01/04/2019	28	-17	253	321	0.076	0.025
IEO-CI-L-303	MC	01/04/2019	28	-17	229	235	0.079	0.034
IEO-CI-L-304	MC	01/04/2019	28	-17	229	211	0.153	0.062
IEO-CI-L-305	MC	01/04/2019	28	-17	232	238	0.055	0.020
IEO-CI-L-306	MC	01/04/2019	28	-17	263	334	0.024	0.006
IEO-CI-L-307	MC	01/04/2019	28	-17	223	234	0.024	0.007
IEO-CI-L-308	MC	03/04/2019	27	-17	262	293	0.477	0.265
IEO-CI-L-309	MC	03/04/2019	27	-17	256	320	0.797	0.834
IEO-CI-L-310	MC	03/04/2019	27	-17	234	256	0.026	0.007
IEO-CI-L-311	MC	03/04/2019	27	-17	245	294	0.520	0.346
IEO-CI-L-312	MC	03/04/2019	27	-17	239	242	0.106	0.070
IEO-CI-L-313	MC	03/04/2019	27	-17	229	237	0.017	0.003
IEO-CI-L-314	MC	01/04/2019	28	-17	222	215	0.040	0.014
IEO-CI-L-315	MC	01/04/2019	28	-17	244	252	0.010	0.002
IEO-CI-L-316	MC	01/04/2019	28	-17	250	281	0.028	0.008
IEO-CI-L-317	MC	02/04/2019	28	-17	200	154	0.072	0.035
IEO-CI-L-318	MC	02/04/2019	28	-17	224	216	0.054	0.017
IEO-CI-L-319	MC	02/04/2019	28	-17	223	174	0.020	0.005
IEO-CI-L-320	MC	05/04/2019	28	-17	248	271	0.209	0.199
IEO-CI-L-321	MC	05/04/2019	27	-17	215	199	0.219	0.187
IEO-CI-L-322	MC	02/04/2019	28	-17	234	225	0.049	0.019
IEO-CI-L-323	MC	05/04/2019	28	-17	262	357	0.039	0.003
IEO-CI-L-324	MC	05/04/2019	28	-17	239	238	0.049	0.009
IEO-CI-L-325	MC	03/04/2019	28	-17	247	232	0.425	0.237
IEO-CI-L-326	MC	05/04/2019	28	-17	258	287	0.919	0.866
IEO-CI-L-327	MC	05/04/2019	28	-17	250	241	0.067	0.030
IEO-CI-L-328	MC	02/04/2019	28	-17	262	273	0.413	0.288
IEO-CI-L-329	MC	03/04/2019	28	-17	228	213	0.091	0.049
IEO-CI-L-330	MC	03/04/2019	28	-17	220	196	0.574	0.308
IEO-CI-L-331	MC	05/04/2019	27	-17	249	280	0.779	0.655
NRIF-CA-L-2885	CA	19/09/2017	43	-48	225	298	0.990	0.984
NRIF-CA-L-2886	CA	19/09/2017	43	-48	244	281	0.090	0.052
NRIF-CA-L-2887	CA	20/09/2017	43	-48	233	276	0.082	0.023
NRIF-CA-L-2888	CA	20/09/2017	43	-48	217	174	0.207	0.189
NRIF-CA-L-2889	CA	21/09/2017	43	-48	244	263	0.206	0.151
NRIF-CA-L-2890	CA	21/09/2017	43	-48	254	284	1.000	1.000
NRIF-CA-L-2891	CA	21/09/2017	43	-48	266	278	0.234	0.149
NRIF-CA-L-2892	CA	21/09/2017	43	-48	278	371	0.622	0.510
NRIF-CA-L-2893	CA	22/09/2017	43	-48	248	313	0.401	0.290
NRIF-CA-L-2894	CA	24/09/2017	44	-48	213	187	0.523	0.445
NRIF-CA-L-2895	CA	25/09/2017	44	-48	254	291	0.912	0.863
NRIF-CA-L-2896	CA	26/09/2017	44	-48	253	349	1.000	1.000
NRIF-CA-L-2897	CA	29/09/2017	45	-48	243	262	1.000	1.000
NRIF-CA-L-2898	CA	29/09/2017	45	-48	220	197	0.737	0.824
NRIF-CA-L-2899	CA	29/09/2017	45	-48	250	295	1.000	1.000
NRIF-CA-L-2900	CA	29/09/2017	45	-48	255	300	0.350	0.429
NRIF-CA-L-2901	CA	30/09/2017	45	-48	263	350	0.969	0.951
NRIF-CA-L-2902	CA	30/09/2017	45	-48	236	235	0.483	0.513

NRIF-CA-L-2903	CA	30/09/2017	45	-48	224	174	0.197	0.183
NRIF-CA-L-2904	CA	06/10/2017	45	-47	230	189	0.858	0.927
NRIF-CA-L-2905	CA	08/10/2017	45	-48	211	182	0.995	0.985
NRIF-CA-L-2906	CA	08/10/2017	45	-48	233	254	0.999	0.999
NRIF-CA-L-2907	CA	09/10/2017	45	-48	258	295	0.472	0.345
NRIF-CA-L-2908	CA	10/10/2017	45	-48	207	146	0.333	0.191
NRIF-CA-L-2909	CA	10/10/2017	45	-48	236	251	0.354	0.393
NRIF-CA-L-2910	CA	11/10/2017	45	-48	243	209	0.994	1.000
NRIF-CA-L-2911	CA	16/10/2017	42	-50	240	296	0.545	0.349
NRIF-CA-L-2912	CA	16/10/2017	42	-50	261	298	0.186	0.109
NRIF-CA-L-2913	CA	22/10/2017	42	-50	170	124	0.728	0.769
NRIF-CA-L-2914	CA	01/10/2017	59	-21	225	218	0.136	0.100
NRIF-CA-L-2915	CA	01/10/2017	59	-21	218	162	0.079	0.039
NRIF-CA-L-2916	CA	01/10/2017	59	-21	230	238	0.067	0.024
NRIF-CA-L-2917	CA	02/10/2017	59	-20	215	179	0.698	0.645
NRIF-CA-L-2918	CA	02/10/2017	59	-20	215	194	0.977	0.989
NRIF-CA-L-2919	CA	03/10/2017	59	-20	212	173	0.134	0.057
NRIF-CA-L-2920	CA	04/10/2017	59	-20	195	154	0.595	0.632
NRIF-CA-L-2921	CA	04/10/2017	59	-20	190	136	0.620	0.477
NRIF-CA-L-2922	CA	04/10/2017	59	-20	233	225	0.265	0.187
NRIF-CA-L-2923	CA	04/10/2017	59	-20	231	241	0.750	0.793
NRIF-CA-L-2924	CA	05/10/2017	58	-20	201	158	0.233	0.218
NRIF-CA-L-2925	CA	05/10/2017	58	-20	194	157	0.156	0.108
NRIF-CA-L-2926	CA	05/10/2017	58	-20	231	264	0.108	0.056
NRIF-CA-L-2927	CA	08/10/2017	60	-14	239	276	0.525	0.532
NRIF-CA-L-2928	CA	08/10/2017	60	-14	219	219	0.283	0.266
NRIF-CA-L-2929	CA	09/10/2017	60	-14	210	182	0.098	0.060
NRIF-CA-L-2930	CA	09/10/2017	60	-14	229	264	0.152	0.132
NRIF-CA-L-2931	CA	11/10/2017	59	-16	199	151	0.046	0.017
NRIF-CA-L-2932	CA	11/10/2017	59	-16	209	186	0.085	0.046
NRIF-CA-L-2933	CA	14/10/2017	58	-16	213	173	0.049	0.015
NRIF-CA-L-2934	CA	15/10/2017	58	-16	220	218	0.010	0.002
NRIF-CA-L-2935	CA	15/10/2017	58	-16	234	248	0.077	0.036
NRIF-CA-L-2936	CA	16/10/2017	58	-16	208	187	0.196	0.132
NRIF-CA-L-2937	CA	16/10/2017	58	-16	236	290	0.061	0.022
NRIF-CA-L-2938	CA	01/11/2017	57	-16	206	189	0.067	0.031
NRIF-CA-L-2939	CA	02/11/2017	57	-16	216	190	0.496	0.631
NRIF-CA-L-2940	CA	03/11/2017	57	-16	207	171	0.128	0.092
NRIF-CA-L-2941	CA	04/11/2017	57	-16	203	173	0.026	0.005
NRIF-CA-L-2942	CA	05/11/2017	56	-16	207	177	0.285	0.176
NRIF-CA-L-2943	CA	08/11/2017	56	-22	200	147	0.054	0.019
NRIF-CA-L-2944	CA	08/11/2017	56	-22	180	122	0.937	0.935
NRIF-CA-L-2945	CA	09/11/2017	56	-21	217	200	0.182	0.155
NRIF-CA-L-2946	CA	09/11/2017	56	-21	192	148	0.095	0.049
NRIF-CA-L-2947	CA	10/11/2017	56	-22	193	137	0.028	0.008
NRIF-CA-L-2948	CA	10/11/2017	56	-22	207	159	0.119	0.072
NRIF-CA-L-2949	CA	10/11/2017	56	-22	205	165	0.034	0.010
NRIF-CA-L-2950	CA	10/11/2017	56	-22	203	173	0.024	0.006
NRIF-CA-L-2951	CA	11/11/2017	56	-22	190	131	0.059	0.023
NRIF-CA-L-2952	CA	12/11/2017	56	-23	202	154	0.340	0.341
NRIF-CA-L-2953	CA	12/11/2017	56	-23	199	155	0.145	0.093
NRIF-CA-L-2954	CA	12/11/2017	56	-23	217	203	0.594	0.590
NRIF-CA-L-2955	CA	13/11/2017	56	-23	202	153	0.369	0.453
NRIF-CA-L-2956	CA	13/11/2017	56	-23	230	231	0.086	0.039
NRIF-CA-L-2957	CA	14/11/2017	56	-24	206	174	0.041	0.013
NRIF-CA-L-2958	CA	14/11/2017	56	-24	205	182	0.256	0.297
NRIF-CA-L-2959	CA	16/11/2017	56	-23	192	147	0.597	0.727
NRIF-CA-L-2960	CA	16/11/2017	56	-23	221	217	0.052	0.018
NRIF-CA-L-2961	CA	18/11/2017	56	-23	194	165	0.108	0.039
NRIF-CA-L-2962	CA	18/11/2017	56	-23	203	145	0.251	0.331
NRIF-CA-L-2963	CA	19/11/2017	56	-23	207	164	0.152	0.117
IMR-NW-L-582	NW	11/09/2019	63.62	7.77	212	194	0.227	0.098
IMR-NW-L-584	NW	11/09/2019	63.62	7.77	222	188	0.079	0.022
IMR-NW-L-585	NW	11/09/2019	63.62	7.77	224	199	0.098	0.027
IMR-NW-L-591	NW	11/09/2019	63.62	7.77	192	157	0.056	0.020
IMR-NW-L-598	NW	11/09/2019	63.62	7.77	217	181	0.250	0.325

IMR-NW-L-602	NW	11/09/2019	63.62	7.77	214	194	0.049	0.018
IMR-NW-L-612	NW	11/09/2019	63.62	7.77	214	196	0.018	0.003
IMR-NW-L-679	NW	25/09/2019	63.53	4.48	233	266	0.052	0.020
IMR-NW-L-681	NW	25/09/2019	63.53	4.48	221	189	0.108	0.058
IMR-NW-L-691	NW	24/09/2019	61.41	4.45	219	191	0.030	0.005
IMR-NW-L-693	NW	24/09/2019	61.41	4.45	218	204	0.145	0.085
IMR-NW-L-695	NW	24/09/2019	61.41	4.45	248	327	0.011	0.002
IMR-NW-L-696	NW	24/09/2019	61.41	4.45	227	215	0.199	0.195
IMR-NW-L-698	NW	24/09/2019	61.41	4.45	226	212	0.253	0.204
IMR-NW-L-701	NW	24/09/2019	61.41	4.45	222	212	0.062	0.026
IMR-NW-L-702	NW	24/09/2019	61.41	4.45	220	184	0.077	0.038
IMR-NW-L-703	NW	24/09/2019	61.41	4.45	223	194	0.010	0.001
IMR-NW-L-706	NW	24/09/2019	61.41	4.45	225	229	0.027	0.007
IMR-NW-L-708	NW	25/09/2019	60	5.22	242	313	0.010	0.002
IMR-NW-L-720	NW	31/03/2019	57.77	-9.85	173	90	0.219	0.189

5. CALIBRATION OF FISH AGEING SERVICES OTOLITH AGE ESTIMATES IN PHASE 9.

Participants:
AZTI: Patricia L. Luque
IEO: Isabel Castillo, Aida Parejo, Pablo Quelle.
IU.: Saadet Karakulak
NMFS: Robert Allman
SABS: Dheeraj S. Busawon
UNICA: Piero Addis, Andrea Bellodi
UNIGE: Fulvio Garibaldi

5.1. Introduction

The Fish Ageing Services laboratory (FAS) was contracted by ICCAT GBYP in Phase 9 to provide age estimates from 2000 Atlantic bluefin tuna otolith samples. A calibration exercise was performed with the objective of ensuring that there was no systemic bias in age readings performed by SCRS experts compared to FAS age estimates. This is the second calibration performed with FAS readings, since another one has already been done with the readings carried out by FAS in ICCAT GBYP Phase 7. In the first calibration, a one-year bias in the count of bands in older specimens was found, with a lower count by FAS compared to the rest of the laboratories starting from 10-13 years of age. This bias appears to be due to the fact that FAS counts the bands in a different area of the ventral arm of the otolith (Rodriguez-Marin et al. 2020a). To address this issue a second calibration exercise was carried out ensuring that all parties were following the ICCAT reviewed reading protocol (Rodriguez-Marin et al., 2020b). This paper presents the result of the second calibration exercise which will serve as quality control monitoring for ageing consistency. In addition, the samples used in the calibration will enlarge the new reference collection.

5.2. Material and methods

Seven research centers have participated in this task, four from Europe (AZTI; University of Cagliari, UNICA; University of Genoa, UNIGE and Spanish Institute of Oceanography, IEO), one from Turkey (Istanbul University, IU), one from Canada (St. Andrews Biological Station, SABS) and one from USA (National Marine Fisheries Service, NMFS). The collaboration of these laboratories is

necessary for the participation of researchers from both sides of the Atlantic. The researchers involved have experience in direct ageing of Atlantic bluefin tuna and contribute with age-length data to the assessment of this species. Furthermore, to assess the effectiveness of the new reading protocols, two inexperienced readers participated in the calibration.

Laboratories read a sub-sample of 10% of the otoliths aged by FAS in Phase 9 GBYP, to determine a measure of inter-laboratory precision. Based on the 1st calibrations results (Rodriguez-Marin et al., 2020a), this subsample favored larger specimens (>200 cm straight fork length). However, all sizes were still represented (Figure 28). In the ageing precision analysis, IEO and AZTI aged using the physical otolith sections while the rest of the laboratories involved used digital images as they are easier to share among partners, and allowed, to a limited extent, the comparison between both sets of readings. Additionally, both sets, physical sections and digital images, will be added to the new reference collection using the consensus age obtained from expert readers.

A modal reading has been used: "Mode Experts" (Mod_E) for the readings of all laboratories including the readings of both physical otolith sections and digital images but not including the readings of the two inexperienced readers. FAS used live readings and for the rest of the readers the reading mode is indicated at the end of the name (reader acronym name_L for live and reader name_P for pictures).

According to the reviewed protocol, age estimates consisted in the counting of opaque bands using transmitted light. The preparations, consisting of sections of physical otoliths, were read twice. A third and final band count was completed if the first two band estimations differ, to produce the final band estimate. All band counts were performed blindly without knowledge of fish size or catch date. The final band estimate was done with knowledge of the first two counts. Band counts were transformed to ages by applying the procedure described in Rodriguez-Marin et al. (2020b).

A reading form was provided and the following information was recorded for each sample: number of annual bands (opaque), ventral arm edge type (wide translucent, narrow translucent or opaque), edge confidence (1= no confident; 2= confident in completeness and not with the type and 3= confident), sample readability code (1= pattern present-no meaning, 2= pattern present-unsure with age estimate, 3= good pattern present-slightly unsure in some areas, 4= good pattern-confident with age estimate), reading date and notes with observations about the sample. This form also included the measurement of the first five annual bands to see if there are differences between readers and to have a check of the readers' reading criteria. Annual band measurements during otolith reading were done following the "measurement line" defined in Rodriguez-Marin et al. (2020b).

Precision was estimated through Coefficient of Variation (CV), Average Percent Error (APE), tests of symmetry and age bias plots (Campana et al., 1995; McBride, 2015). Annotated images and annual band measurements were produced for control quality of age estimates.

The Covid-19 pandemic induced a delay in the shipment and delivery of the physical otolith sections and have restricted the use of laboratories and equipment necessary for sample access and analysis.

5.3. Results and discussion

In terms of precision, age estimates from FAS and SCRS readers were within the acceptable limits (CV<10) except for two expert readers. Despite the good precision, the symmetry test indicated a bias for all expert readers. Interestingly, the non-expert readers showed no bias and were within the acceptable level of precision (Table 17).

Marginal edge agreement was high between readers and FAS, reaching an average of 50% when all three edge types (O, NT and WT) are used, and 75% when only opaque and translucent edge types are taken into account (table 1 and Figure 29). The high level of agreement supports the use of transmitted light for band counting of otolith sections (Rodriguez-Marin et al., 2020b). Readers rated the readability of images as good and had high confidence in edge type assignment (Table 17).

The use of transmitted light, as compared to reflected light, not only improves agreement on the marginal edge type, but also allows a clearer view of the entire otolith section, including the dorsal arm. However, readers who have used reflected light to read the sections state that in the inner part, at the end of the ventral arm, the bands are very clearly visible in old specimens, whereas with transmitted light this final area of the ventral arm sometimes appears hard to interpret, while the bands are visible in the outer area.

The distribution plots of differences between band counts and bias plots show that in general expert readers count more bands than FAS from 10 annual bands onwards (Figure 30, Figure 31, Figure 32 and Figure 33). There are only three readers that show practically no bias up to specimens with more than 13 bands and two of them are precisely the inexperienced ones.

The measurements of the first annual bands show that there are two readers that are interpreting the bands differently from the rest of the readers and they are precisely the two readers with the lowest

accuracy and CV higher than 10 (Table 17 and Figure 34). The misinterpretation of the first bands influences the total band count of the sample and final age estimation.

The influence of sample quality (with respect to readability code and edge confidence) on the differences between the band counting of FAS and the other readers was analyzed for specimens with more than 10 bands. No trend was observed with either the best or the worst quality samples. The differences in band counts occur for samples with an average readability code of around 2.6. These differences are mainly due to a different band count at the end of the ventral arm, with a higher band count in the inner part of the ventral arm compared to the outer part (Figure 35).

A survey on the use of each reading Zone within the otolith section was conducted for each reader (Figure 36). Results show that all readers mainly use Zone 2 of the ventral arm (agreed in the reading protocol). They use Zone 3 to corroborate or check the continuity of the opaque bands over the entire width of the ventral arm, especially in the first 3-4 first annual bands. Zone 1 is used to double-check when the bands are not seen very clearly in Zone 2 or to check the total number of bands, taking into account that in this Zone 1 the count is underestimated.

Five readers (PLL, RAL, DBU, SKA and FGA) follow the same reading pattern; using Zone 1 as double-checking of the number of bands in Zone 2; FGA corroborates the number of bands in Zone 1, especially in large specimens; PLL considers the number of bands counted in Zone 1 as the minimum number it expects to count in Zones 2 and 3; RAL uses the Zone 2 reading for the first 4-5 bands and tries to find continuity in Zone 3, thereafter he counts in Zone 2.

ABE and PAD use Zone 1 only to double check the other two Zones, Zone 2 for reading and measuring and Zone 3 as the main double-checking zone. ICG almost never uses Zone 1, only if it has a lot of doubts on the reading done in Zone 2. APL uses Zone 1 when Zone 2 is unclear when reading the last bands. ERM almost never uses Zone 3, except for the first annuli.

FAS uses all zones of the otolith section and uses Zone 2 to take the third reading when there is a disagreement of more than 1 band between the first and second readings.

In order to compare the age estimates obtained in the present and previous calibrations with the growth curves of both stocks, data from the experts mode (Mod_E) and FAS age estimates were fitted to the Von Bertalanffy equation and plotted together with growth functions from the eastern stock, Cort (1991) based on 1st dorsal fin spine reading and length frequency analysis, and from the western stock, Ailloud et al., (2017) based on otolith readings and tagging. Using the growth models of both stocks at ages 0 to 20 years, which are the ages covered in both calibrations, and where there are practically no differences between the both stocks growth models, it is observed that the fit of the expert mode (Mod_E) is coincident with the growth functions of both stocks, while the fit of the FAS readings, diverges from 10 years and shows from this age onwards higher length-at-age values than

those of the stock growth functions (Figure 37). These results are not entirely conclusive, since the fit to the length-at-age data is sensitive to the extreme values of the oldest specimens being well represented, which is not the case.

To try to determine which of the two readings is more appropriate, the strong 2003 cohort (ICCAT, 2018) was used to see which of the two readings would identify it better. For this purpose, the abundance per year class of the batch 1 and batch 2 specimens (4000 samples) read by FAS in previous phases of the GBYP was obtained. The abundance of these samples was also obtained from the Mod_E readings by applying a correction vector. The ageing bias vector was produced using data from present and previous calibrations. A vector of bias-corrected aged otoliths was created by taking the weighted average of the FAS band counts associated with each band count group of the corresponding Mod_E. This vector was applied only to otoliths with more than 10 bands (Table 18). The cohort tracking analysis showed that the FAS readings identify the 2004 cohort as the most abundant, while the Mod_E readings identify the 2003 year class as the most abundant. The year classes preceding and following the most abundant ones estimated by FAS and Mod_E also showed some abundance (Figure 38). These results indicate that Mod_E readings are more appropriate.

Residual plots were made comparing the growth curves of both stocks predicted ages to readers age estimates. A bias in the residual plots for fish measuring more than 250 cm SFL was observed for all readers, including FAS. This bias is slightly more pronounced with the Richards model than with the Von Bertalanffy model (Figure 39, Figure 40 and Figure 41). A similar divergence from the validated samples from Neilson and Campana (2008) was found with a bias at older ages compared to the growth curves from Ailloud et al. (2017), specifically with the Richards model (Figure 42).

5.4. Conclusion

There are differences in band counts between ICCAT SCRS expert readers and FAS readings. These differences start from specimens with more than 10 bands and are more pronounced for older specimens. The results of the present calibration (GBYP Phase 10) are very similar to those of the previous one (GBYP Phase 9). These differences in readings appear to be due to the fact that FAS uses the entire section of the otolith to count annual bands, whereas ICCAT readers focus on the inner part of the ventral arm. Analyses conducted to establish which reading is more appropriate, growth

function estimation and cohort follow-up analysis, seem to indicate that ICCAT readers are more accurate than FAS readers.

References

Ailloud, Lisa E., Matthew V. Lauretta, Alex R. Hanke, Walter J. Golet, Robert J. Allman, Matthew R. Siskey, David H. Secor, and John M. Hoenig. 2017. Improving growth estimates for Western Atlantic bluefin tuna using an integrated modeling approach. Fish Res, 191: 17-24.

Campana, S.E.; Annand, M.C.; McMillan, J.I. 1995. Graphical and statistical methods for determining the consisteny of age determinations. Transactions of the American Fishery Society. 124:131-138.

Cort, J. L. (1991). Age and growth of bluefin tuna Thunnus thynnus (L.) of the Northeast Atlantic. ICCAT Collective Volume of Scientific Papers 35, 213–230.

ICCAT. 2018. Report of the 2017 ICCAT bluefin stock assessment meeting. Col. Vol. Sci. Pap. ICCAT, 74 (6): 2372-2535.

McBride. R.S. 2015. Diagnosis of paired age agreement: a simulation of accuracy and precision effects. ICES J Mar Sci; doi:10.1093/icesjms/fsv047.

Neilson, J. D. & Campana, S. E. (2008). A validated description of age and growth of western Atlantic bluefin tuna (Thunnus thynus). Canadian Journal of Fisheries and Aquatic Sciences 65, 1523–1527. doi: 10.1139/F08-127

Rodriguez-Marin E., Addis P., Allman R., Bellodi A., Busawon D., Garibaldi F., Luque, P.L. and Quelle P. 2020a. Calibration of the Fish Ageing Services readings, carried out in GBYP Phase 7, to estimate age of bluefin tuna from the eastern Atlantic stock. Standing Committee on Research and Statistics Doc. SCRS/2020/068.

Rodriguez-Marin E., Quelle P., Addis P., Alemany F., Bellodi A., Busawon D., Carnevali O., Cort J.L., Di Natale A., Farley J., Garibaldi F., Karakulak S., Krusic-Golub K., Luque P.L., and Ruiz M. 2020b Report of the ICCAT GBYP international workshop on Atlantic bluefin tuna growth. Collect. Vol. Sci. Pap. ICCAT, 76(2): 616-649

Table 17. Diagnosis of paired band counting agreement for all data (n = 200). Precision indices: CV = Coefficient of Variation, APE = Average Percent Error, Evans-Hoenig and Bowker symmetry tests, symmetry bias (*, ** = significant differences in one or both symmetry tests, $p < 0.01$), marginal edge type agreement with FAS (%) using three edge types (O, NT and WT) and two edge types (O, T), and mean readability score and mean edge type confidence by reader. Reader's acronyms are explained in material and methods section.

Readers comparison	CV	APE	Evans-Hoenig (p)	Bowker (p)	Symmetry bias	Edge 3 type agreement with FAS (%)	Edge 2 type agreement with FAS (%)	Mean sample readability by reader	Mean edge type confidence by reader
FAS - ModE	5,8	4,1	0,0005	0,0921	*	49	74	2,9	2,5
FAS - ERM_L	6,5	4,6	0,0000	0,0098	* *	40	71	2,4	2,5
FAS - PLL_L	7,2	5,1	0,0025	0,1449	*	44	83	2,6	2,6
FAS - ABE_P	8,9	6,3	0,0053	0,0621	*	51	88	3,0	2,6
FAS - PAD_P	16,6	11,7	0,0000	0,0001	* *	49	79	2,9	2,4
FAS - DBU_P	7,1	5,0	0,0044	0,0859	*	45	74	2,6	2,4
FAS - SKA_P	11,5	8,1	0,0033	0,1292	*	21	49	3,1	2,4
FAS - RAL_P	6,8	4,8	0,0000	0,0429	*	50	79	3,0	2,2
FAS - FGA_P	7,5	5,3	0,0005	0,0624	*	47	88	3,0	2,5
FAS - ICG_P (non expert)	7,8	5,5	0,0127	0,1044		36	72	3,0	2,7
FAS - APL_P (non expert)	7,8	5,5	0,7137	0,4196		47	69	3,1	2,5

Table 18. Band counts from present and previous calibrations obtained from 423 individuals and resulting differences in bands counting between FAS and Mod_E. The ageing bias vector applied to otoliths with more than 10 bands appears framed (A.b.v.).

Band counting from Mod_E \ Band counting from otoliths aged by FAS	0	1	2	3	4	5	6	7	8	9	10	11	12	13	14	15	16	A.b.v.
0	0,00	0,00	0,00	0,00	0,00	0,00	0,00	0,00	0,00	0,00	0,00	0,00	0,00	0,00	0,00	0,00	0,00	**0,00**
1	0,00	0,77	0,46	0,00	0,00	0,00	0,00	0,00	0,00	0,00	0,00	0,00	0,00	0,00	0,00	0,00	0,00	**1,23**
2	0,00	0,03	1,17	1,14	0,00	0,00	0,00	0,00	0,00	0,00	0,00	0,00	0,00	0,00	0,00	0,00	0,00	**2,34**
3	0,00	0,00	0,20	2,50	0,27	0,00	0,00	0,00	0,00	0,00	0,00	0,00	0,00	0,00	0,00	0,00	0,00	**2,97**
4	0,00	0,00	0,00	0,00	2,00	2,33	0,20	0,00	0,00	0,00	0,00	0,00	0,00	0,00	0,00	0,00	0,00	**4,53**
5	0,00	0,00	0,00	0,00	0,57	3,81	0,57	0,00	0,00	0,00	0,00	0,00	0,00	0,00	0,00	0,00	0,00	**4,95**
6	0,00	0,00	0,00	0,00	0,00	1,19	3,43	1,00	0,38	0,00	0,00	0,00	0,00	0,00	0,00	0,00	0,00	**6,00**
7	0,00	0,00	0,00	0,00	0,00	0,36	1,29	4,00	1,14	0,00	0,00	0,00	0,00	0,00	0,00	0,00	0,00	**6,79**
8	0,00	0,00	0,00	0,00	0,00	0,00	0,00	1,75	3,60	0,90	2,00	0,00	0,00	0,00	0,00	0,00	0,00	**8,25**
9	0,00	0,00	0,00	0,00	0,00	0,00	0,00	0,61	2,43	4,70	0,87	0,00	0,00	0,00	0,00	0,00	0,00	**8,61**
10	0,00	0,00	0,00	0,00	0,00	0,00	0,00	0,00	0,33	3,38	3,33	1,83	1,00	0,00	0,00	0,00	0,00	**9,88**
11	0,00	0,00	0,00	0,00	0,00	0,00	0,00	0,21	0,48	1,09	2,12	4,33	1,45	0,79	0,00	0,00	0,00	**10,48**
12	0,00	0,00	0,00	0,00	0,00	0,00	0,00	0,00	0,00	0,41	1,14	2,75	5,45	1,48	0,32	0,00	0,00	**11,55**
13	0,00	0,00	0,00	0,00	0,00	0,00	0,00	0,00	0,00	0,00	0,61	1,33	2,91	5,91	1,27	0,45	0,00	**12,48**
14	0,00	0,00	0,00	0,00	0,00	0,00	0,00	0,00	0,00	0,00	0,00	1,05	2,86	6,81	2,00	0,00	0,00	**12,71**
15	0,00	0,00	0,00	0,00	0,00	0,00	0,00	0,00	0,00	0,00	0,91	0,00	1,09	2,36	5,09	1,36	2,91	**13,73**
16	0,00	0,00	0,00	0,00	0,00	0,00	0,00	0,00	0,00	0,00	0,00	0,00	0,00	2,17	2,33	5,00	5,33	**14,83**
17	0,00	0,00	0,00	0,00	0,00	0,00	0,00	0,00	0,00	0,00	0,00	0,00	0,00	0,00	3,50	3,75	8,00	**15,25**
18	0,00	0,00	0,00	0,00	0,00	0,00	0,00	0,00	0,00	0,00	0,00	0,00	0,00	0,00	0,00	0,00	16,00	**16,00**

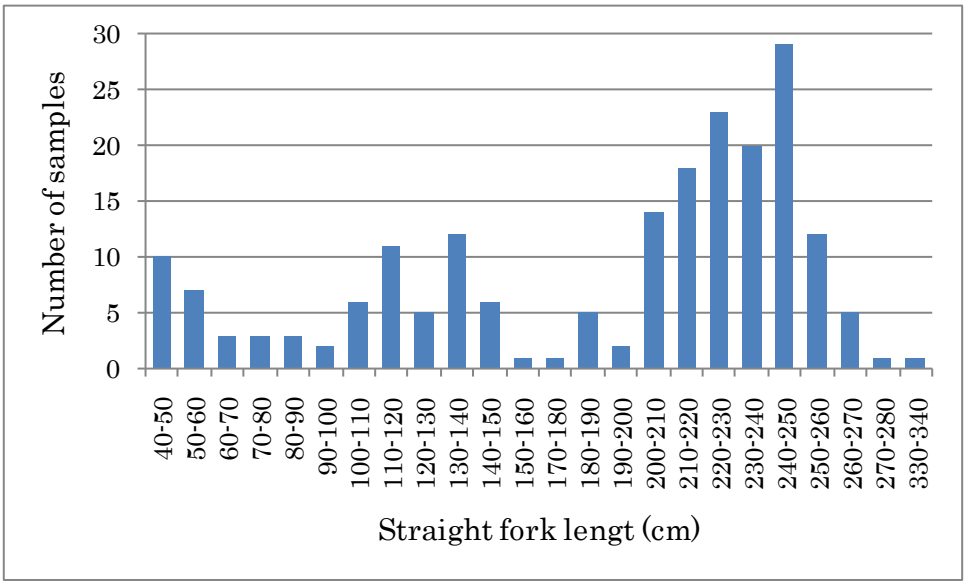

Figure 28. *Length distribution of analyzed specimens used in the calibration by 10 cm size bin.*

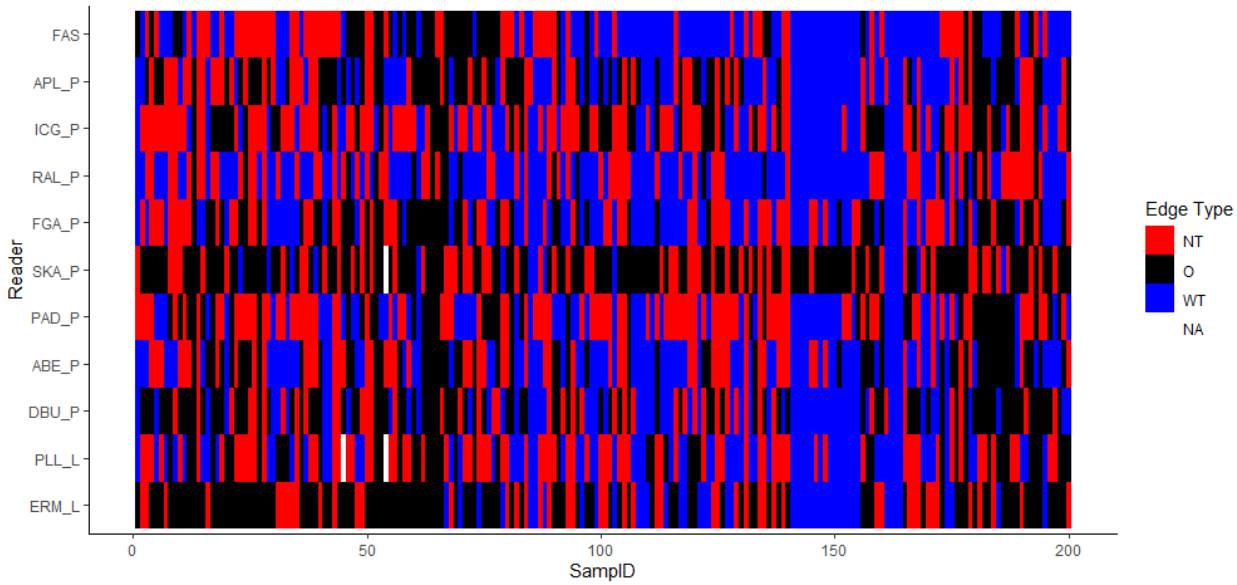

Figure 29. *Tile plot showing otolith marginal edge type assignment (NT= narrow translucent, Opaque= O, WT= wide translucent, NA= missing data) by sample for each reader.*

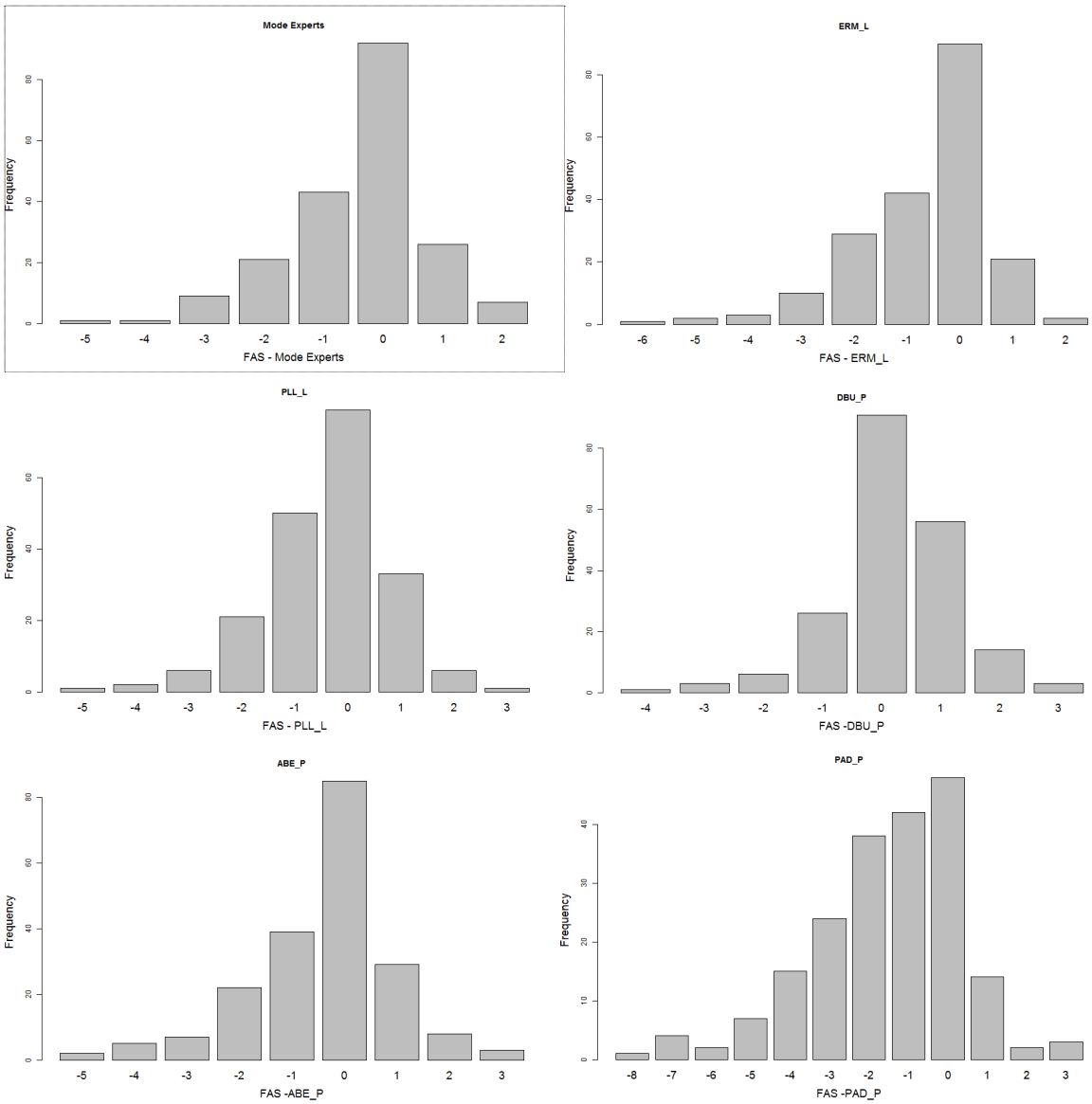

***Figure 30**. Band count difference distributions between FAS and experts mode (boxed figure), and between FAS and each reader.*

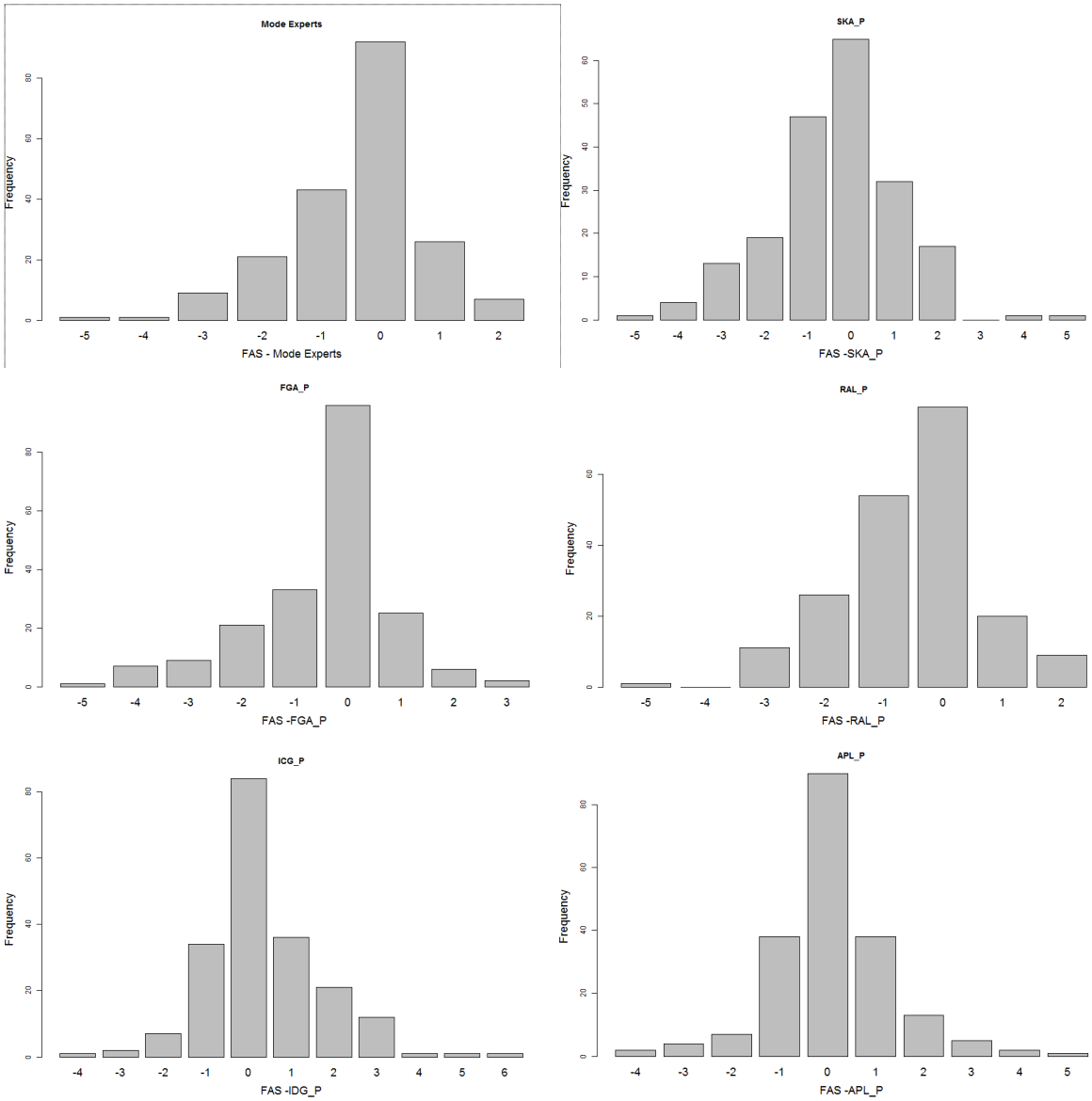

***Figure 31**. Band count difference distributions between FAS and experts mode (boxed figure), and between FAS and each reader. The last two figures at the bottom correspond to inexperienced readers.*

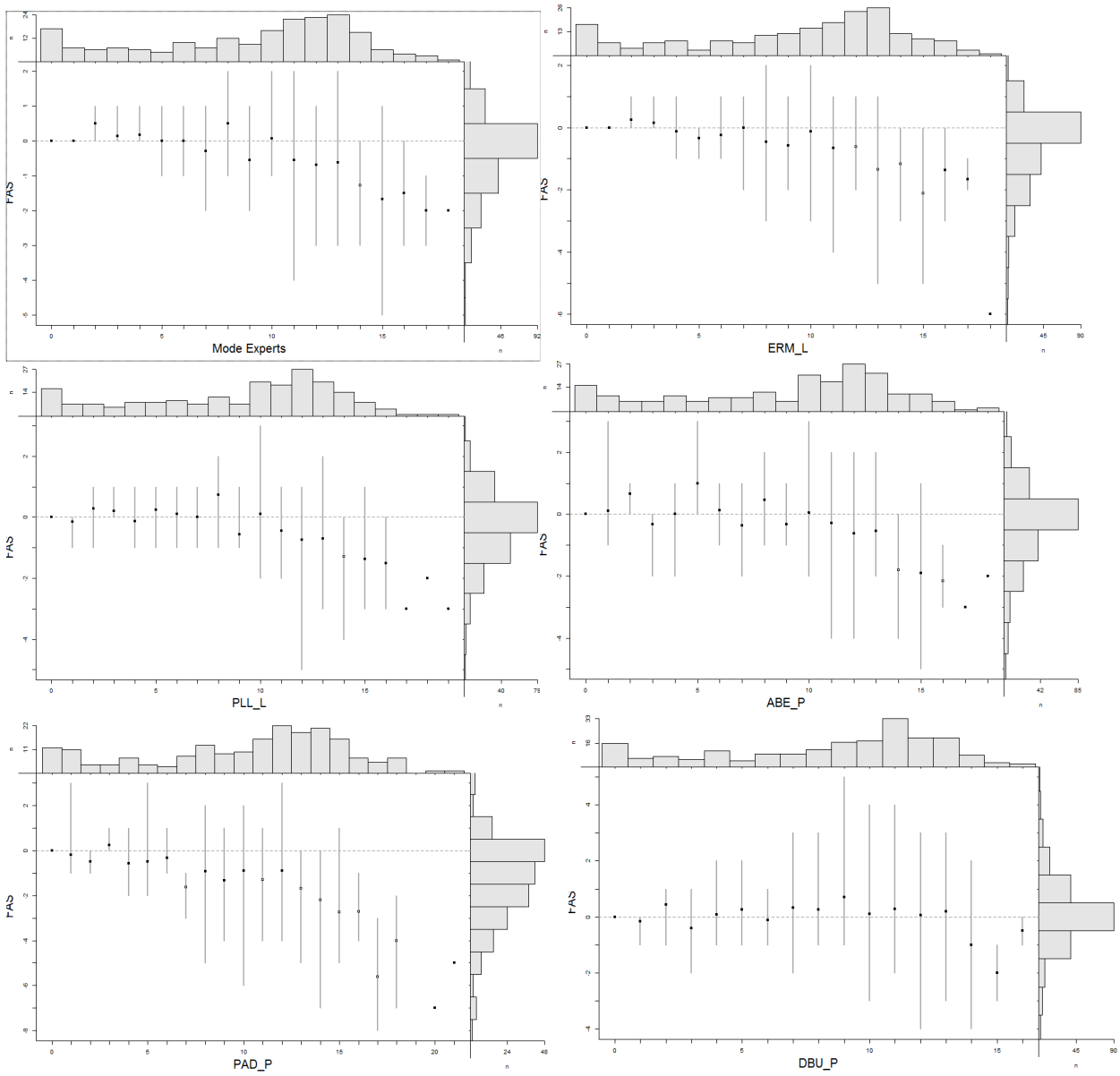

Figure 32*. Band count bias graphs between FAS and each reader (experts mode in the boxed figure) (FAS band count minus reader band count). The number of samples per band count and band differences in the readings appears at the top and right side of each graph.*

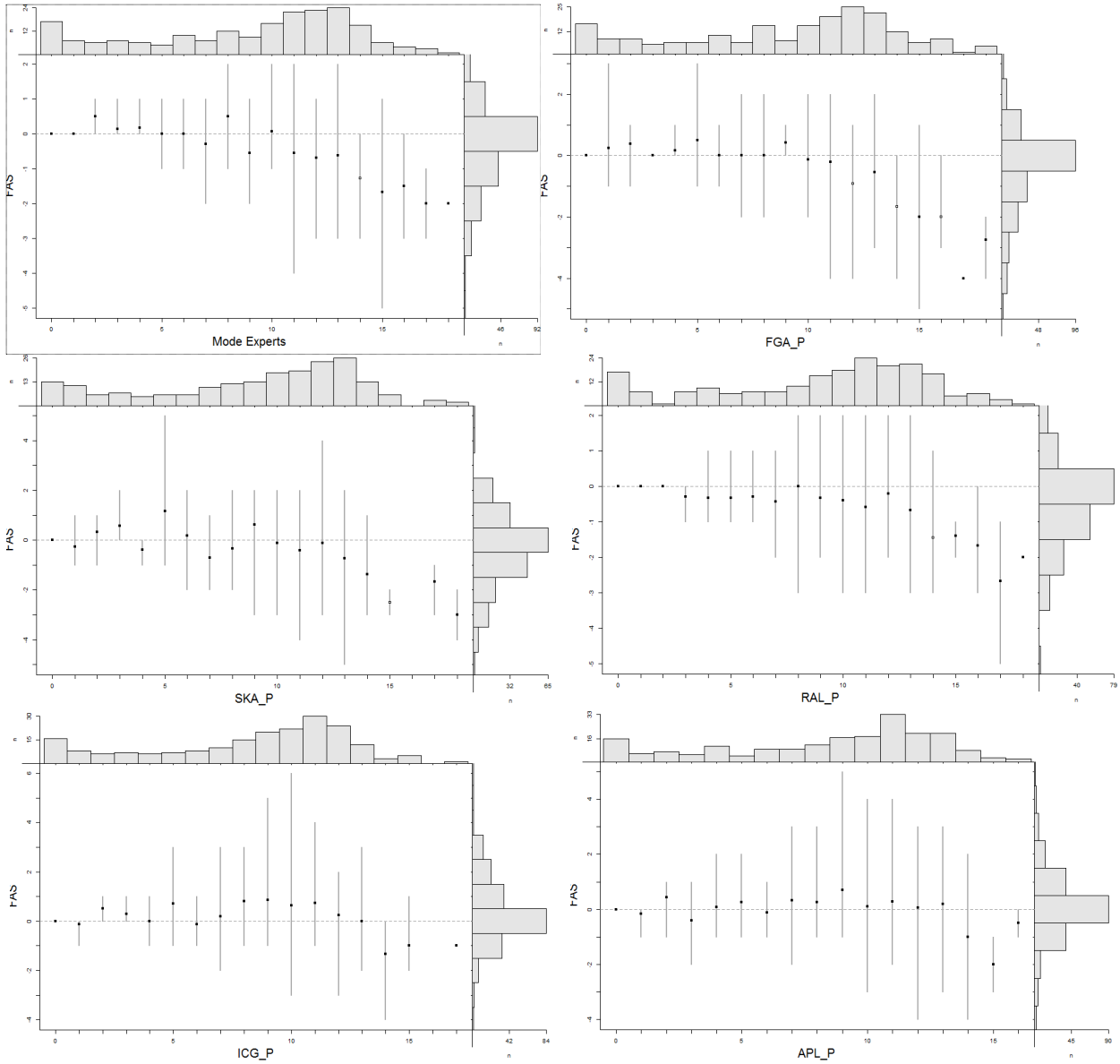

Figure 33*. Band count bias graphs between FAS and each reader (experts mode in the boxed figure) (FAS band count minus reader band count). The number of samples per band count and band differences in the readings appears at the top and right side of each graph.*

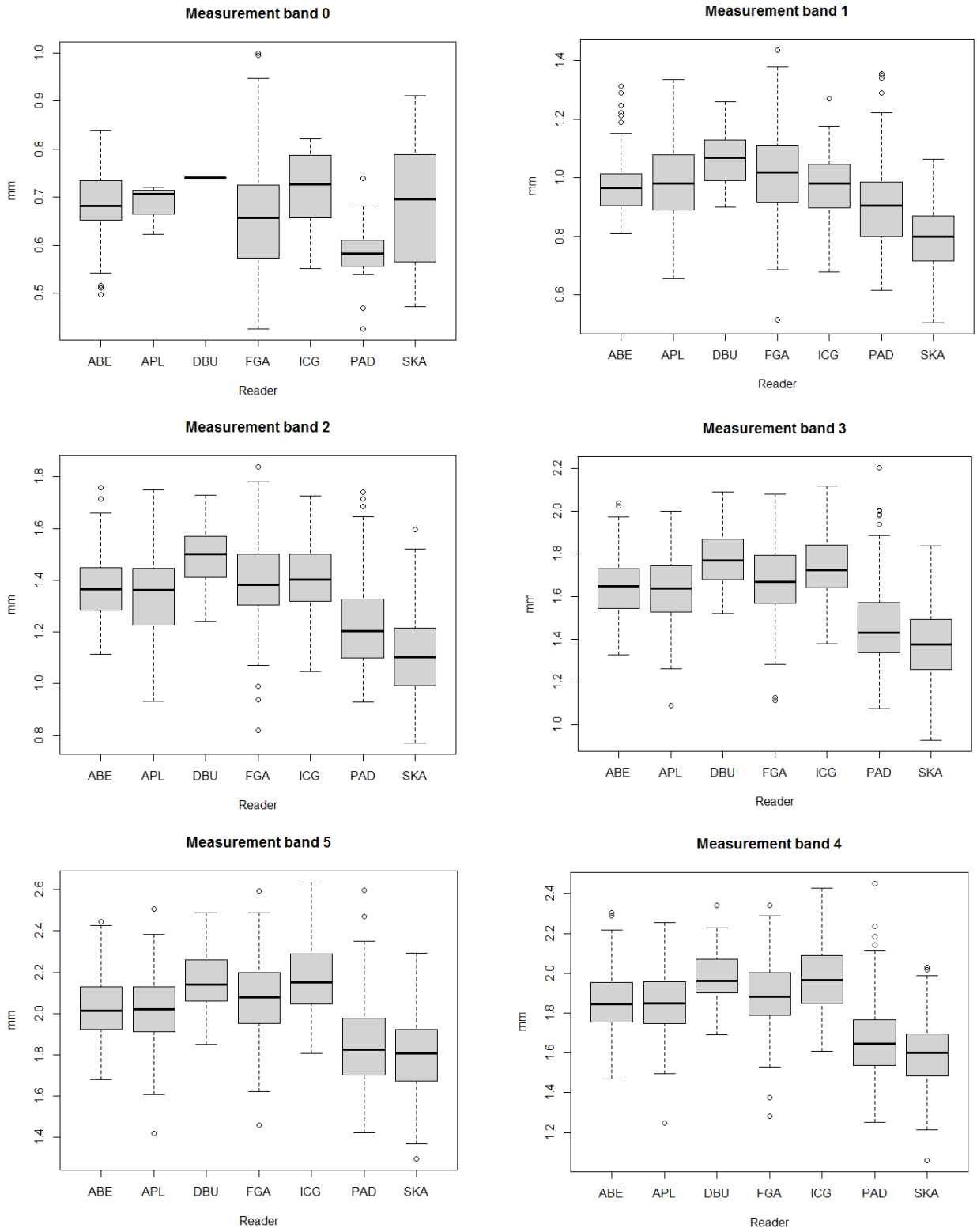

Figure 34. *Box-plot of the measurements of the first five annual and innermost sub-annual bands by some readers.*

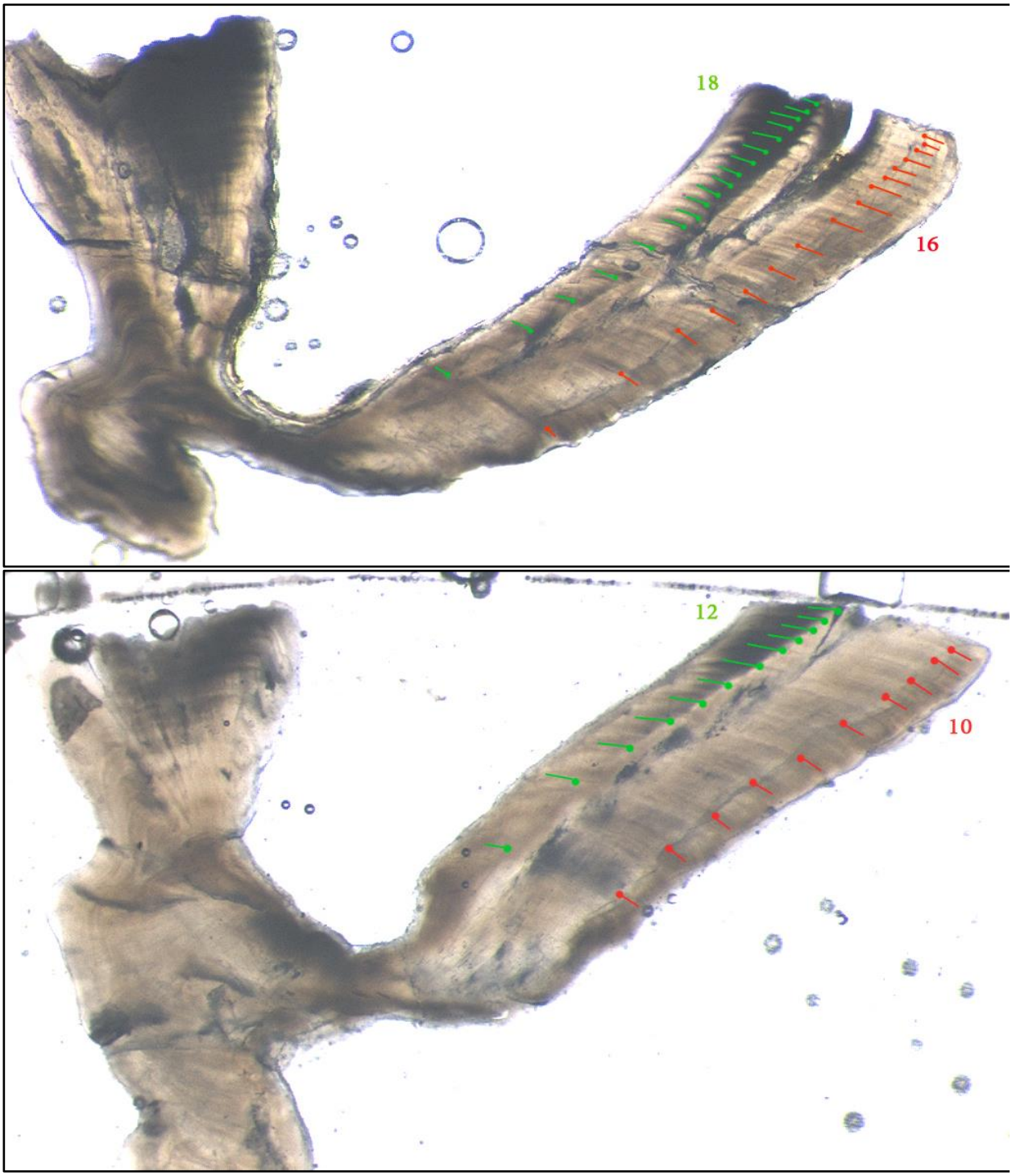

Figure 35*. Images of bluefin tuna otolith sections with different band counts on the inner and outer part of the ventral arm.*

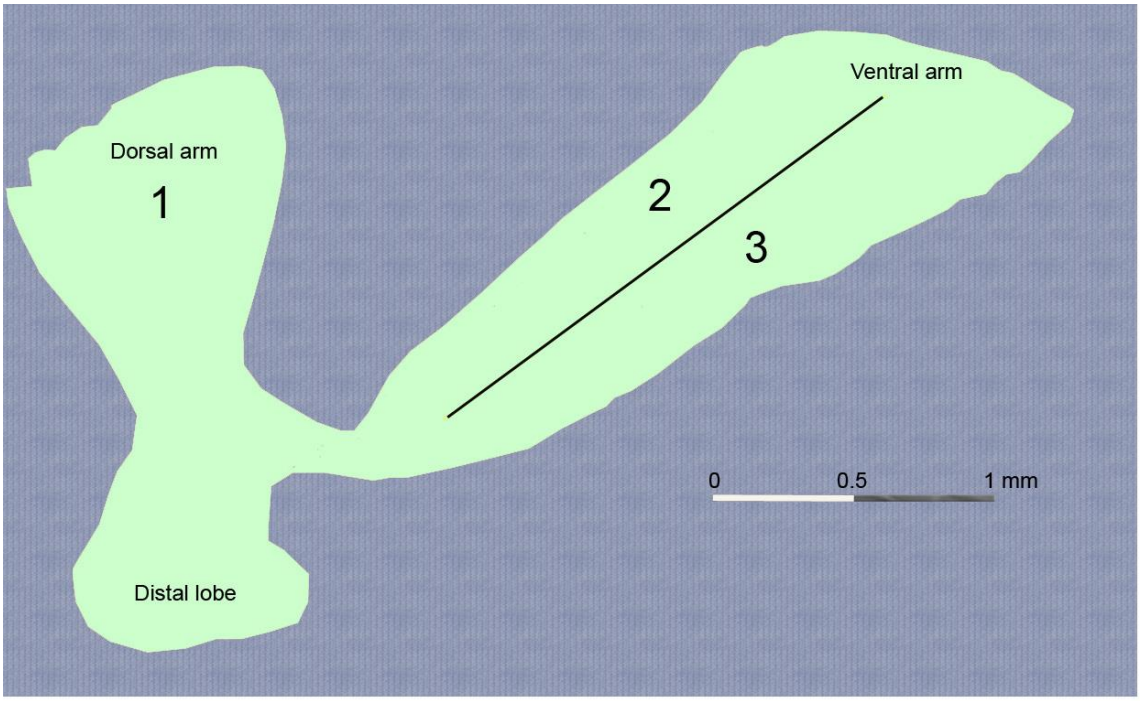

	Use of each reading zone		
Reader	**Zone 1**	**Zone 2**	**Zone 3**
ERM_L	4	1	5
PLL_L	2	1	3
RAL_P	2	1	3
DBU_P	2	1	3
ABE_P	2	1	2
PAD_P	2	1	2
FGA_P	2	1	3
SKA_P	2	1	3
ICG_P	5	1	3
APL_P	4	1	3
FAS	1	1	1

1. Always. The main zone used for reading
2. To double check the band counting in zone 2
3. Very often to corroborate the nº bands throughout the ventral arm
4. Eventually. If bands are not clearly visible in zone 2
5. Hardly ever

Figure 36*. Survey on the use of the different zones of an otolith section for band counting. Top: reading zones. Middle: survey results. Below: coding of the frequency of zones use.*

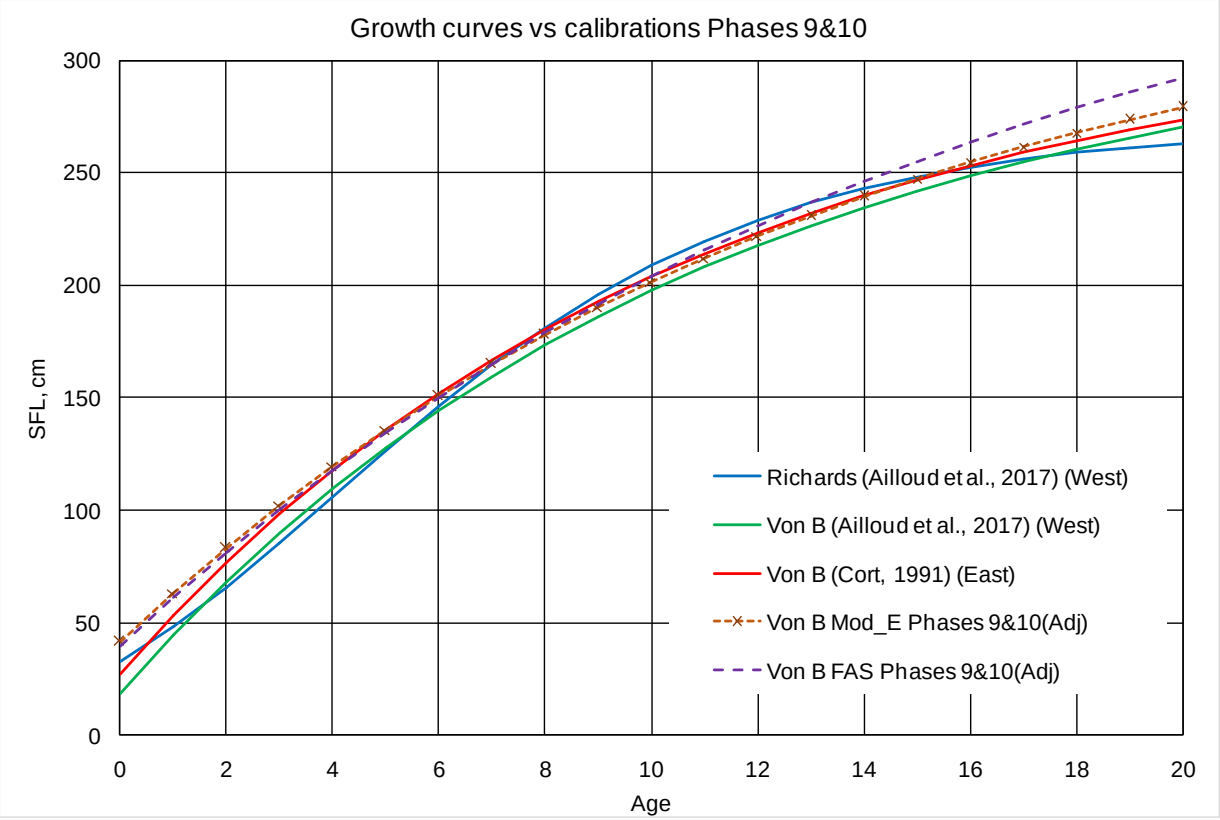

***Figure 37**. Comparison of age estimates obtained in the present and previous calibrations (Phases 9&10) with the growth curves of both stocks.*

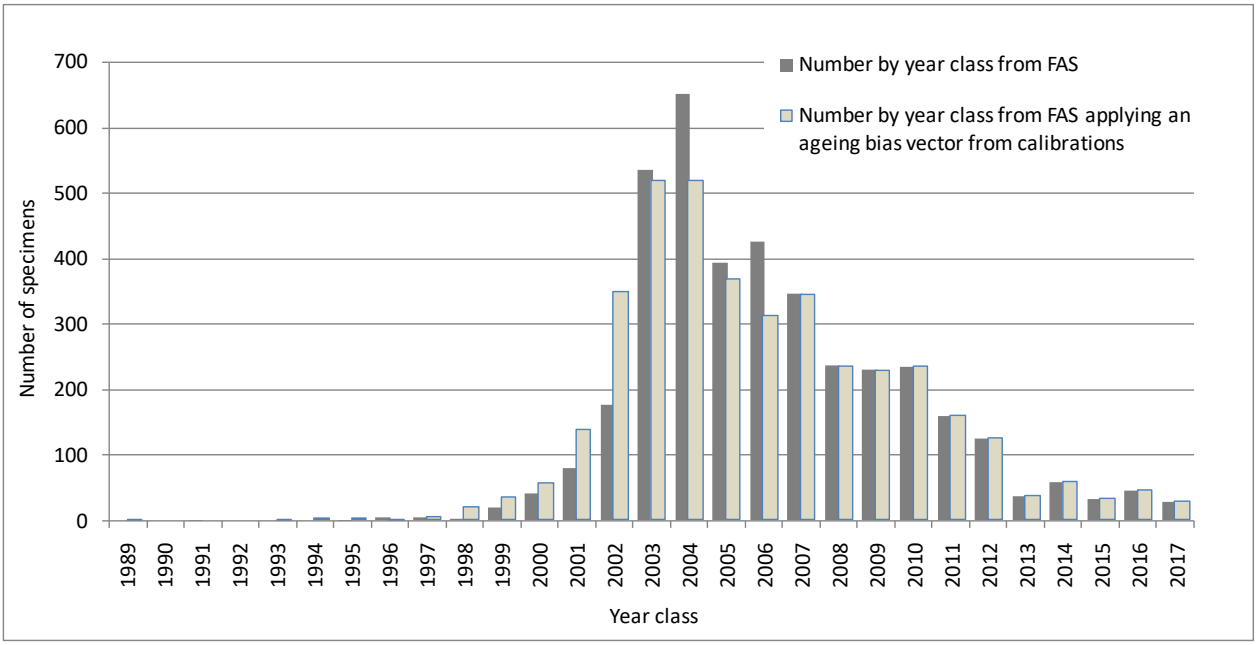

***Figure 38**. Abundance per year class of samples read by FAS and from Mod_E readings by applying a correction vector obtained from calibrations.*

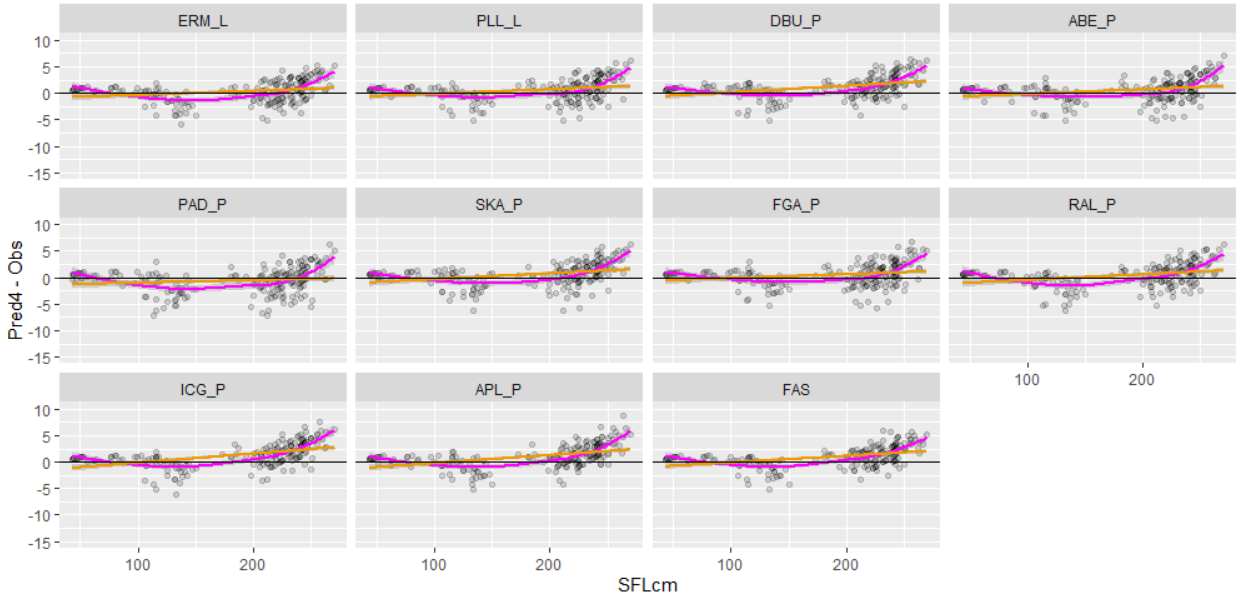

Figure 39. *Residual plots comparing Cort et al. (1991) bluefin tuna Von Bertalanffy predicted ages to reader age estimates (residuals= predicted – observed). Orange lines represent linear regressions and purple lines represent smoothers (Loess) fit to the data using the geom_smooth function in ggplot2.*

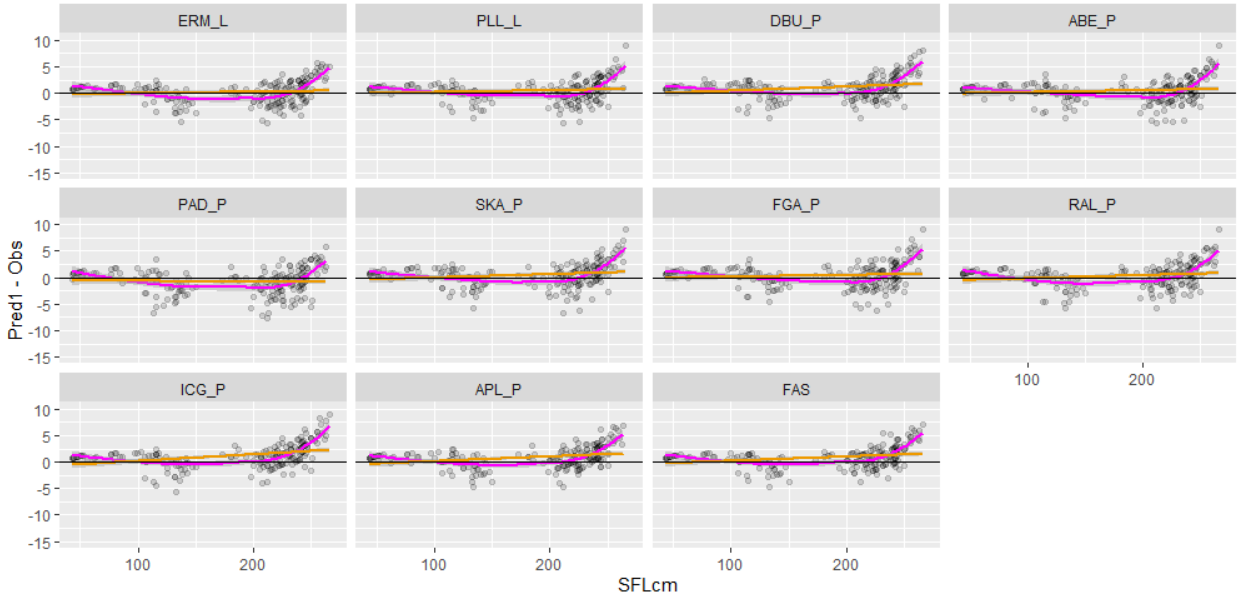

Figure 40. *Residual plots comparing Ailloud et al. (2017) bluefin tuna Richards predicted ages to reader age estimates (residuals= predicted – observed). Orange lines represent linear regressions and purple lines represent smoothers (Loess) fit to the data using the geom_smooth function in ggplot2.*

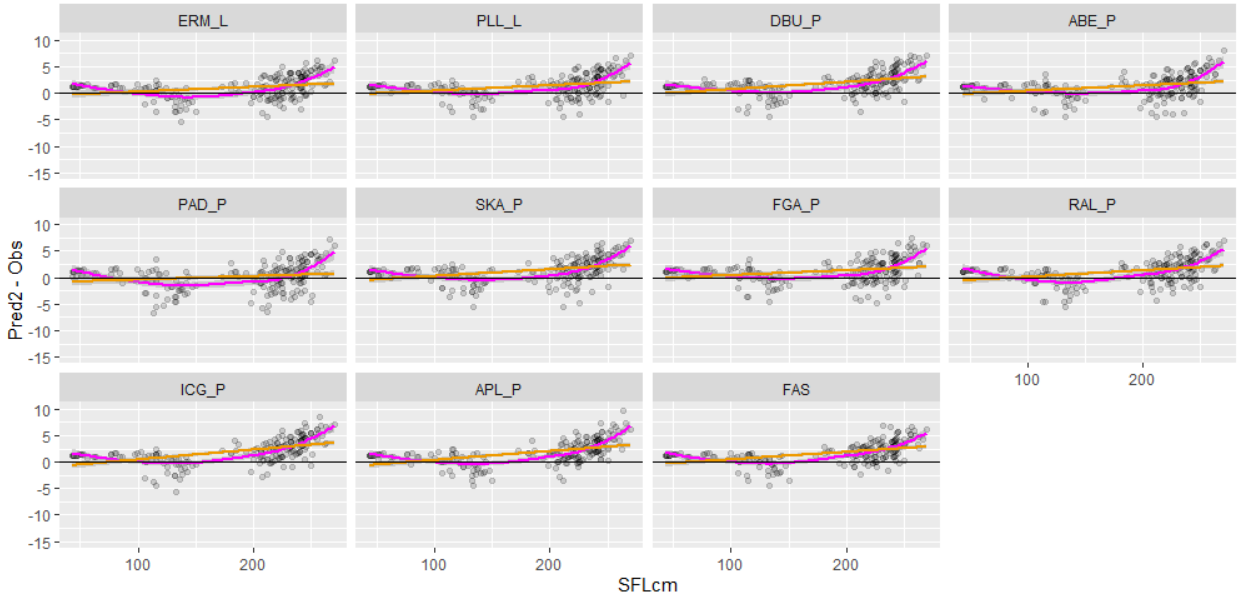

Figure 41. *Residual plots comparing Ailloud et al. (2017) bluefin tuna Von Bertalanffy predicted ages to reader age estimates (residuals= predicted – observed). Orange lines represent linear regressions and purple lines represent smoothers (Loess) fit to the data using the geom_smooth function in ggplot2.*

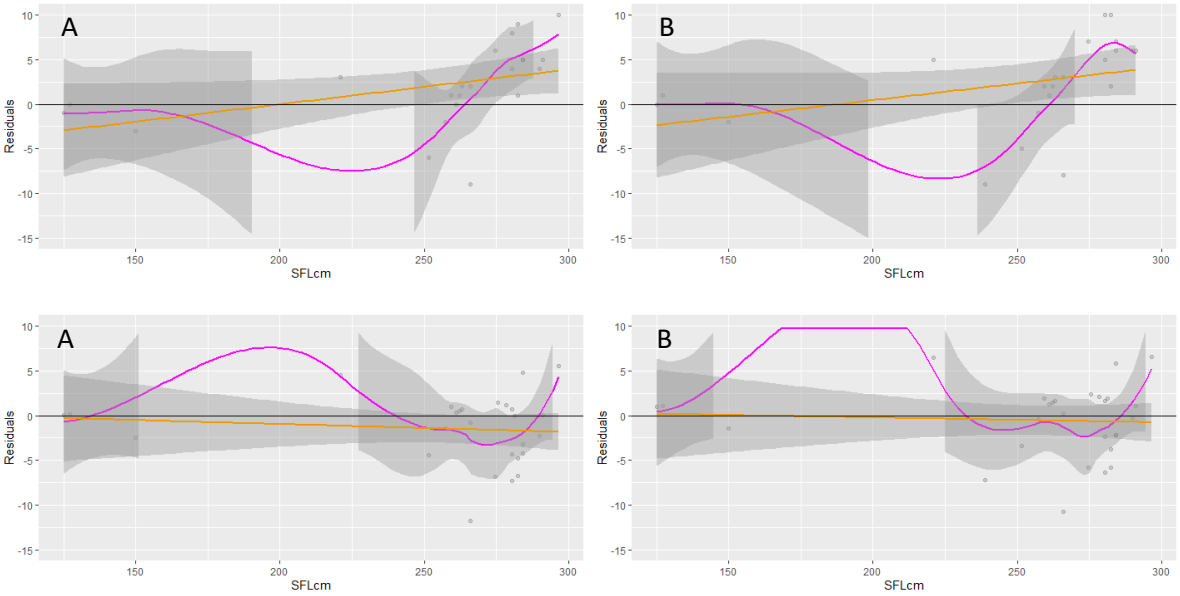

Figure 42. *Residual plots comparing Ailloud et al. (2017) bluefin tuna Richards (top row) and Von Bertalanffy (bottom row) predicted ages to primary reader age estimates (A) and radiocarbon age estimates(B) (residuals= predicted – observed). Orange lines represent linear regressions and purple lines represent smoothers (Loess) fit to the data using the geom_smooth function in ggplot2.*

6. DETERMINATION OF THE OTOLITH EDGE TYPE DEPOSITION ALONG THE YEAR CYCLE.

Task leader: Enrique Rodriguez-Marin (IEO)

Participants:
AZTI: Patricia L. Luque
IEO: Isabel Castillo,
SABS: Dheeraj S. Busawon, Nathan Stewart.

6.1. Introduction

A widely used semi-direct validation method consists of observing the evolution of the marginal areas of calcified structures over time. It is often used to validate seasonal deposition. However, the study of the type of marginal edge and its growth throughout the year is also essential to make the appropriate age adjustment, which consists of converting the number of annual bands found in the structure into ages. To do this, it is necessary to identify properly the type of edge and, in relation on the date of birth and collection, obtain the adjusted age of the specimen. The study of the edge type deposition requires observations throughout the year and the observation of a large number of samples (Campana, 2001; Panfili et al., 2002).

In the case of Atlantic bluefin tuna it is difficult to assess the nature of the otolith edge: opaque vs. translucent (Secor et al., 2014; Busawon et al., 2015; Rodriguez-Marin et al., 2020). The difficulty is related to the visualization of a band partial increase affected by refraction and by the reflection of light at the marginal edge and on the curved surface of the otolith. In order to reduce this source of inconsistency we will use otolith samples with consensus on edge type and number of annual band and samples with high readability pattern and edge type confidence. In the present study, we measured the marginal growth of sagittal otoliths of Atlantic bluefin tuna and verified the formation of marginal edge type throughout the year.

6.2. Material and methods

The timing of marginal band formation was assessed by examining the ventral arm edge. Edge type was identified as of a certain type when it occupies more than 50% of the edge across the width of the ventral arm. Dorsal arm was also used to corroborate this edge type and with the same criterion of 50%.

Marginal increment analysis (MIA) consisted of measuring the distances separating the latest marks at the edge of the otolith. The axis of measurement and the description of the marks being used need to be rigorously standardized. We used the "measurement line" adopted in last BFT ageing workshop (Rodriguez-Marin et al., 2020). It was agreed that the second line, necessary to draw the "measurement line", be placed in the middle of the ventral arm when the "ventral groove" is difficult to identify in the otolith section.

Following Campana (2001) recommendation, a minimum of two complete cycles needs to be examined, therefore, the periodicity in annulus deposition or MIA, was determined using the index of completion C = Wn / ((Wn−1+Wn-2)/2) x 100 (Tanabe et al., 2003); where Wn is the width of the marginal increment (distance from the end of the last opaque zone to the marginal edge, whatever edge nature); and Wn-1 and Wn-2 are widths of the previously completed increments (the distance from the end of the second or third most outer opaque zones to the last and penultimate opaque zone) (Figure 43). This method only allows the analysis of MIA in otoliths of specimens over two years old, for specimens older than one year, only one complete cycle was be used (C = Wn / Wn−1 x 100).

A form was used, containing the following information by sample: Light type (reflected, transmitted), number of annual bands (opaque), reading criterion (1 Busawon et al., 2015; 2 Rodriguez-Marin et al., 2020), ventral arm marginal edge type (wide translucent, narrow translucent or opaque), edge type confidence (1= no confident; 2= confident in completeness and not with the type and 3= confident), readability code (1= pattern present-no meaning, 2= pattern present-unsure with age estimate, 3= good pattern present-slightly unsure in some areas, 4= good pattern-confident with age estimate), Wn, Wn-1 and Wn-2 widths in mm, agreed band count (Yes for agreed and No for individual decision), agreed edge type (Yes for agreed and No for individual decision), measuring date, reader coding and notes with observations about the sample.

MIA should be analyzed by age or by age groups since changes in the seasonal timing of the marginal increment with age may occur (Campana, 2001). The analysis of MIA by age covering the whole year is difficult in this species, due to the fact that fisheries are seasonal and target a certain population size fraction. To analyze MIA by age, age groups with sufficient monthly sample representation throughout the year (more than 5 samples per month) were considered.

6.3. Results and discussion

A total of 784 otolith sections showing 1 to 27 opaque bands were analyzed. The majority of these samples, 69%, came from the Canadian laboratory of St. Andrews Biological Station (SABS), 23% from the ICCAT Atlantic-Wide Research Programme for Bluefin Tuna (GBYP) database and the rest, 8%, from the old reference collection to whose formation several laboratories contributed (Busawon

et al., 2015). The monthly distribution of the samples shows that the months of January, February, April and December are poorly represented (Table 19). It is necessary to improve the sampling of these months to have a complete annual representation of the edge type and MIA.

Exploration of MIA values by number of total otolith bands shows an increasing trend with the number of bands (Figure 44). An almost linear growth is observed up to the specimens with 7 bands and from here the slope of the relationship between MIA and number of bands begins to decrease gradually. Growth rate based on length also show an inflection at this ages/number of bands in other growth studies for bluefin tuna (Murua et al., 2017). With this in account, we decided to divide the MIA analysis for two groups of total number of bands: No. of bands 1-7 and 8-27 (Table 19).

Edge type analysis shows that opaque zones are more frequent from July to November, while the translucent terminal edges are formed from December to July. MIA values are higher from July-August to November for both groups of band numbers (Figure 45). The results for edge type and MIA values are consistent, as the MIA values are maximal when the opaque terminal edge is finishing forming. However, the appearance of edge type throughout the year is not consistent with previous studies (Siskey et al., 2016; Rodriguez-Marin et al., 2020) that analyzed the opaque band formation showing that they were formed during the winter months. Nevertheless, the growth of MIA values for the present study and Rodriguez-Marin et al. (2020) study coincide and show similar results in terms of MIA increase from July to November.

The type of light, reflected vs. transmitted, used to identify the nature of the edge can influence its identification. If we separate the analysis by type of light, we observe that the months from September to November are months identified mostly as opaque with both types of light (Figure 46). The otolith edge identification is a common difficulty in interpreting the age of fish (Vitale et al., 2019), The change from reflected to transmitted light recommended for reading sections of bluefin tuna otoliths (Rodriguez-Marin et al., 2020) has resulted in a considerable increase in agreement with respect to terminal edge type. This improvement along with an increase in the number of samples will allow the MIA analysis to be completed and edge type deposition to be determined throughout the year.

6.4. Conclusion:

Preliminary results of edge type and MIA in otolith of ABFT clearly indicate that opaque bands are fully formed in August to November. However, poor data in the early part of the year are determinant to reach any conclusive results. Further sampling effort during winter months are recommended to fully cover the year and examine the relationship between month and index of completion.

References

Busawon, D.S., Rodriguez-Marin, E., Luque, P.L., Allman, R., Gahagan, B., Golet, W., Koob, E., Siskey, M., Ruiz, M., Quelle, P., Neilson, J.D., Secor, D.H. 2015. Evaluation of an Atlantic bluefin tuna otolith reference collection. Collect. Vol. Sci. Pap. ICCAT 71, 960-982.

Campana, S.E. 2001. "Accuracy, precision and quality control in age determination including a review of the use and abuse of age validation methods." Journal of Fish Biology 59: 197-242.

Murua, H., Rodriguez-Marin, E., Neilson, J. D., Farley, J. H., & Juan-Jordá, M. J. (2017). Fast versus slow growing tuna species: age, growth, and implications for population dynamics and fisheries management. Reviews in Fish Biology and Fisheries, 27(4), 733-773.

Panfili, J., de Pontual, H., Troadec, H., Wright, P.J., 2002. Manual of FishSclerochronology, co-edition. IFREMER-IRD, Brest, pp. 464.

Rodriguez-Marin E., Quelle P., Addis P., Alemany F., Bellodi A., Busawon D., Carnevali O., Cort J.L., Di Natale A., Farley J., Garibaldi F., Karakulak S., Krusic-Golub K., Luque P.L., and Ruiz M. 2020. Report of the ICCAT GBYP international workshop on Atlantic bluefin tuna growth. Collect. Vol. Sci. Pap. ICCAT, 76(2): 616-649

Secor, D. H., et al. 2014. Standardization of otolith-based ageing protocols for Atlantic bluefin tuna.Collect. Vol. Sci. Pap. ICCAT 70(2): 357-363.

Siskey, M., Lyubchich, V., Liang, D., Piccoli, P., Secor, D. 2016. Periodicity of strontium: Calcium across annuli further validates otolith-ageing for Atlantic bluefin tuna (Thunnus thynnus). Fish. Res. 177, 13-17.

Tanabe, T., Kayama, S., Ogura, M., & Tanaka, S. 2003. Daily increment formation in otoliths of juvenile skipjack tuna Katsuwonus pelamis. Fisheries Science, 69(4), 731-7

Vitale, F., Clausen, L. W., & Chonchúir, G. N. 2019. Handbook of fish age estimation protocols and validation methods (CRR 346).

Table 19. Number of samples analyzed per month and group of number of opaque bands.

Month	No. bands 1- 7	No. bands 8-27	Total samples
1	1		1
2	2		2
3	5	12	17
4	1	4	5
5	17	34	51
6	30	2	32
7	18	13	31
8	36	138	174
9	16	186	202
10	20	146	166
11	12	79	91
12	6	6	12
Total samples	164	620	784

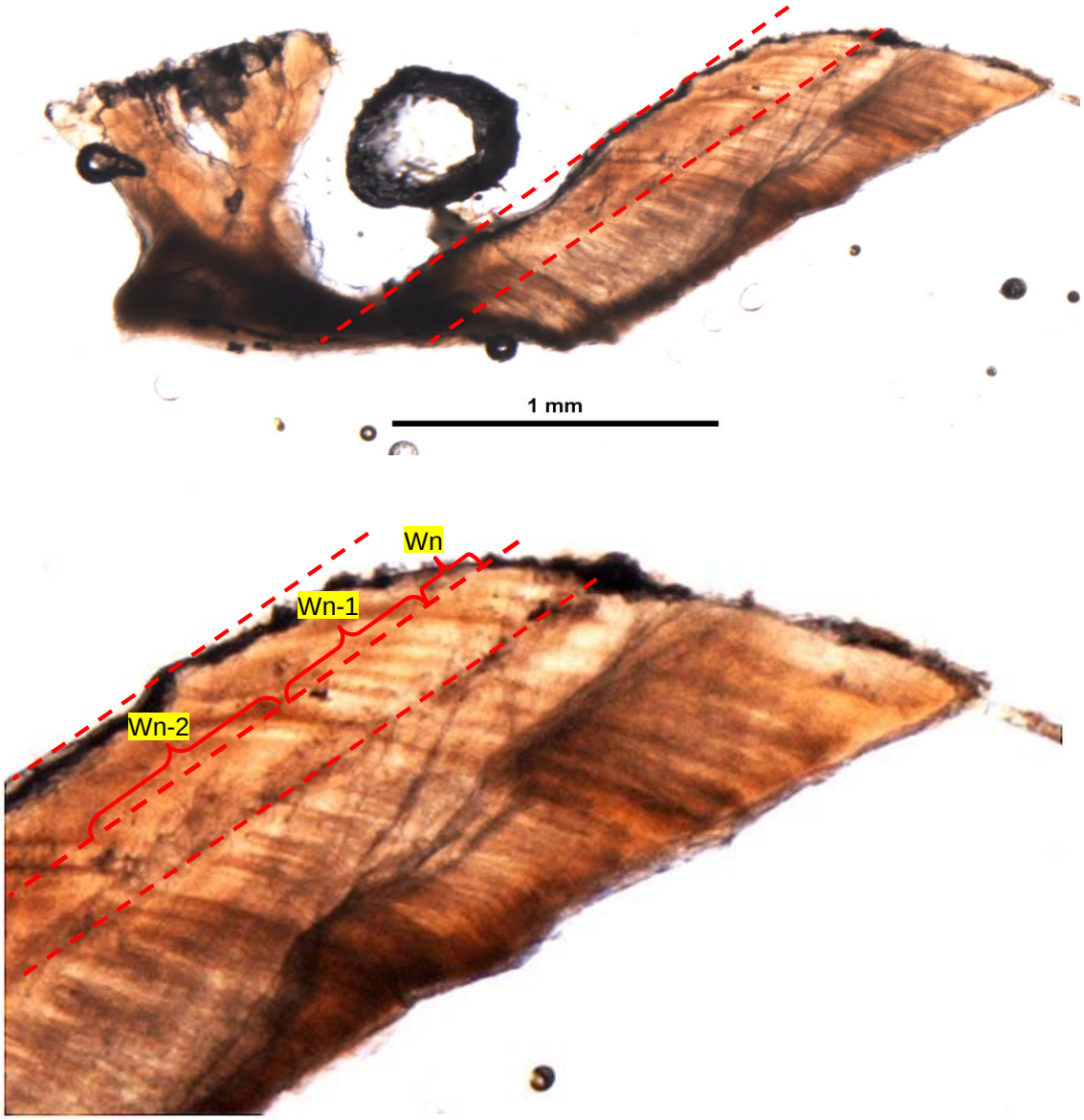

Figure 43. *Transmitted light image of a bluefin tuna otolith section with 3 opaque bands completely formed and translucent edge (top). Enlarged image of the ventral arm end with the measurements obtained to calculate the MIA of this sample (below). MIA = Wn/((Wn-1 + Wn-2)/2) x 100. The red dashed lines indicate the location of the line where the measurements are taken.*

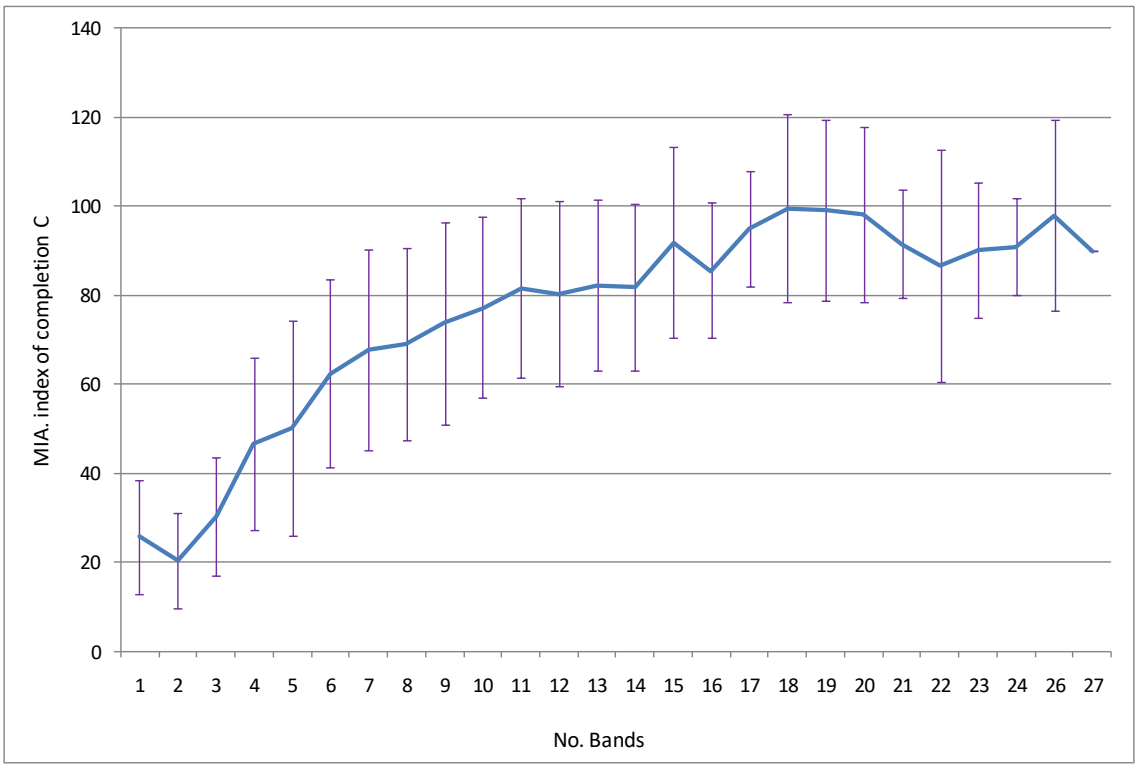

Figure 44. *Marginal increment analysis (MIA), using the index of completion C, by number of otolith bands.*

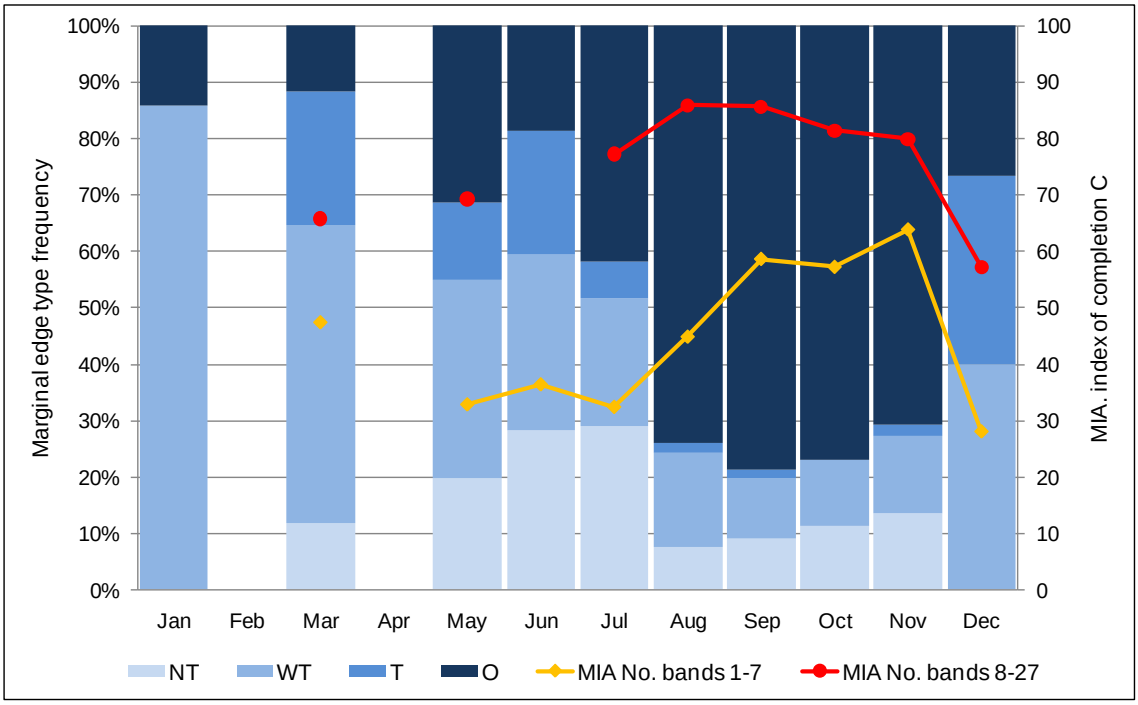

Figure 45. *Marginal state and Marginal Increment Analysis (MIA) for two groups of number of bands: No. of bands 1-7 and 8-27, of eastern Atlantic bluefin tuna otoliths plotted against month.*

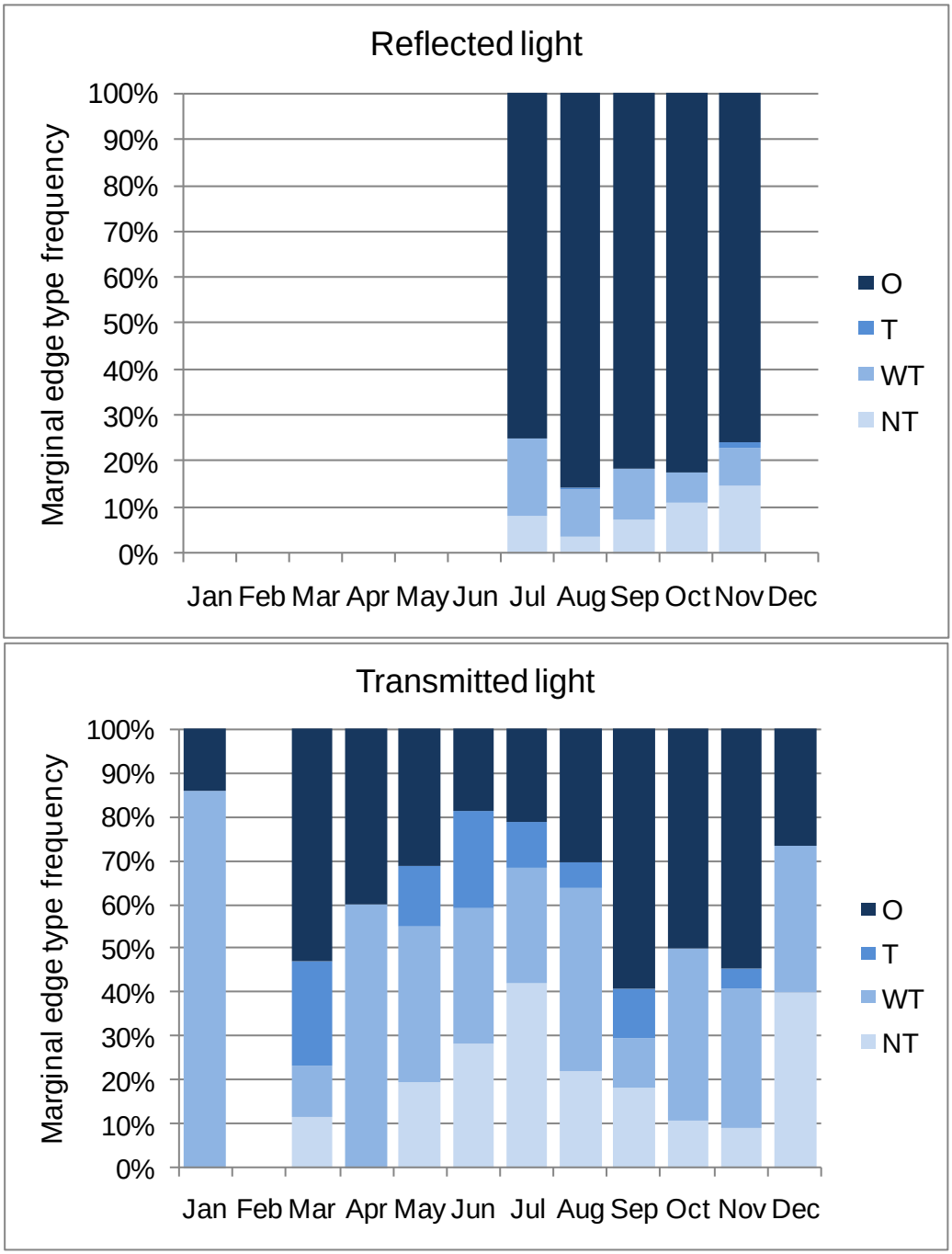

Figure 46. *Marginal state of eastern Atlantic bluefin tuna otoliths plotted against month. Otolith sections read with reflected light (top) and transmitted light (below).*

7. PROCESSING PLANKTON SAMPLES FROM THE BAY OF BISCAY IN SEARCH OF ATLANTIC BLUEFIN TUNA LARVAE

Task Leader: María Santos (AZTI)

Participants: Beatriz Beldarrain and Nicolas Goñi (AZTI)

7.1. Introduction

Atlantic bluefin tuna (*Thunnus thynnus*) is managed so far as two separate populations in the Atlantic and Mediterranean. Their two spawning areas are widely separated. The western stock spawns in the Gulf of Mexico (including the Straits of Florida), and the eastern stock spawns in several spawning areas of the Mediterranean Sea. Although the western stock was the first to be under regulation (since 1999), the number of reproductive studies is lower than those undertaken for the eastern stock (Susca *et al*., 2001; Corriero *et al*., 2003; Karakulak *et al*., 2004; Aranda *et al*., 2011; MacKenzie & Mariani, 2012). Recently, Richardson *et al*. (2016) used larval collections to demonstrate a spawning ground in the Slope Sea, between the Gulf Stream and the northeast United States continental shelf (Richardson *et al*.2016).

Eastern Atlantic bluefin tuna (ABFT) migrates from the Mediterranean to the Bay of Biscay for feeding (Arrizabalaga *et al*.2019; Arregui *et al*.2018). But recently, there were indications that ABFT was spawning also in the Bay of Biscay since larvae of the species have been found in this area (Rodriguez *et al*.2019). For that reason, the search for ABFT larvae in samples collected in past surveys in the Bay of Biscay was performed in 2019 founding one larva of ABFT. In 2020, taking advantage of the ABFT index acoustic survey, specific plankton samples were collected to find ABFT larvae.

7.2. Material and Methods

7.2.1. Field samples

Taking into advance of the ABFT acoustic survey, on board a commercial vessel (*Tuku-tuku*), in the Bay of Biscay (15-22 June 2020) (ABFT laying period Jun-Jul-Aug), plankton samples were performed to look for ABFT larvae in this area.

The study area in the Bay of Biscay was from 3ºW to the French coast and from the Cantabric coast to 45ºN (**Fig. 47**). The survey was carried out outside the platform (200m depth), were the probability to find ABFT was higher, initially. There was a systematic sampling: at sunset, after the acoustic transects and fishing activities were performed during the day, a plankton haul was performed. In total there were 6 plankton samples.

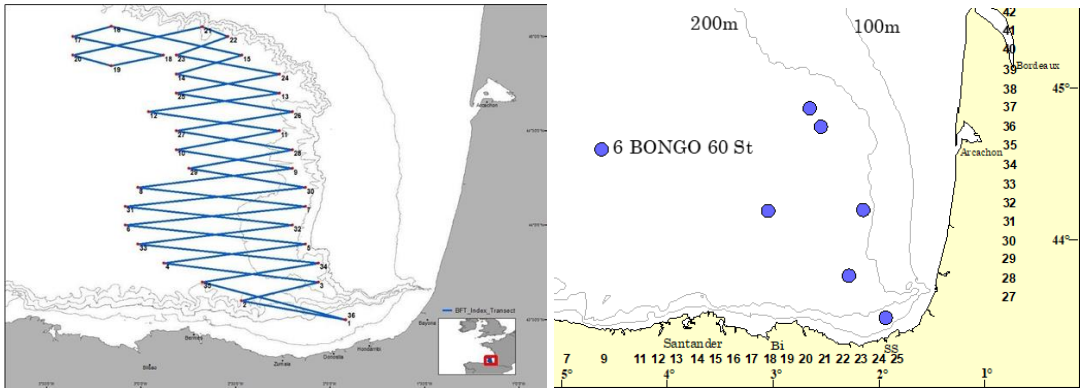

Figure 47*: Area of study with acoustic transects (blue lines) (left) and Bongo 60 plankton stations (right*)

At each station, an oblique plankton haul was performed using a BONGO60 net with a net mesh size of 250 µm with the vessel navigating at 2 knots during 20 min. The net was lowered to a maximum depth of 30-40m. A 35 kg depressor was used to allow for correctly deploying the net. "G.O. 2030" flowmeters were used to estimate afterwards the filtered volume. Sample depth, temperature, salinity, and fluorescence profiles were obtained at each sampling station using a CTD RBR-XR420 coupled to the net. Immediately after the haul, the net was washed, and the sample obtained was fixed in ethanol 96%. **Table 20** shows the information for each plankton station.

Table 20*: Plankton samples collected during the BFT Index survey, looking for BFT larvae*

station	date	gmt hour_end	lat_end	lon_end	duration(mn)	speed(knots)	net
1	20200616	16:30	432939	15512	20	2	bongo 60(250um)
2	20200618	17:35	441162	30183	20	2	bongo 60(250um)
3	20200619	20:50	444487	23193	20	2	bongo 60(250um)
4	20200620	20:55	445218	23819	20	2	bongo 60(250um)
5	20200621	20:25	441200	20785	20	2	bongo 60(250um)
6	20200622	20:50	434600	21600	20	2	bongo 60(250um)

7.2.2. BFT larvae identification

Larvae species other than clupeids were extracted from the plankton samples under the binocular. ABFT larvae were looked for under a stereoscopic microscope. BFT identification was based on pigmentation patterns, number of myomers, morphologic and meristic characteristics, taking advantage of the last year identification experience and following the descriptions by Alemany

(1997), Fahay (2007), Rodriguez *et al*. (2017), Puncher *et al*. (2015) and ABFT larvae photos from an incubation experiment carried out in 2012 by AZTI, in the laboratory of IEO Mazarrón-Murcia (Spain) and from a survey carried out in 2012 in the Balearic Sea.

7.3. Results and discussion

Few adult ABFT individuals were detected in the area during the survey; Even and all, plankton hauls were carried out, although the probability of finding an ABFT egg was very low since few adults were sighted. Moreover, there were performed very few plankton samples. Among the 6 plankton samples obtained, none ABFT larvae were found (**Table 21**)

Table 21*: larvae found in the plankton samples analyzed for ABFT larvae*

station	BFTlarvae	other larvae
1	0	74
2	0	2
3	0	14
4	0	2
5	0	0
6	0	7

Two main factors may contribute to explain the lack of bluefin tuna larvae in the area prospected. The first one, the absence of adult bluefin tuna in the prospected area during the survey days; There were found juvenile or pre-adult fish mostly, whereas adult aggregations were locally observed in onshore areas nearby the Cap Breton canyon, outside of the survey area. The second one the few plankton samples that were performed during the survey. Other factors may be the big amount of salps in the survey area and the overall number of fish larvae that was low in the area for this time of the year

The plankton collection took place again in 2021. Big salp aggregations were not observed this year in the study area but in the rest of the Bay of Biscay at least in May. Adult ABFT were spotted at least at one of the plankton sampling locations, which may increase the likelihood of finding bluefin tuna larvae in the samples collected.

References

Alemany F, Quintanilla L, Velez-Belchi P, Garcia A and others (2010) Characterization of the spawning habitat of Atlantic bluefin tuna and related species in the Balearic Sea (western Mediterranean). Prog Oceanogr 86: 21−38

Arregui, I., Galuardi, B., Goñi, N., Lam, C.H., Fraile, I., Santiago, J., Lutcavage, M. and Arrizabalaga, H. (2018) Movements and geographic distribution of juvenile bluefin tuna in the Northeast Atlantic, described through internal and satellite archival tags. ICES Journal of Marine Science doi:10.1093/icesjms/fsy056.

Arrizabalaga, H., Arregui, I., Medina, A., Rodríguez-Ezpeleta, N., Fromentin, J.-M. and Fraile, I. (2019) Life History and Migrations of Mediterranean Bluefin Tuna In: The Future of Bluefin Tunas: Ecology, Fisheries Management, and Conservation.B. Block (ed.) Johns Hopkins University Press, pp. 67-93.

Corriero A, Desantis S, Deflorio M, Acone F, Bridges CR, De la Serna JM, Megalofonou P, De Metrio G. Histological investigation on the ovarian cycle of the bluefin tuna in the western and central Mediterranean. Journal of Fish Biology. 2003;63(1):108–119. doi: 10.1046/j.1095-8649.2003.00132.x.

Goñi, N., Uranga, J., Arregui, I., Onandia, I., Martinez, U., Boyra, G., Melvin, G.D., Godard, I. and Arrizabalaga, H. (2018) ACOUSTIC-BASED FISHERY-INDEPENDENT ABUNDANCE INDEX OF JUVENILE BLUEFIN TUNAS IN THE BAY OF BISCAY: RESULTS FROM THE FIRST THREE SURVEYS AND CHALLENGES. Collect. Vol. Sci. Pap. ICCAT, 76(x): SCRS/2018/145

Karakulak S, Oray I, Corriero A, Deflorio M, Santamaria N, Desantis S, De Metrio G. Evidence of a spawning area for the bluefin tuna (Thunnus thynnus L.) in the eastern Mediterranean. Journal of Applied Ichthyology. 2004;20(4):318–320. doi: 10.1111/j.1439-0426.2004.00561.x

Mackenzie, Brian & Mariani, Patrizio. (2012). Spawning of Bluefin Tuna in the Black Sea: Historical Evidence, Environmental Constraints and Population Plasticity. PloS one. 7. e39998. 10.1371/journal.pone.0039998.

Puncher, G N, Alemany F, Arrizabalaga H, Cariani A and Tinti F. Misidentification of bluefin tuna larvae: a call for caution and taxonomic reform. Rev Fish Biol Fisheries (2015) 25:485–502 DOI 10.1007/s11160-015-9390-1

Reglero P., Ciannelli L., Alvarez-Berastegui D., Balbín R., Lopez-Jurado J.L., Alemany F., (2012) Geographically and environmentally driven spawning distributions of tuna species in the western Mediterranean Sea, Marine ecology progress series, 2012, 463:273-284 pp.

Richardson DE, Marancik KE, Guyon JR, Lutcavage ME, Galuardi B, Lam CH, Walsh HJ, Wildes S, Yates DA, Hare JA. Discovery of a spawning ground reveals diverse migration strategies in Atlantic bluefin tuna (Thunnus thynnus) Proceedings of the National Academy of Sciences of the United States of America. 2016;113(12):3299–3304. doi: 10.1073/pnas.1525636113.

Rodriguez J.M., Johnstone C.and Lozano-Peral D.2019. Is the southern Bay of Biscay a spawning ground for Thunnus thynnus and Sarda Sarda? SCRS/2019/201.

Rodriguez, J.M., Alemany, F. and Garcia A. 2017. A guide to the eggs and larvae of 100 common Western Mediterranean Sea bony fish species. FAO, Rome, Italy, 256 pp.

Susca V, Corriero A, Deflorio M, Bridges CR, De metrio G. New results on the reproductive biology of bluefin tuna (Thunnus thynnus) in the Mediterranean. ICCAT Collective Volume of Scientific Papers. 2001;52:745–751.

8. SORTING, IDENTIFICATION AND COUNTING OF ATLANTIC BLUEFIN TUNA LARVAE FOR GENETICS TO BE APPLIED IN UNDERSTANDING POPULATION STRUCTURE IN THE EASTERN STOCK

Task leader: Patricia Reglero.

Subcontracted party: CBBA

8.1. Introduction

The collection of Atlantic bluefin tuna larvae in the main spawning area of the NW Mediterranean provides a novel opportunity to genetically mark actively spawning adult fish through DNA analysis and to assess the genetic diversity and population structure in the spawning ground. Besides, the collection of Atlantic bluefin tuna larvae provides a novel opportunity to genetically mark actively spawning adult fish through DNA analysis. The ability to acquire larvae quickly means that larval collections can be useful for further work on EBFT population structure considering also the early life stage besides the information inferred from the larvae and related to the adults. Sample sorting, initial ID and curation are critical to the success of obtaining high quality DNA. National programs ensure collecting tuna larvae every summer in the main spawning ground for Bluefin tuna using Bongo nets. One collector is formalin preserved and these samples that are routinely used to identify bluefin tuna larvae since formalin is the best preservation method for the maintenance of pigments used for taxonomic identification and it is further used for the estimation of the larval index used in the assessments. The other Bongo collector is preserved in alcohol since 2019. To ensure the quality of the DNA in the larvae is high, it is important to separate the larvae and storage them separately in ethanol.

8.2. Field sampling and laboratory processing

We sorted and identified bluefin tuna fish larvae from 60 stations randomly selected from a cruise that took place around the Balearic Islands, western Mediterranean Sea, during June-July 2020. The larvae were separated and identified from a Bongo net (90-cm diameter and 500-µm mesh size) that was towed obliquely down to 30-m depth for 8-12 minutes at 2 knots cruising speed and preserved directly in 100% ethanol for further processing. We used a dissection microscope to identify bluefin tuna larvae and sorting them from the total plankton sample. In addition, the different stages described in the larvae development were identified: yolk sac, preflexion, flexion, or postflexion. The individuals

sorted were preserved in 100% ethanol in different 4 ml jarks, each for stage sampled, and kept in the freezer for the perfect conservation.

8.2. Results

We identified 2258 individuals from 49 samples with the presence of bluefin tuna larvae (stations positive; Table 22). In the remaining 11 samples, the absence of bluefin tuna larvae was confirmed (Table 23).

Table 22. *Number of bluefin tuna larvae identified by stage of development from station positives sampled.*

Survey	Station	Order	Bongo	Nets	Specie	Stage	Nº larvae
TB0620	1402	9	B90	500	BFT	PREFLEXION	82
TB0620	1589	15	B90	500	BFT	PREFLEXION	17
TB0620	1793	17	B90	500	BFT	PREFLEXION	9
TB0620	1317	26	B90	500	BFT	PREFLEXION	6
TB0620	1690	16	B90	500	BFT	PREFLEXION	35
TB0620	1226	27	B90	500	BFT	PREFLEXION	7
TB0620	1131	28	B90	500	BFT	PREFLEXION	10
TB0620	1131	28	B90	500	BFT	POSTFLEXION	4
TB0620	1228	29	B90	500	BFT	PREFLEXION	17
TB0620	1228	29	B90	500	BFT	FLEXION	2
TB0620	1319	30	B90	500	BFT	PREFLEXION	9
TB0620	1319	30	B90	500	BFT	FLEXION	1
TB0620	1319	30	B90	500	BFT	POSTFLEXION	1
TB0620	1410	31	B90	500	BFT	PREFLEXION	9
TB0620	1499	32	B90	500	BFT	FLEXION	7
TB0620	1696	34	B90	500	BFT	PREFLEXION	3
TB0620	1597	35	B90	500	BFT	PREFLEXION	9
TB0620	1597	35	B90	500	BFT	FLEXION	1
TB0620	1501	36	B90	500	BFT	PREFLEXION	10
TB0620	1412	37	B90	500	BFT	PREFLEXION	26
TB0620	1412	37	B90	500	BFT	FLEXION	1
TB0620	1321	38	B90	500	BFT	PREFLEXION	20
TB0620	1321	38	B90	500	BFT	POSTFLEXION	2
TB0620	1230	39	B90	500	BFT	FLEXION	18
TB0620	1135	41	B90	500	BFT	PREFLEXION	51
TB0620	1232	42	B90	500	BFT	PREFLEXION	22
TB0620	1323	43	B90	500	BFT	YOLK SACK	5
TB0620	1234	46	B90	500	BFT	YOLK SACK	93
TB0620	1234	46	B90	500	BFT	PREFLEXION	83
TB0620	1139	48	B90	500	BFT	PREFLEXION	74
TB0620	1139	48	B90	500	BFT	FLEXION	5
TB0620	1139	48	B90	500	BFT	YOLK SACK	2
TB0620	1236	49	B90	500	BFT	PREFLEXION	111
TB0620	1236	49	B90	500	BFT	YOLK SACK	5
TB0620	1327	50	B90	500	BFT	PREFLEXION	72
TB0620	1329	51	B90	500	BFT	PREFLEXION	212
TB0620	1331	52	B90	500	BFT	PREFLEXION	47
TB0620	1331	52	B90	500	BFT	FLEXION	1
TB0620	1331	52	B90	500	BFT	POSTFLEXION	1

TB0620	1333	53	B90	500	BFT	PREFLEXION	64
TB0620	1333	53	B90	500	BFT	FLEXION	1
TB0620	1239	54	B90	500	BFT	PREFLEXION	8
TB0620	1241	55	B90	500	BFT	PREFLEXION	18
TB0620	1241	55	B90	500	BFT	FLEXION	3
TB0620	1144	56	B90	500	BFT	PREFLEXION	102
TB0620	1144	56	B90	500	BFT	FLEXION	6
TB0620	1335	57	B90	500	BFT	PREFLEXION	24
TB0620	1243	58	B90	500	BFT	PREFLEXION	4
TB0620	1146	59	B90	500	BFT	PREFLEXION	36
TB0620	975	64	B90	500	BFT	FLEXION	4
TB0620	893	67	B90	500	BFT	PREFLEXION	23
TB0620	893	67	B90	500	BFT	FLEXION	3
TB0620	1056	69	B90	500	BFT	PREFLEXION	10
TB0620	1056	69	B90	500	BFT	FLEXION	1
TB0620	891	72	B90	500	BFT	PREFLEXION	30
TB0620	1052	75	B90	500	BFT	PREFLEXION	81
TB0620	1052	75	B90	500	BFT	FLEXION	2
TB0620	1052	75	B90	500	BFT	POSTFLEXION	2
TB0620	1050	76	B90	500	BFT	PREFLEXION	25
TB0620	1050	76	B90	500	BFT	FLEXION	18
TB0620	703	77	B90	500	BFT	PREFLEXION	12
TB0620	701	78	B90	500	BFT	FLEXION	2
TB0620	792	83	B90	500	BFT	PREFLEXION	21
TB0620	794	84	B90	500	BFT	PREFLEXION	296
TB0620	794	84	B90	500	BFT	FLEXION	1
TB0620	794	84	B90	500	BFT	POSTFLEXION	2
TB0620	882	85	B90	500	BFT	PREFLEXION	43
TB0620	882	85	B90	500	BFT	FLEXION	3
TB0620	882	85	B90	500	BFT	POSTFLEXION	1
TB0620	878	87	B90	500	BFT	PREFLEXION	124
TB0620	876	88	B90	500	BFT	PREFLEXION	10
TB0620	962	89	B90	500	BFT	PREFLEXION	5
TB0620	964	90	B90	500	BFT	PREFLEXION	35
TB0620	966	91	B90	500	BFT	PREFLEXION	148

Table 23. Stations sampled with an absence of bluefin tuna larvae.

Survey	Station	Order	Bongo	Nets	Specie	Nº larvae
TB0620	1046	1	B90	500	BFT	0
TB0620	1044	2	B90	500	BFT	0
TB0620	1127	5	B90	500	BFT	0
TB0620	1492	10	B90	500	BFT	0
TB0620	1585	12	B90	500	BFT	0
TB0620	1694	20	B90	500	BFT	0
TB0620	1593	23	B90	500	BFT	0
TB0620	1408	25	B90	500	BFT	0
TB0620	1137	47	B90	500	BFT	0
TB0620	1148	60	B90	500	BFT	0
TB0620	788	81	B90	500	BFT	0

8.3. Conclusion and perspectives

We have been able to ensure high quality bluefin tuna larvae preserved in ethanol. Different developmental stages within the first month of life of this species were identified and separately preserved. Including early life stages, such as larvae, in the biological sampling program for Atlantic and Mediterranean bluefin tuna is a main task to ensure n holistic view of the life cycle of the species. Survival upon reproduction is the ultimate goal of the species. On one hand, explanations of the timing, selection of spawning sites and many other biological and ecological aspects of bluefin tuna can be understood from the perspective of the fate and needs of the offspring and therefore recruitment. On the other hand, having larvae well preserved provide a novel opportunity to genetically mark actively spawning adult fish through DNA analysis in the future, explore genetic connectivity and ensure sampling that can help to solve uncertainties in current knowledge of the species.

9. ACKNOWLEDGEMENTS

This work was carried out under the provision of the ICCAT Atlantic Wide Research Programme for Bluefin Tuna (GBYP), funded by the European Union, by several ICCAT CPCs, the ICCAT Secretariat and by other entities (see: https://www.iccat.int/GBYP/en/Overview.asp). The contents of this report do not necessarily reflect the point of view of ICCAT or of the other funders, which have not responsibility about them, neither do them necessarily reflect the views of the funders and in no ways anticipate the Commission's future policy in this area.

10. APPENDICES

Appendix 1: Database as of 8th July 2021 (see “DATABASE_2021_4_ICCAT.xlsx).